AD-A149 552 LITHOGRAPHY RADIATION EFFECTS STUDY(U) SPIRE CORP 1/2
BEDFORD MA B W MURRAY NOV 84 RADC-TR-84-233
F19628-80-C-0196

UNCLASSIFIED F/G 14/5 NL

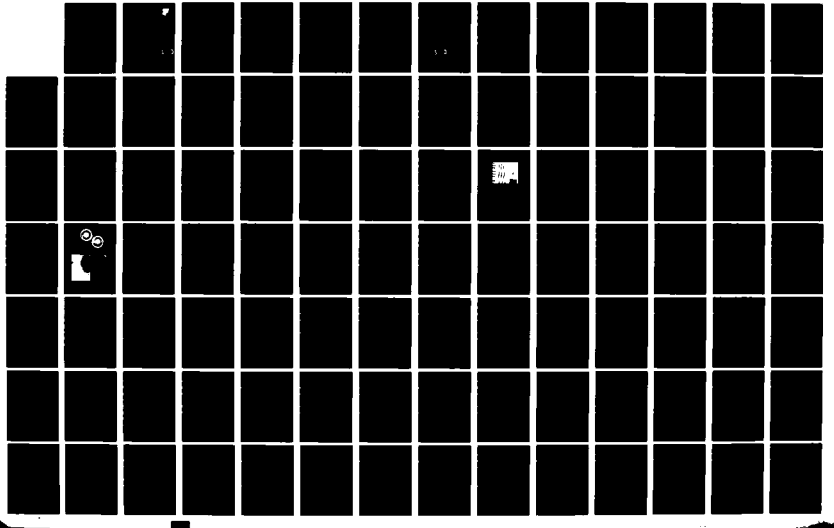

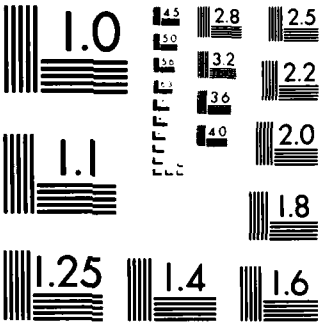

(12)

RADC-TR-84-233
Final Technical Report
November 1984

LITHOGRAPHY RADIATION EFFECTS STUDY

Spire Corporation

Brian W. Murray

APPROVED FOR PUBLIC RELEASE; DISTRIBUTION UNLIMITED

ROME AIR DEVELOPMENT CENTER
Air Force Systems Command
Griffiss Air Force Base, NY 13441-5700

This report has been reviewed by the RADC Public Affairs Office (PA) and is releasable to the National Technical Information Service (NTIS). At NTIS it will be releasable to the general public, including foreign nations.

RADC-TR-84-233 has been reviewed and is approved for publication.

APPROVED: John C. Garth

JOHN C. GARTH
Project Engineer

APPROVED: Harold Roth

HAROLD ROTH, Director
Solid State Sciences Division

FOR THE COMMANDER: John A. Ritz

JOHN A. RITZ
Acting Chief, Plans Office

If your address has changed or if you wish to be removed from the RADC mailing list, or if the addressee is no longer employed by your organization, please notify RADC (ESR) Hanscom AFB MA 01731. This will assist us in maintaining a current mailing list.

Do not return copies of this report unless contractual obligations or notices on a specific document requires that it be returned.

REPORT DOCUMENTATION PAGE

1a. REPORT SECURITY CLASSIFICATION UNCLASSIFIED	1b. RESTRICTIVE MARKINGS N/A
2a. SECURITY CLASSIFICATION AUTHORITY N/A	3. DISTRIBUTION/AVAILABILITY OF REPORT Approved for public release; distribution unlimited.
2b. DECLASSIFICATION/DOWNGRADING SCHEDULE N/A	
4. PERFORMING ORGANIZATION REPORT NUMBER(S) N/A	5. MONITORING ORGANIZATION REPORT NUMBER(S) RADC-TR-84-233
6a. NAME OF PERFORMING ORGANIZATION Spire Corporation 6b. OFFICE SYMBOL (If applicable)	7a. NAME OF MONITORING ORGANIZATION Rome Air Development Center (ESR)
6c. ADDRESS (City, State and ZIP Code) Patriots Park Bedford MA 01730	7b. ADDRESS (City, State and ZIP Code) Hanscom AFB MA 01731
8a. NAME OF FUNDING/SPONSORING ORGANIZATION AFOSR 8b. OFFICE SYMBOL (If applicable)	9. PROCUREMENT INSTRUMENT IDENTIFICATION NUMBER F19628-80-C-0196
8c. ADDRESS (City, State and ZIP Code) Bolling AFB DC 20332	10. SOURCE OF FUNDING NOS. PROGRAM ELEMENT NO. 61102F; PROJECT NO. 2306; TASK NO. J3; WORK UNIT NO. 31

11. TITLE (Include Security Classification)
LITHOGRAPHY RADIATION EFFECTS STUDY

12. PERSONAL AUTHOR(S)
Brian W. Murray

13a. TYPE OF REPORT	13b. TIME COVERED	14. DATE OF REPORT (Yr., Mo., Day)	15. PAGE COUNT
Final	FROM Nov 80 TO Nov 83	November 1984	106

16. SUPPLEMENTARY NOTATION
N/A

17 COSATI CODES			18. SUBJECT TERMS (Continue on reverse if necessary and identify by block number)
FIELD	GROUP	SUB. GR.	
06	18		X-Ray Lithography; PBS Resist
18	06		Dove Profile Measurement Technique; X-Ray Phoelectrons

19. ABSTRACT (Continue on reverse if necessary and identify by block number)

An experimental x-ray lithography facility for irradiating thin films of a photoresist next to a gold mask is described. The x-ray irradiance and PMMA irradiation times are estimated for several target elements with characteristic x-ray lines in the 1-3 keV energy range. A gold mask (6800 A thick) deposited with films of carbon 100, 220, 520 and 710 A thick were placed next to films of PBS resist and irradiated with x-rays from Al, Ag, and Ti targets bombarded by 10 keV electrons. The exposed PBS was etched for a fixed time interval, and the thickness of the etched resist next to the varying film thickness of carbon was measured by optical ellipsometry. The plot of etched PBS thickness vs. carbon film thickness gave a measure of the depth of penetration of x-ray photoelectrons from the gold mask into the resist and a possible method of measuring dose-depth profiles at material interfaces at soft x-ray energies. A realistic, calculational model that includes source bremsstrahlung predicts fairly well experimental dose profile for the Au/C mask.

20. DISTRIBUTION/AVAILABILITY OF ABSTRACT UNCLASSIFIED/UNLIMITED ☒ SAME AS RPT ☐ OTIC USERS ☐	21. ABSTRACT SECURITY CLASSIFICATION UNCLASSIFIED
22a. NAME OF RESPONSIBLE INDIVIDUAL John C. Garth	22b. TELEPHONE NUMBER (Include Area Code) (617) 861-2360 22c. OFFICE SYMBOL RADC (ESR)

A 7000 A-thick Ag mask, deposited with 13 films of carbon ranging in thickness from 35 A to 1688 A, was placed next to films of PBS resist and irradiated with x-rays from Al, Ag, Ti and Cr targets bombarded by 10 keV electrons. The resultant profiles were consistent with the previous profiles obtained using the Au mask. All profiles exibited a strong asymptote indicating that the thicker carbon films used absorbed all the x-ray generated radiations from the Ag mask. For Al, the asymptote was reached at 180 A of carbon; Ag, 380 A; Ti, 500 A and Cr, around 580 A. The corresponding characteristic x-ray energies are: Al, 1.49 keV; Ag, 2.98 keV; Ti, 4.51 keV and Cr, 5.41 keV. Even though commercial x-ray lithography sources will be operated at 20-25 keV for greater x-ray efficiency, one may still conclude from this data that loss of spatial resolution due to high x/low Z interfaces should be minimal and in the range of 1000 A or less, depending on the source used. Further, mask-generated radiations which can reduce exposure contrast can be eliminated by depositing a thin organic (low Z) film to the resist side of an x-ray lithography mask.

SUMMARY

An experimental x-ray lithography facility for irradiating thin films of a photoresist next to a gold mask is described. The x-ray irradiance and irradiation times for PMMA and PBS resists are estimated for several target elements with characteristic x-ray lines in the 1-5 keV energy range. A gold mask (6800 A thick) deposited with films of carbon 100, 220, 520 and 710 A thick were placed next to films of PBS resist and irradiated with x-rays from Al, Ag, and Ti targets bombarded by 10 keV electrons. The exposed PBS was etched for a fixed time interval, and the thickness of the etched resist next to the varying film thicknesses of carbon was measured by optical ellipsometry. The plot of etched PBS thickness vs. carbon film thickness gave a measure of the depth of penetration of x-ray photoelectrons from the gold mask into the resist and a possible method of measuring dose-depth profiles at material interfaces at soft x-ray energies.

A Ag mask (7000 A thick), deposited with 13 separate films of carbon ranging in thickness from 35 A to 1688 A, was placed next to PBS resist films and irradiated with x-rays from Al, Ag, Ti and Cr targets bombarded with 10 keV electrons. The resultant dose profiles (etched PBS depth vs. carbon thickness), obtained in the same way as those for the Au mask, were in basic agreement with the data for the Au mask. However, every profile for the Ag mask exhibited an asymptote with depth of carbon which implies that, within the range of carbon thickness used, the x-ray generated radiations from the Ag mask were completely absorbed. For the Al source (K_α = 1.49 keV), the asymptote began at a carbon thickness of about 180 A; for Ag (L_α = 2.98 keV), 380 A; for Ti (K_α = 4.51 keV), 500 A and for Cr (K_α = 5.41 keV), 580 A. Comparison of these data with existing theoretical models were not carried out.

The implications for commercial x-ray lithography that can be derived from these experiments are the following. One, by coating the Au (or whatever metal is used) mask with a thin (~2000 A), low Z organic film, the problem of unwanted mask-generated radiation that reduce contrast between exposed and unexposed resist will be eliminated. Two, the loss of spatial resolution due to a dose profile being generated at a high Z/low Z interface would seem to be in the range of 1000 A or less, depending on the source used.

PREFACE

The author would like to express his appreciation to Mr. Russell Dolan (consulting scientist at Spire) and Mr. Joseph Cooner (RADC, Hanscom AFB) for their assistance and contributions to this program. The author would like to especially thank the technical monitor of this contract, Dr. John Garth (RADC, Hanscom AFB) for his scientific contribution to the work reported here.

TABLE OF CONTENTS

TABLE OF CONTENTS (Concluded)

LIST OF ILLUSTRATIONS

LIST OF ILLUSTRATIONS (Concluded)

LIST OF TABLES

1.0 INTRODUCTION

The X-Ray Lithography Radiation Effects Contract (No. F19628-80-C-0196) is a 30-month program which has the following major objectives:

a. The development of methods for submicron depth dose measurements in low Z materials in the vicinity of interfaces with high Z materials. The measurements will be restricted to one-dimensional geometries, and will measure the dose contributions of 1-10 keV characteristic x-rays, continuum x-rays, and electrons produced in the high Z material.

b. One method to be developed will physically measure energy deposited in materials by monitoring transmitted radiations with a solid state detector. The detector will also provide additional information on the transmitted photoelectron spectrum as well as the x-ray spectrum.

c. The second method to be developed will be dose profile measurements in low Z materials using well characterized photoresists as detectors.

d. The comparison of experimental data with calculational results of available codes and theoretical models to check the accuracy of these calculational methods.

e. The development of a list of guidelines based on the results of this program to help optimize further work in x-ray lithography.

Commercial x-ray sources, with the flexibility for performing the measurements necessary for this program, are not available. As a result, a major part of the initial effort is, therefore, the design and assembly of a highly reliable, variable energy x-ray source. This source is not designed to have high brightness, but it will be intensity and voltage stabilized.

The techniques by which thin films (filters, photoresist, oxides, etc.) are constructed and the accuracy to which their dimensions are known are critical in obtaining reliable data. In addition, techniques will need to be developed to utilize photoresist materials as sensitive dose monitors. A second major element, then, in

the initial efforts of this program will be to fully develop and utilize these techniques for this program. Spire Corporation will employ its internal semiconductor processing laboratory to fabricate precision films using photoresist spinning, evaporation and sputtering methods.

2.0 X-RAY LITHOGRAPHY EXPERIMENTAL FACILITY

2.1 X-Ray Source Vacuum Chamber

After a thorough review , the vacuum chamber illustrated in Figure 1 was chosen to house the x-ray source and experimental components. The outside diameter of the main chamber is 6 inches, with the largest conflat flanges being 8-inches in diameter. Six vacuum ports have rotatable conflat flanges. This chamber design allows for the flexibility needed for the experimental studies. The two ports along the vertical direction (normal to page) connect to the vacuum pump (below) and other experiments (above). The four horizontal ports in the plane of the page will house the x-ray target anode, the electron gun, the residual gas analyzer (RGA), and the Faraday cup electron beam monitor.

Oil-free vacuum pumping is accomplished with a 30 l s^{-1} ion pump with a sorption pump for initial rough pumping. The 1-1/2-inch pumpout port in Figure 1 is used to rough pump the chamber. A bake-out mantle is needed to bake out the chamber to at least 200°C so that ultra high vacuum (UHV) pressures of residual gases can be realized. The RGA will be especially useful in determining the quality of the vacuum environment of the chamber, and can be used to detect the presence of leaks and to monitor the effectiveness of various bake-out procedures.

The vacuum system was tested to pump down the bare vacuum chamber closed off with conflat flanges. With minimum chamber bakeout (using heating tapes), the vacuum pressure obtained was 2 X 10^{-7} torr.

2.2 Electron Gun

2.2.1 General Description

After an extensive search, a suitable electron gun was purchased from Nuclide Corporation of Acton. It is designed for 30 kV, 300 mA operation, but the upper limits of the HV power supply is 15 kV and 50 mA. The current regulation is 1 percent or better, while the voltage regulation is better than 5 percent.

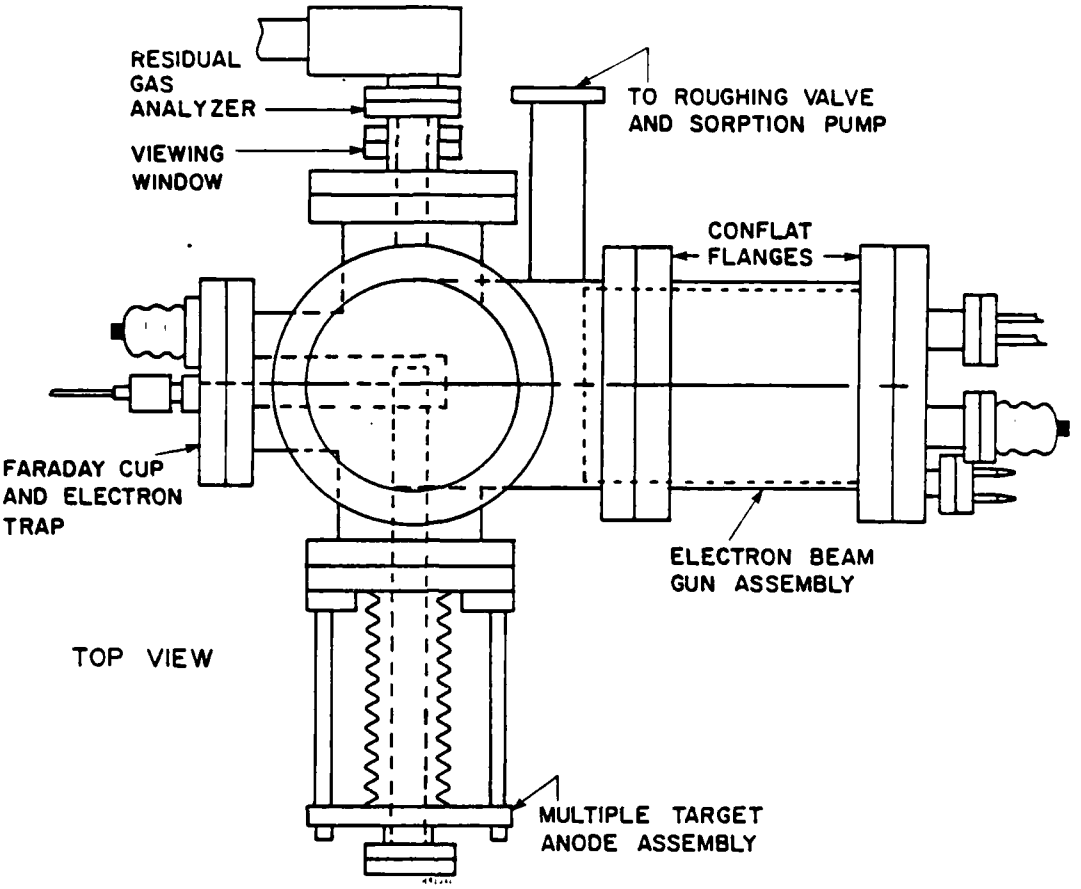

FIGURE 1. TOP VIEW ILLUSTRATION OF VACUUM CHAMBER CONFIGURATION. (The conflat flanges contain Cu-metal-gaskets which provide the UHV seals.)

The gun comes as a system with power supplies and controls which can operate in a stable fashion in the microamp range as well as at 50 mA. This is due to a manually adjusted anode-cathode gap in the gun assembly. The lowest accelerating voltage at which it can operate in a stable manner and with some current is not yet fully known. This gun model has been shown by other users to yield up to 84 mA when operated at 5 kV. The chances of operating it at 3 kV with a stable current are very good. Since the cathode can be adjusted to change the perveance ($I(amps)/V^{3/2}$), a current of 20 mA and an operating voltage of 2.2 kV yields a perveance of 2×10^{-7}. As long as the perveance is below 10^{-6}, stable operation should be obtainable.

The electron beam is focused with a magnetic coil which allows the distance between the coil and the anode target to be very large. This gun model has been operated at an 18-inch working distance with a 4-mm spot size. The filament material (Ta ribbon) has a vapor pressure of 6×10^{-7} torr at its surface when operated at 2200°C. Neutral Ta atoms can be boiled off and land on any cold, nearby surface. Having the capability of a long working distance minimizes the risk of contaminating an x-ray anode target surface with Ta from the cathode. Nevertheless, direct site between the filament and anode target does imply eventual contamination of the target with Ta.

2.2.2 Electron Gun Configuration Within the Vacuum Chamber

Although the electron gun is a purchased component, a significant amount of engineering effort was required to insure that this component will perform with the flexibility required for this program. In order to steer the electron beam to the x-ray target anode, the gun must first be mounted properly inside the vacuum chamber so that adjustments can be made. Figure 2 is a schematic sketch illustrating the mounting of the gun and its focus coil within the 6-inch tubulation off the main vacuum chamber. The electron gun body is fastened to two OFHC copper plates which, in turn, are attached to an adjustable copper plate by two (or three) 1/2-inch copper rods. This kind of mechanical adjustment will be necessary, also, for the x-ray target anode assembly and the electron trap. By making proper adjustments to this plate, the direction of the electron beam will be aimed toward the x-ray target anode. This plate, in turn, is attached to the 8-inch (O.D.) conflat flange which has the feedthroughs for high voltage, focus coil current and cooling water. The cooled copper vacuum shroud is necessary to shield the source housing from the heat generated by the electron gun, during long operating periods.

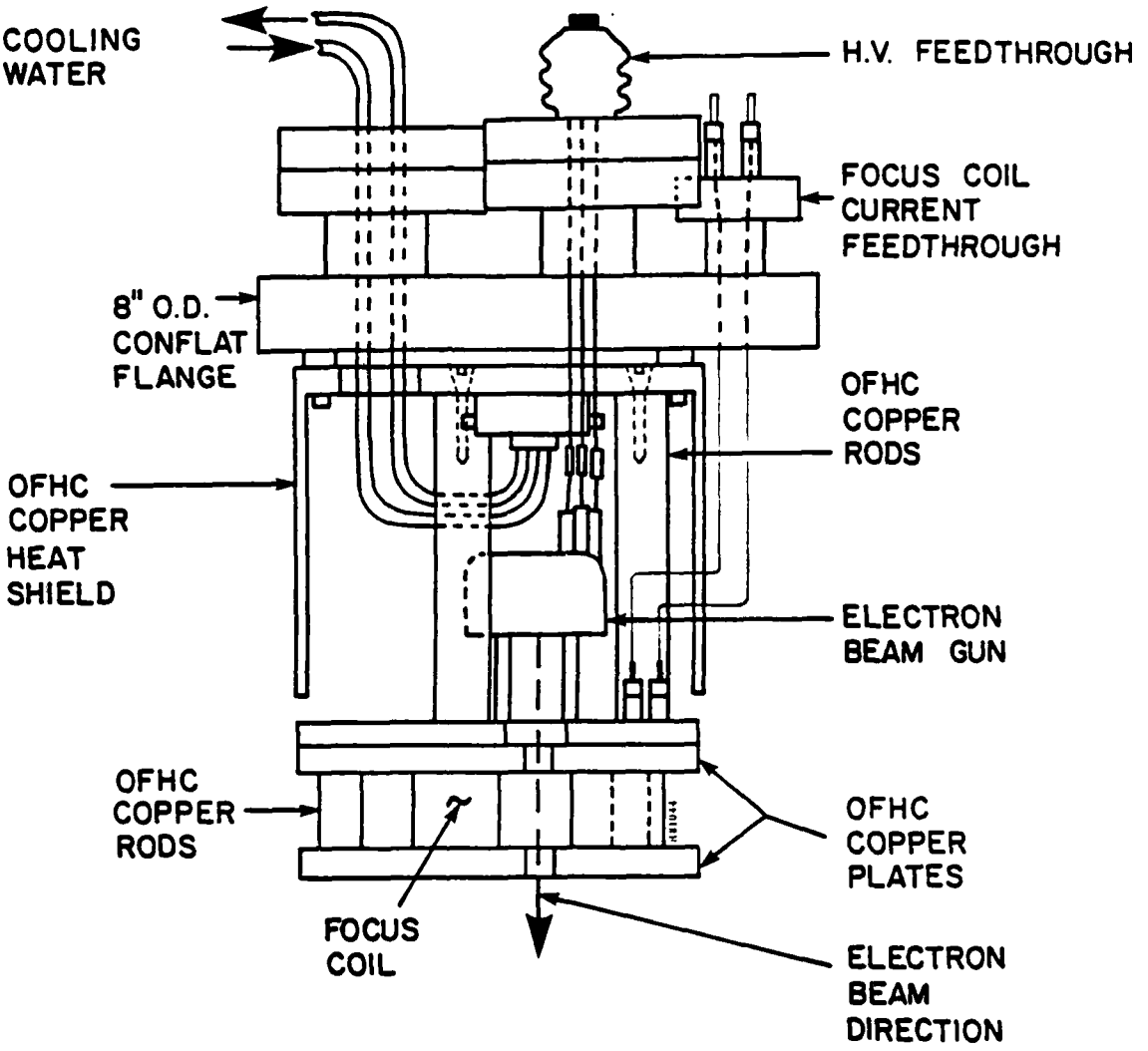

FIGURE 2. SCHEMATIC SKETCH OF ELECTRON BEAM GUN MOUNT WITHIN VACUUM CHAMBER (not to scale).

2.2.3 Focus Coil Adaptation

The focus coil, as supplied by Nuclide Corporation, was adapted for use in an UHV environment. The least costly way to adapt this coil for a UHV environment was to encapsulate it in a welded, vacuum-tight steel canister. Vacuum feedthroughs were used to bring the coil leads out of the canister. Since up to 20 watts of electrical power can be fed to the focus coil during operation, cooling of the coil is necessary. This is accomplished by placing the canister between copper plates which are water cooled through the 1/2-inch copper support rods. There are no demountable waterline connections within the electron gun mounting configuration. The coil itself is potted within the canister under vacuum to insure a long service life and to promote heat conduction from the coil to the water-cooled copper plates.

2.3 X-Ray Target Anode Assembly

Since the program calls for a variety of x-ray energies, a means of changing the energies of the x-rays produced had to be devised. To provide the means to change the energy of the characteristic x-ray produced in this facility, a moveable anode assembly was designed as illustrated in Figure 3. The x-ray anode is a water-cooled, multiple target, designed for remote positioning in the electron beam. The main anode body will have a cross section approximately 1-inch square and 4-inches long. It will be bevelled at the end which faces the incident electron beam. Selected x-ray target materials, such as aluminum, silver, titanium and chromium will be deposited on the substrate at well specified locations.

Each of these target materials can be brought into alignment with the electron beam by moving the anode linearly in or out of the chamber as permitted by the linear motion feedthrough arrangement. A long welded metal type bellows provides about 5 inches of linear movement. The motion feedthrough is designed to provide small amounts of lateral and tilting adjustment similar to the kind of adjustments for the electron beam gun.

When the bevelled end of the anode body is brought into alignment with the electron beam, the spot formed by the beam can be viewed through a 1-1/2-inch diameter viewing window placed in the vacuum port opposite the anode port. Beam focussing can be accomplished with the anode in this position. The anode may be also fully retracted from the beam so that the electron beam strikes a Faraday cup collector fixed in the beam line behind the anode.

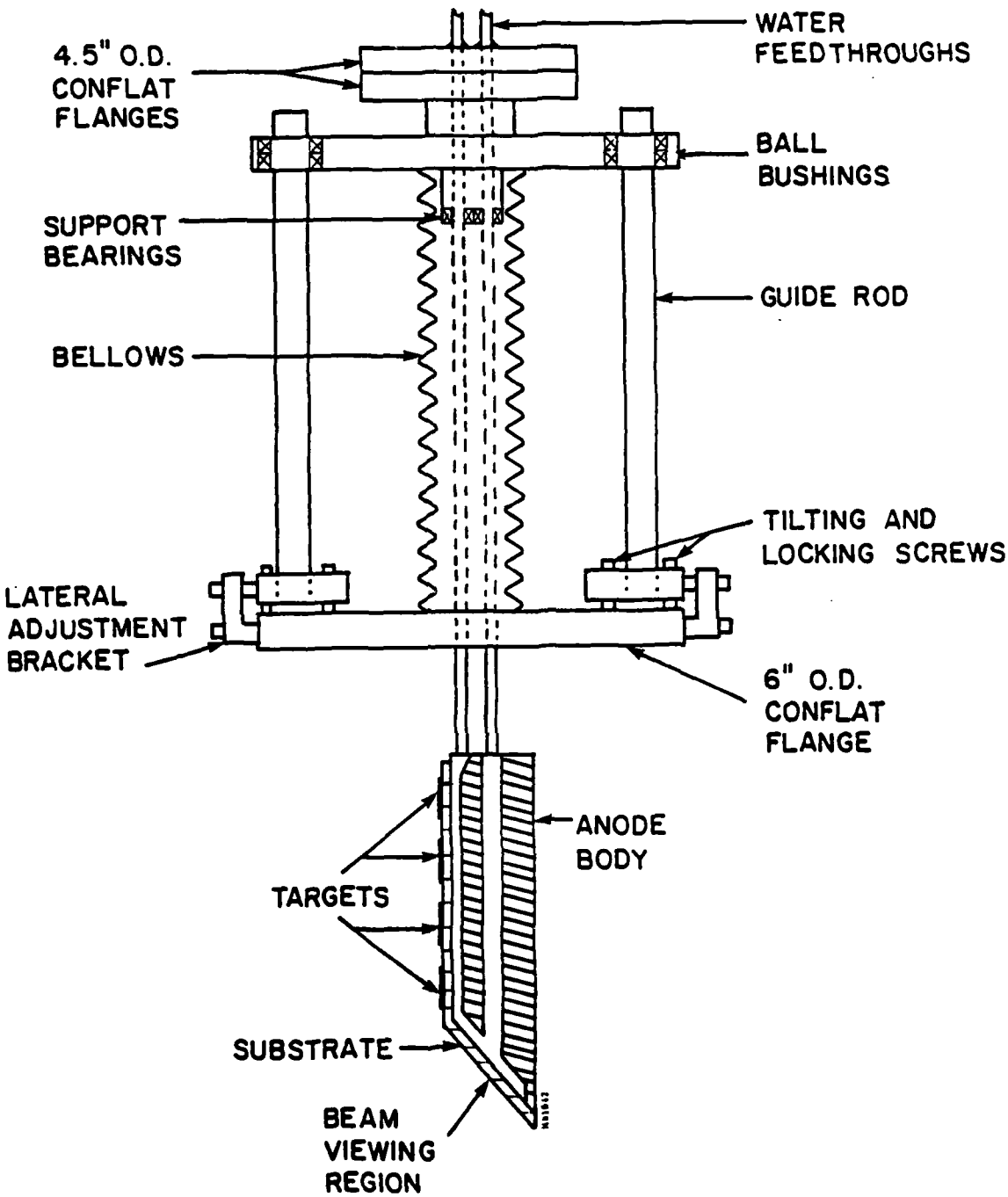

FIGURE 3. SCHEMATIC SKETCH OF X-RAY TARGET ANODE ASSEMBLY. (To change an x-ray target element, the anode assembly manually moved externally to align a new target element in the electron beam.)

Water cooling of the anode target is necessary to allow as much electron beam power on target as possible before melting occurs. The maximum power is 750 watts (15 keV, 50 mA). Because of the high water flow rate anticipated, a closed circulating distilled water system will probably be needed to insure trouble-free water cooling of the anode body.

2.4 Residual Gas Analyzer (RGA) and Viewing Window

An important component of the vacuum system will be an RGA mounted to the vacuum port opposite the x-ray anode assembly port (see Figure 1). The RGA will be a commercial quadropole mass spectrometer and will extend into the 4-inch housing tabulation a small distance. Mounted alongside the RGA on the 6-inch (O.D.) conflat flange will be a 1-1/2-inch diameter viewing window. This window is mounted within a 2-3/4-inch conflat flange and small tubulation to provide a direct view of the anode assembly. The electron beam spot should be visible when the anode body is placed so that the beam strikes the bevelled end of the anode body.

2.5 Faraday Cup Electron Beam Monitor and Electron Trap

The engineering assembly drawing for the Faraday cup monitor and electron trap is shown in Figure 4. The monitor has a deep cup (2 3/4 inches) and a suppressor electrode to capture all the incident electrons. This design should ensure a true measurement of the electron beam current. The enclosure is grounded, and the current measuring lead is shielded electrostatically to reduce noise and pickup from the nearby high voltage leads. The Faraday cup, fixed to a solid boron nitride base, also forms the support for the electron trap.

The electron trap is a parallelopiped with four copper sides and two graphite collimators. A high voltage lead (with the same potential as the accelerating voltage) passes through one of the copper walls to form an electrostatic field transverse to the x-ray beam. The choice of graphite for the collimator material has been made initially on the basis of low cost.

Figure 5 is a schematic illustration of the electron trap. When the anode body is pulled out of the way, the electron beam is incident upon the Faraday cup. When the anode is in a selected position, x-rays are generated in, and electrons are scattered from

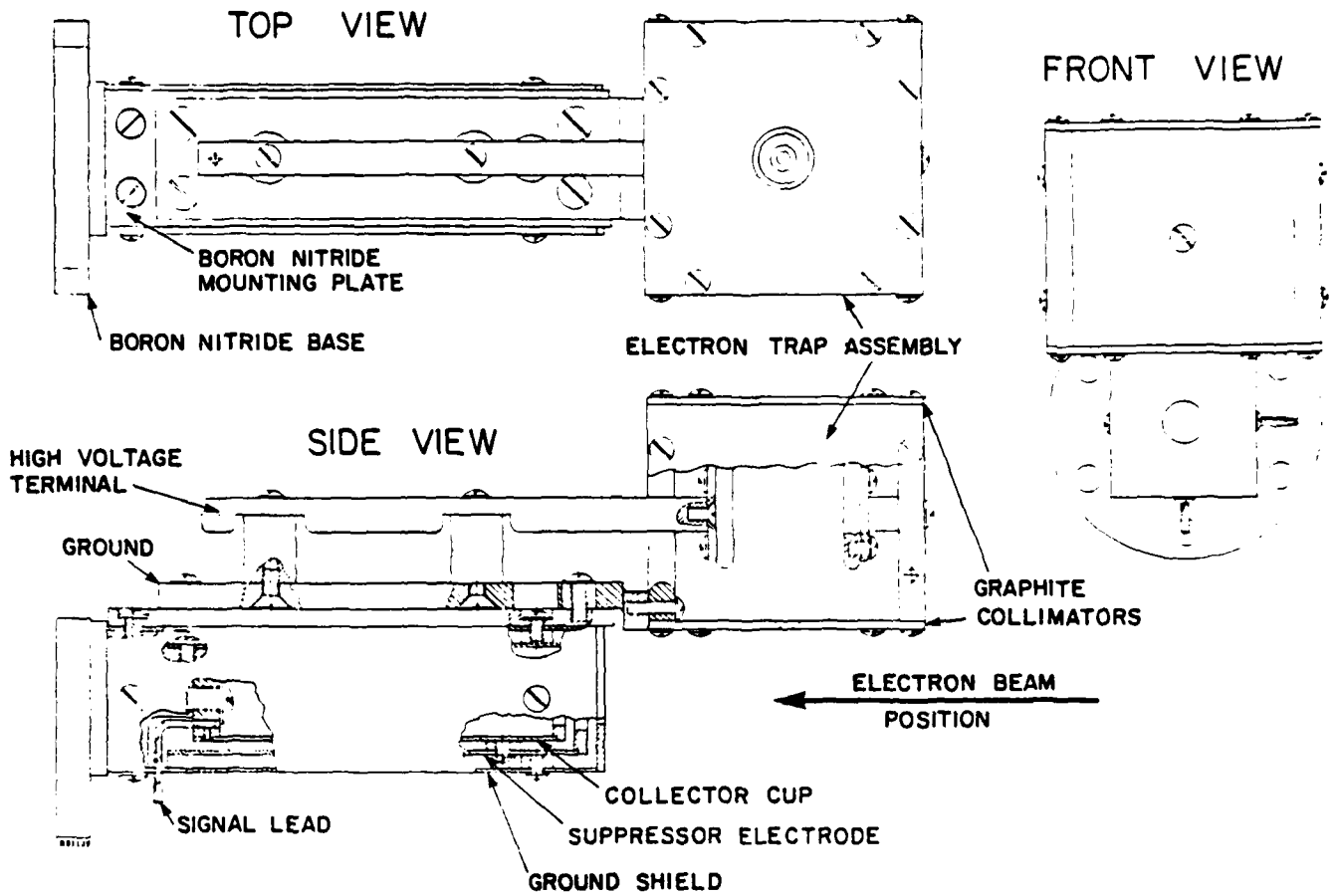

FIGURE 4. FULL SIZE ASSEMBLY DRAWING OF FARADAY CUP AND ELECTRON TRAP. (The collector cup, suppressor electrode and ground shield are all made with molybdenum sheet stock. Boron nitride was chosen for the insulator material due to its low outgassing characteristics.)

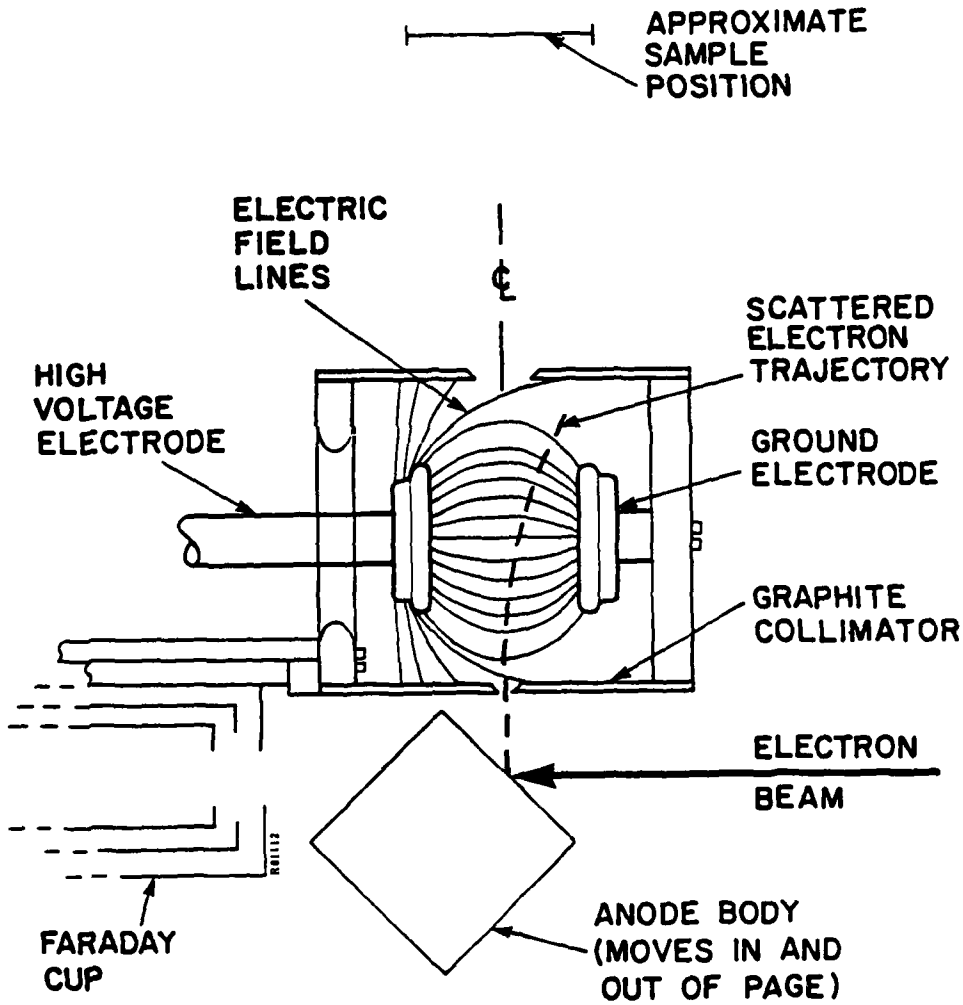

FIGURE 5. SCHEMATIC VIEW OF ELECTRON TRAP. (The electric field lines are approximate, and are drawn to illustrate the effect of the trap on a scattered electron. The collimator holes have been designed to produce a 3/4-inch diameter beam at the sample position.)

one of the anode targets. The lower graphite collimator allows a certain fraction of these x-rays and electrons to enter the electron trap. The high voltage and ground electrode form a transverse electric field to sweep the electrons out of the beam of x-rays. An estimate for the transverse distance which these electrons are moved by such a field is as follows:

Let d_T = fixed distance between electrodes

V_T = voltage drop between electrodes

E_T = V_T/d_T = transverse electric field

qE_T = transverse force on electron

qVs = energy of scattered electron

S_T = transverse length electron travels due to qE_T

Δt = transit time of electron to pass through the electrode region

Then: $$S_T = \frac{1}{2} \frac{qe_T}{m} (\Delta t)^2 = \frac{1}{2} \frac{qV_T}{md_T} (\Delta t)^2$$

and $$\Delta t = \frac{d_T}{(\frac{2qVs}{m})} 1/2$$

Hence: $$S_T = \left(\frac{V_T}{4Vs}\right) d_T$$

If the scattered electron has its original energy, and the potential applied to the electron trap is the accelerating voltage of the electron gun, then V_T = Vs and $S_T = d_T/4$. For the present design, d_T = 0.8 inches, so that S_T = 0.2 inches. The parabolic curve drawn in Figure 5 illustrates this amount of transverse movement by a scattered electron entering the electron trap along the center line.

One could imagine a scattered electron which experiences a second scatter event at the collimator orifice, and leaves that scatter site heading in the direction of the high voltage electrode. The transverse electric field may deflect this electron, depending upon its kinetic energy, so that it exits the trap through the upper orifice. However, its trajectory would not be collinear with the center line and, because of the distance to the sample, there would be little chance of it striking the sample. Extra graphite baffles can be placed above the electron trap to capture escaping electrons if deemed necessary.

3.0 PRODUCTION OF X-RAYS

3.1 Estimated X-Ray Irradiance and PMMA Exposure Times

From Green and Cosslett's paper,[1] the x-ray radiation yield, generated by an electron beam impinging upon a solid thick target, is:

$$N_x = G\,(E_o - E_x)^n \quad \text{(quanta/electron)}$$

where:

N_x = yield of x-rays per incident electron

G = generation efficiency factor

E_o = shell ionization energy (keV)

E_x = incident electron energy (keV)

n = 1.63 (a constant)

For K_α and L_α characteristic lines, curve fitting of Green and Cosslett's data produced the relation:

$$G_{K\alpha} = 3.2 \times 10^{-4} \exp(-Z/10.92) \quad \text{(quanta/electron)}$$

$$G_{L\alpha} = 8.5 \times 10^{-5} \exp(-Z/32.0) \quad \text{(quanta/electron)}$$

The irradiance of a given target irradiated with 15 keV electrons is given by

$$I_s = \frac{N_x}{4\pi} \text{Eph } (5.6 \times 10^4) \quad (\frac{\mu W}{Sr-W})$$

where:

Eph = characteristic photon energy in keV.

The irradiance, I_s, for five different target elements is tabulated in Table 1.

TABLE 1. X-RAY SOURCE IRRADIATION AND PMMA IRRADIATION TIMES

Target element	Eph (keV)	$G_{K\alpha}$ or $GL\alpha$	Yield (#ph/e)	I_s (μW/Sr-W)	X-Ray power on resist ($\mu W/cm^2$)	PMMA incident sensitivity (J/cm^2)	PMMA irrad. time (minutes)
Pd	2.84	2.0×10^{-5}	1.1×10^{-3}	15.9	71.6	3.65	850
Si	1.74	8.9×10^{-5}	5.9×10^{-3}	54.2	243.0	0.92	63
Al	1.49	9.7×10^{-5}	6.7×10^{-3}	52.6	237.0	0.59	41
Cu	0.93	3.4×10^{-5}	2.5×10^{-3}	12.2	54.9	0.16	49
C	0.28	1.8×10^{-4}	1.5×10^{-2}	21.8	98.1	0.12	21

If a 10 cm x-ray source-to-resist distance is assumed with 450 watts of electron beam power on the anode target, then the estimated x-ray power fluences on resist targets can be calculated. To estimate the time required to fully irradiate PMMA to a dose of 575 J cm^{-3}, the absorption coefficient curve for PMMA is required. This is plotted in Figure 6, the x-ray wavelengths noted for five elements. The major absorption edge in PMMA is, of course, the 284 eV $K\alpha$ edge of carbon. The PMMA sensitivity to a given x-ray energy is determined by dividing 575 J cm^{-3} by the appropriate absorption coefficient for that energy. With the x-ray power fluence on the resist and the sensitivity of the resist known, the required irradiation time using each target element can be calculated.

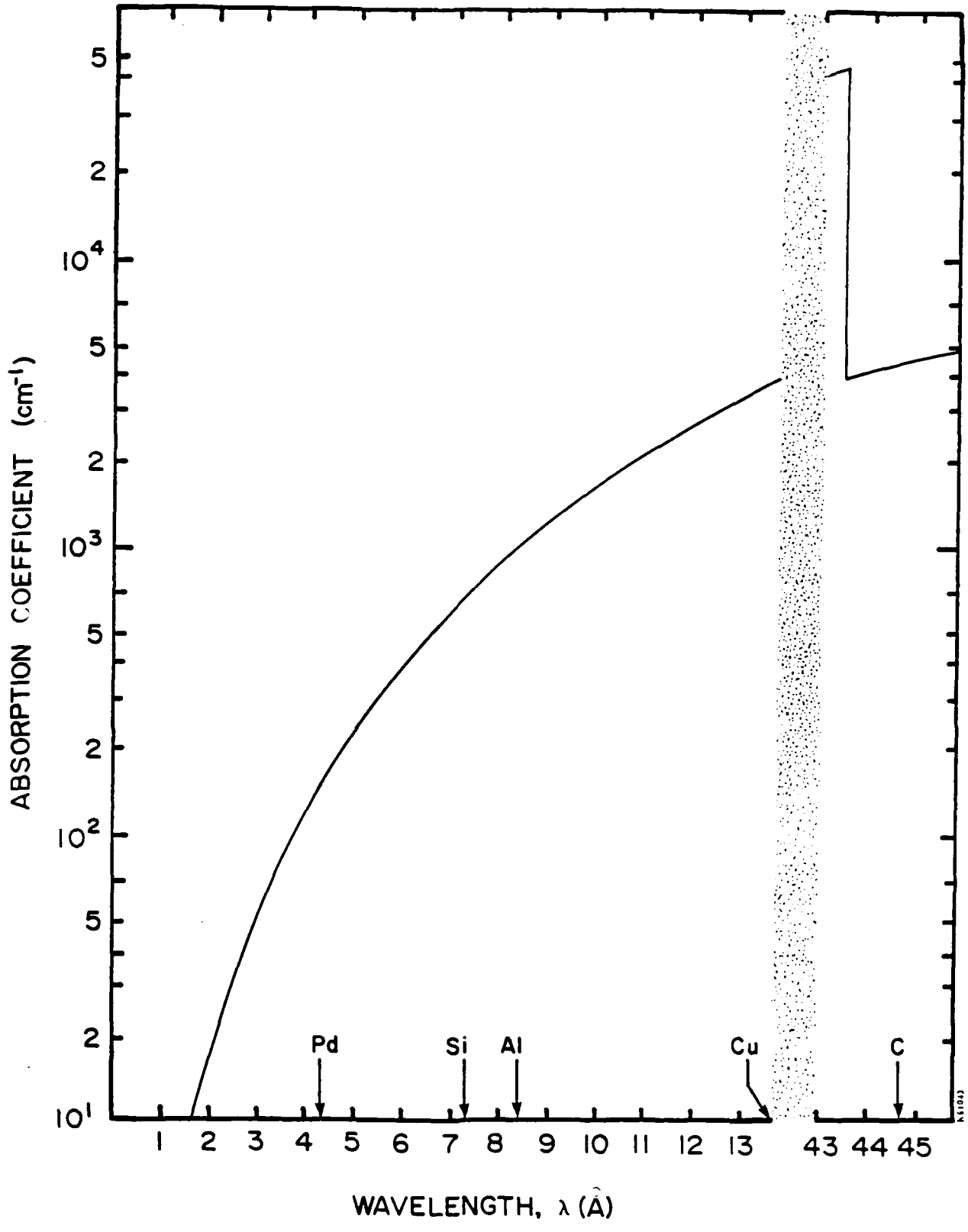

FIGURE 6. X-RAY ABSORPTION COEFFICIENT FOR POLY(METHYL METHACRYLATE), $H_8C_5O_2$ PMMA.

3.2 Experimental Check of Calculation

To check the calculations performed using the Green and Cosslett empirical formulation,[1] the results can be compared directly to experimental data for Al with the x-ray lithography facility built for the U. S. Air Force by Hughes Research. Sullivan[2] measured the x-ray yield for an Al anode bombarded with 7 keV electrons using PMMA resist as a detector. The comparison is as follows:

	Sullivan (7 kV)	Spire (15 kV)
Yield (#ph/e)	1.53×10^{-3}	6.7×10^{-3}
Irradiance (μW/Sr-W)	12.9*	52.6

Using the Green and Cosslett formula for x-ray yield, the two yields listed above were calculated. The ratio 6.7/1.53 = 4.37, when multiplied by the measured irradiance of 12.9 μW/Sr-W, gives 56.3 μW/Sr-W as the comparison estimated irradiance for 15 kV. The Spire estimate of 52.6 μW/Sr-W for the irradiance of Al bombarded with 15 keV electrons is at least consistent with Sullivan's data.

3.3 Dosimetry

To aid the calculational efforts required for this contract, a Fortran program called NRLXRF has been ordered from COSMIC (Computer Software Management & Information Center, University of Georgia). NRLXRF, developed by John W. Criss of NRL, was created to aid in the analysis of x-ray fluorescence spectrometry data. One of its uses will be to predict characteristic x-ray line and bremsstrahlung intensities for most elements located in targets of varied composition, thickness, homogeneity, etc. The program incorporates physical theory and numerical methods to perform calculations employing one or the other, or both as needed. Phillip Blais (Westinghouse Research Center, Pittsburgh, PA) highly recommends NRLXRF as he has used it extensively for his studies.

---

*Experimentally measured

4.0 INITIAL MEASUREMENTS USING A RESIST MATERIAL

4.1 Electron Beam Evaporator

To produce low energy x-rays for the purpose of measuring dose profiles near high Z/low Z material interfaces, an electron beam evaporator unit is well suited. A Sloan E-beam evaporator unit, which is available for this work, has a 10 keV electron beam. The beam is deflected 270^{o} before striking a water cooled solid metal target. This configuration is illustrated in Figure 7.

4.2 Photoresist Materials as Dosimeters

A number of resists could be used as x-ray dosimeters. All are hydrocarbon-based materials which have the same kind of x-ray energy absorption (see Figure 6). The detector chosen for these experiments will be a positive electron beam resist called PBS (Poly(butene-1 sulfone))[3]. This resist was chosen because of its high sulfur content which enhances its sensitivity to Ag L_{α} radiation. PBS, like other organic resists, behaves as:[4]

$$\chi = K D^{\beta}$$

where χ is the dissolution rate (nm/min), K and β are constants, and D is the dose (J/cm^3). Its behaviour over the dose range of 10-50 J/cm^2 is nearly linear as shown in Figure 8[5]. This implies that spatial variations in surface dose will result in initial etch rates which vary, above a threshold dose D_c of about 10 J/cm^3, nearly linearly with $D-D_c$.

It needs to be stated explicitly that such an x-ray dosimeter cannot be used in any absolute sense. Rather, its primary use would be as a working dosimeter to monitor dose from one experiment to the other. With an optimized, standard resist handling protocol (spinning, prebake, storage, irradiation, development), PBS can be a very useful x-ray dose monitor.

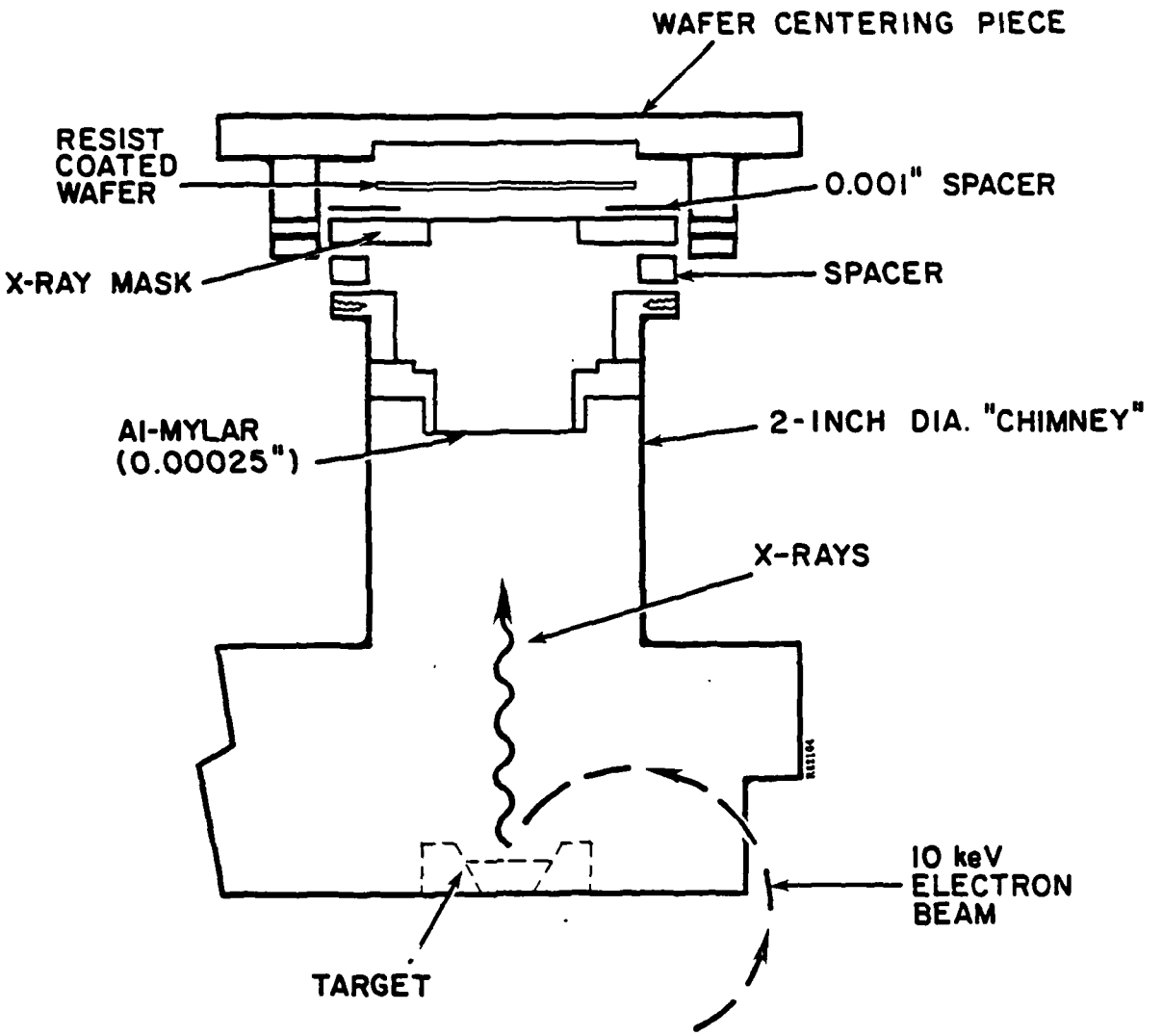

FIGURE 7. E-BEAM EVAPORATOR APPARATUS FOR X-RAY IRRADIATIONS.

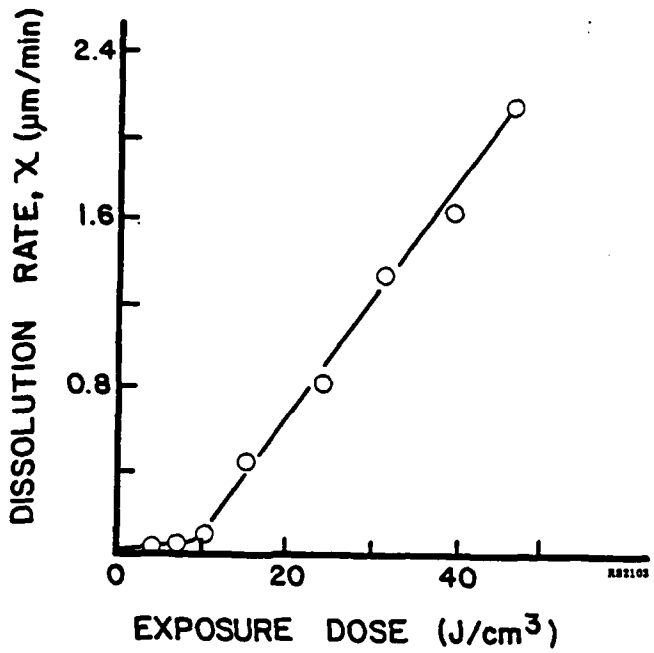

FIGURE 8. CHARACTERISTIC EXPOSURE CURVE FOR PBS USING Ag Lα RADIATION.

4.3 X-ray Irradiation of PBS

Figure 9 shows the x-ray absorption coefficient curve for PBS. The K-edge absorption peak shown is due to the sulphur in this material. Note that while the silver Ag L_α radiation is approximately twice the energy of the Al K_α irradiation, its absorption in PBS is about 60% of that for Al. The sulphur incorporated into PBS raises the sensitivity of the material for these higher energy x-rays by about a factor of 4.

Using the x-ray absorption coefficient curve (Figure 9) and the PBS characteristic exposure curve (Figure 8), the exposure times required to fully irradiate PBS at different x-ray energies can be calculated. Table 2 gives the pertinent data to calculate the estimated irradiation times. Note that the calculated exposure times are based on an assumed 200 W of electron beam power on the target and a target to resist layer distance of 15 cm. From these numbers it appears that Ni would not be a likely candidate for our planned experiments due to the large exposure time required. This time is due to two factors: 1) the relatively low energy of the incident electrons (10 keV) and, 2) the relative insensitivity of the PBS material to the Ni radiation. If the electron beam energy could be raised to 20 keV, then the K_α radiation for Ni would increase by a factor of 24, reducing the exposure time to 2.8 hours.

TABLE 2. X-RAY IRRADIATION OF PBS DATA

Element	X-ray energy (keV)	E (keV)	G (10^{-5})	Yield (ph/e$^-$) (10^{-4})	X-ray power (μW/Sr-W)	Power* at resist (μW/cm^2)	PBS** sens (mJ/cm^2)	Exp time (min)
Al	1.49	1.56	9.7	3.1	24.2	20.8	16.6	13.3
Pd	2.84	3.60	2.0	4.1	6.1	5.2	28.5	91.3
Ag	2.98	3.80	1.96	3.8	6.0	5.1	33.3	108.0
Ti	4.51	4.96	4.3	5.9	14.0	12.0	117.0	2.7h
Ni	7.47	8.33	2.5	0.58	2.3	1.98	500	69

*Power delivered to resist surface for a 200 W electron beam power level on target and a target-resist distance of 15 cm.

**Based on a sensitivity value of 20 J/cm^2 for PBS.

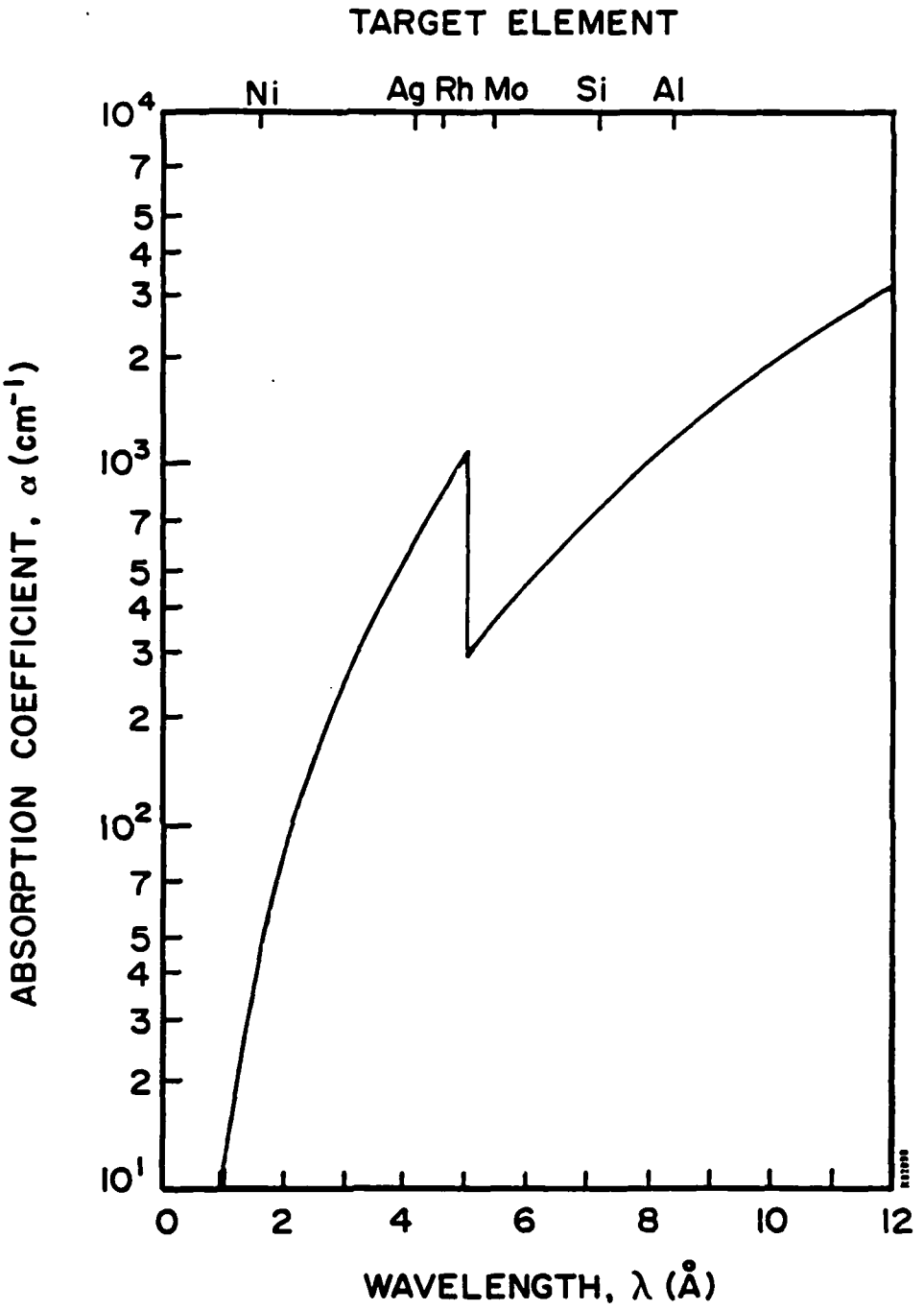

FIGURE 9. X-RAY ABSORPTION COEFFICIENT AND TRANSMISSION FOR POLY(BUTENE-1-SULFONE) RESIST.

4.4 Poly (Butene-1 Sulfone) (PBS) Resist as a Detector

Four ounces of this material with developer and rinse solutions were purchased from KTI Chemicals (Wallingford, CT). Since this material is proprietary (Bell Telephone Laboratories, Princeton, NJ), user information is sparse. Brian Murray traveled to Hunt Chemical (East Providence, RI) to work with Mr. Medhat Poukhey to learn how to best spin coat Si wafers with this material and to understand its development characteristics.

Since PBS is a non-viscous material with less than 4% solids, spin speeds during coating need to be kept fairly low if a thick layer is desired. It was found that the most uniform coatings were obtained by first flooding the wafer while stationary with resist material and then turning on the spinner with a ramp acceleration to reach its pre-set speed. Coating speeds of 1000 rpm, 1500 rpm, 2000 rpm, and 3000 rpm were tried. The 3000 rpm coated wafer appeared to be spotty and streaky in spots, due to a very thin layer of material. The pre-bake temperature used was 120°C for 30 minutes[5] After the pre-bake, a small scratch was made in the resist layer of each wafer so that Dektac thickness measurements could be done. Figure 10 illustrates the measurement data for the 1000 rpm and 3000 rpm cases. Since 1000 rpm on most wafer spinners is the minimum speed, resist thickness in the range of 3500 Å will be the thickest resist layer obtainable with this material. The application of a second layer over the first layer was attempted, but little was added to the thickness of resist on the wafer. This was probably due to the fact that the resist solvents dissolved the first layer during the spin coating of the second layer.

4.5 Experiments with An X-ray Mask

A mask, with the Air Force 1951 pattern, was kindly given to us by Mr. Phillip Blais from Westinghouse Research Center, (Pittsburg, PA). Its substrate is 6 microns of polyimide and the high Z absorber is gold with a thickness of 6000 Å. Figure 7 illustrates the experimental apparatus used to obtain the x-ray mask patterns on a PBS coated wafer. A 0.001 inch thick Mylar spacer was placed between the wafer and the mask. The 0.00025 inch thick aluminized Mylar is used to absorb electrons which scatter from the target and to help reflect the infrared radiation that is generated from the target itself.

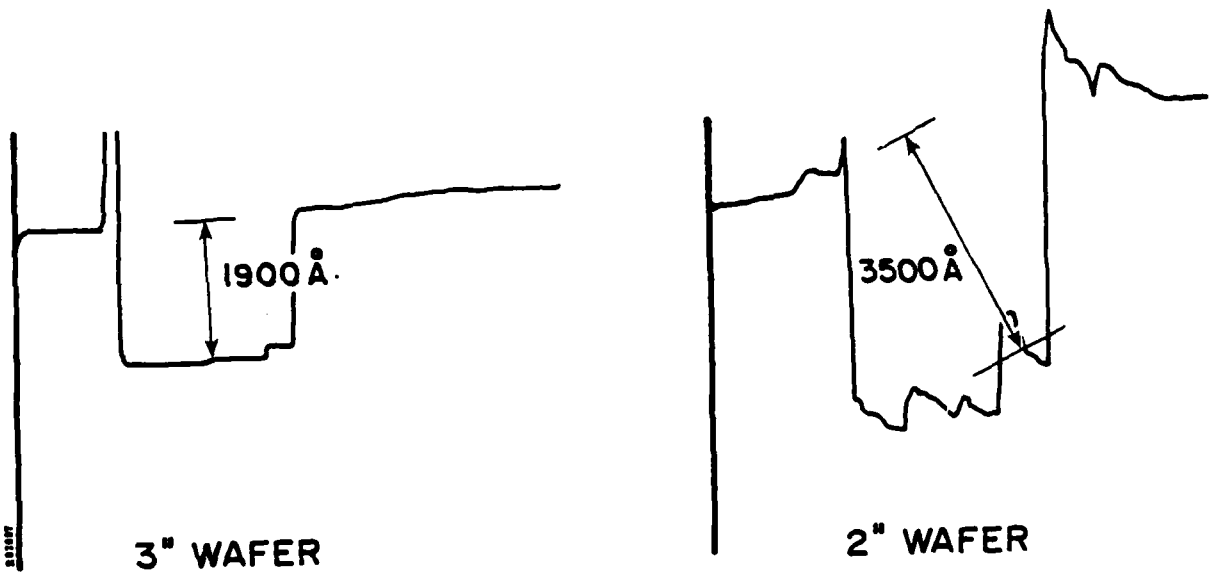

FIGURE 10. DEKTAK THICKNESS MEASUREMENTS OF PBS SPUN COATINGS ON Si WAFERS. (Spun at 3000 rpm (left) and at 1000 rpm (right)).

The two targets used for the initial experiments were Al and Ag. By experimentation it was determined that 80 mA of electron beam could fall on the Ag target before melting occurred and about 40 mA could be used for the Al target. This means that the electron beam power on target for Ag is about 800 watts and for Al about 400 watts. However, the Al-Mylar electron/heat shield does absorb some x-rays, so that taking the irradiation time in Table 1 and dividing by the appropriate electron beam power factor does not take into account the absorption in this shield material. As a result of this, it was decided to use a 45 minute irradiation for the Ag target and a 10 minute irradiation time for the Al target.

Figure 11 illustrates a masked pattern developed on a PBS coated Si wafer. The wafer was coated with a 2700 Å thick layer of PBS. The development time was 20 seconds. Regions of the resist which were not under the gold absorbor were completely removed in this 20 second development time. The pattern seen in Figure 11 is the gold absorber pattern on the mask. It appears that some overdevelopment did take place as these resist regions appear somewhat speckled.

5.0 DOSE PROFILE MEASUREMENTS USING PBS RESIST

5.1 Rationale for Experimental Approach

The rationale for the experiments performed may be described as follows. By using Au as the high Z material, a measurement of the dose profile (produced by soft x-rays) in a low Z material adjacent to the Au can be carried out using various thicknesses of low Z absorbers. If the dosimeter material (PBS) is placed adjacent to the low Z absorbing layers, various dose levels will result in the dosimeter according to the absorber thickness. In this way, dose levels varying with low Z absorber thicknesses are determined and, as a result, a dose profile is measured.

Ideally, if PBS is the dosimeter, the low Z absorbing layers on the Au should be PBS as well. However, since thicknesses of the order of 100 Å are anticipated for the determination of a dose profile, carbon is a more practical first choice for the low Z absorbing material. Dose profiles can be found for the material configuration Au:C:PBS. To a first approximation, carbon and PBS are considered as a single material.

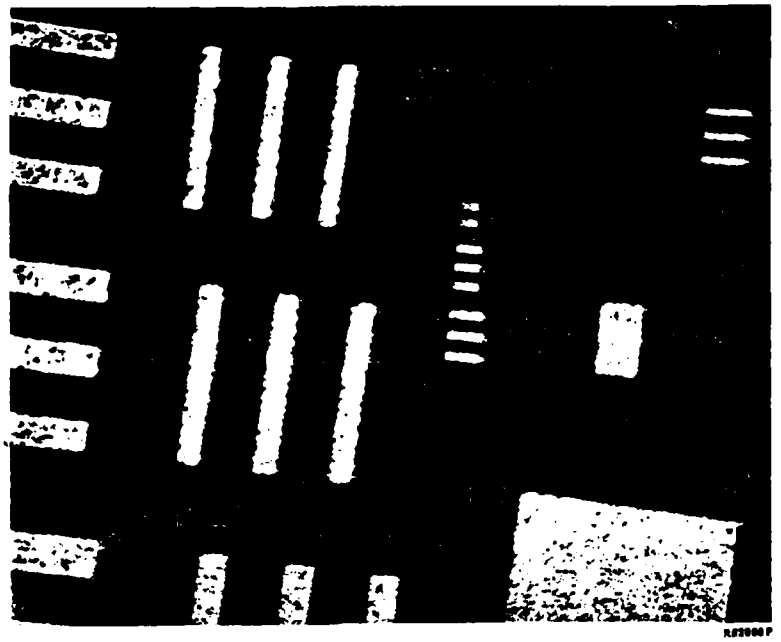

FIGURE 11. DEVELOPED X-RAY MASK PATTERN USING PBS. (The smallest bar length is shown about 10 microns. The dark regions are bare Si substrate.)

5.2 High Z/Low Z X-ray Masks

To make appropriate material interfaces for these experiments, very thin material layers are required. A convenient substrate material is 2.5 micron thick mylar suspended on a 1-inch diameter circular frame. This object is called a pellicle and is available from the National Photocolor Corporation (Mamaroneck, NY). A layer of Au is first evaporated onto the mylar to a preselected thickness. Carbon, is then evaporated onto different regions of the Au layer to various thicknesses. Placing the detector material, PBS resist, which has been spun as a thin film onto a silicon wafer, next to the Au/C interface then completes the experimental configuration. Some regions of the PBS will be next to the mylar only, some regions next to the gold only, and a number of regions next to the variously thick layers of carbon. Figure 12 illustrates the experimental configuration for these studies.

5.2.1 Metal Evaporation

Mr. Joe Lorenzo of Hanscom Air Force Base carried out the metal evaporations onto the mylar pellicles for these experiments. Three separate evaporation runs were performed, two for gold and one for silver. A crystal oscillator rate deposition monitor was used to measure the deposition rate of the gold or silver during each evaporation run. A glass slide, placed in the evaporator at the same distance from the evaporation source as the pellicle, served as an independent monitor of the metal thickness evaporated on the pellicle.

Figure 13 shows the Dektak measurements of the Au and C layers of the first mask used in these experiments. Figure 13 shows the measurement on a glass slide of the Au thickness (6800 Å) which was deposited on the mylar pellicle. In Figure 14, the Dektak measurements are shown for the deposited silver layer. The Ag evaporation was carried out in two separate runs because the silver charge in the evaporation boat ran out after 1500 Å was deposited. The chamber had to be opened up and a new silver charge placed in the boat. The figure shows two measured thicknesses, one of 1500 Å and the other of 2000 Å, measured on two separate glass slides. The sum is the Ag layer deposited on the pellicle surface. The third thickness measurement (Figure 14C) is that of the silver on the pellicle itself. This was done by placing the pellicle on a 1-inch diameter Si wafer supported by a machined Al support. The Dektak measurement on the pellicle surface

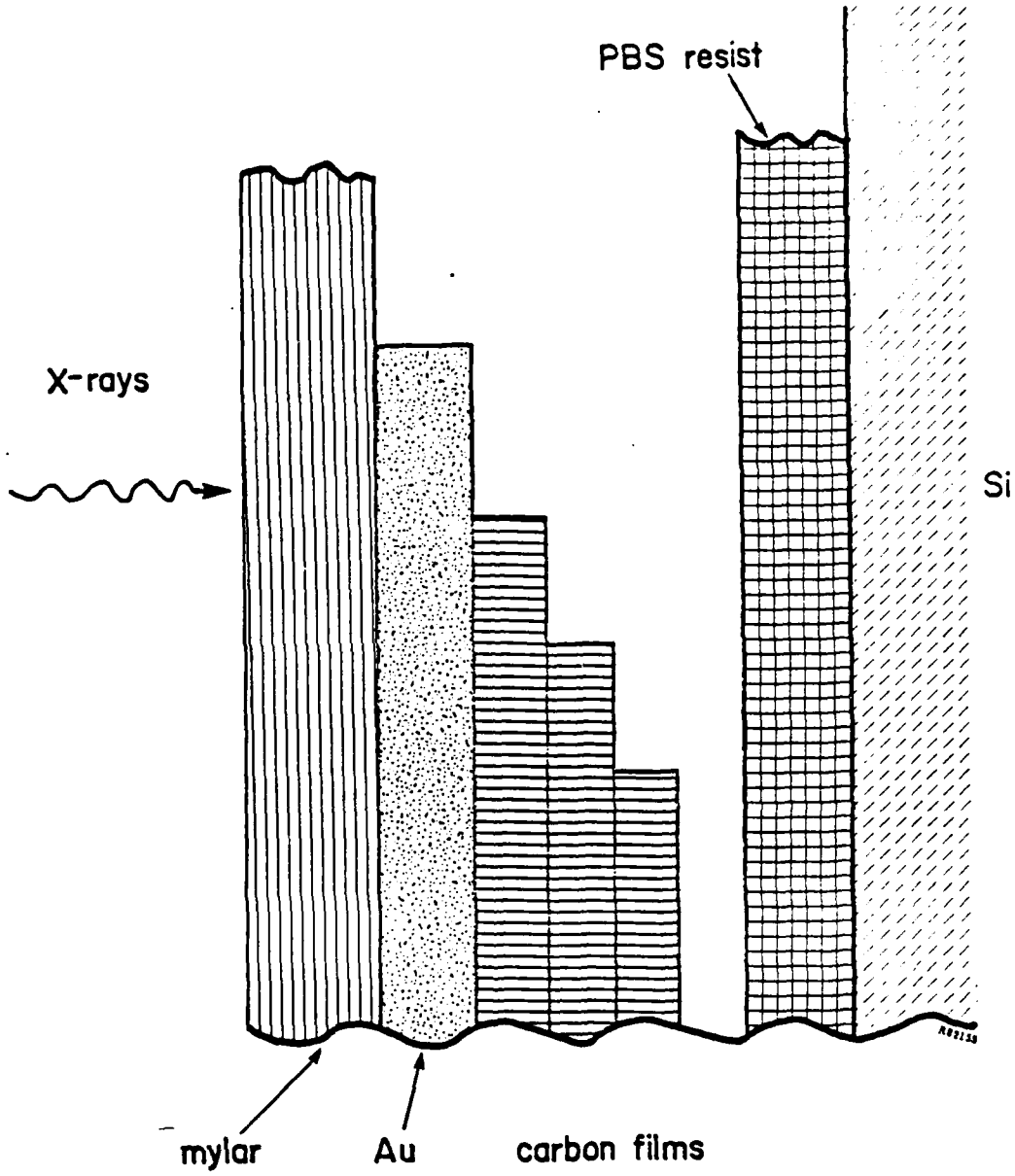

FIGURE 12. EXPERIMENTAL CONFIGURATION FOR MEASURING DOSE PROFILES NEAR Au/C INTERFACE.

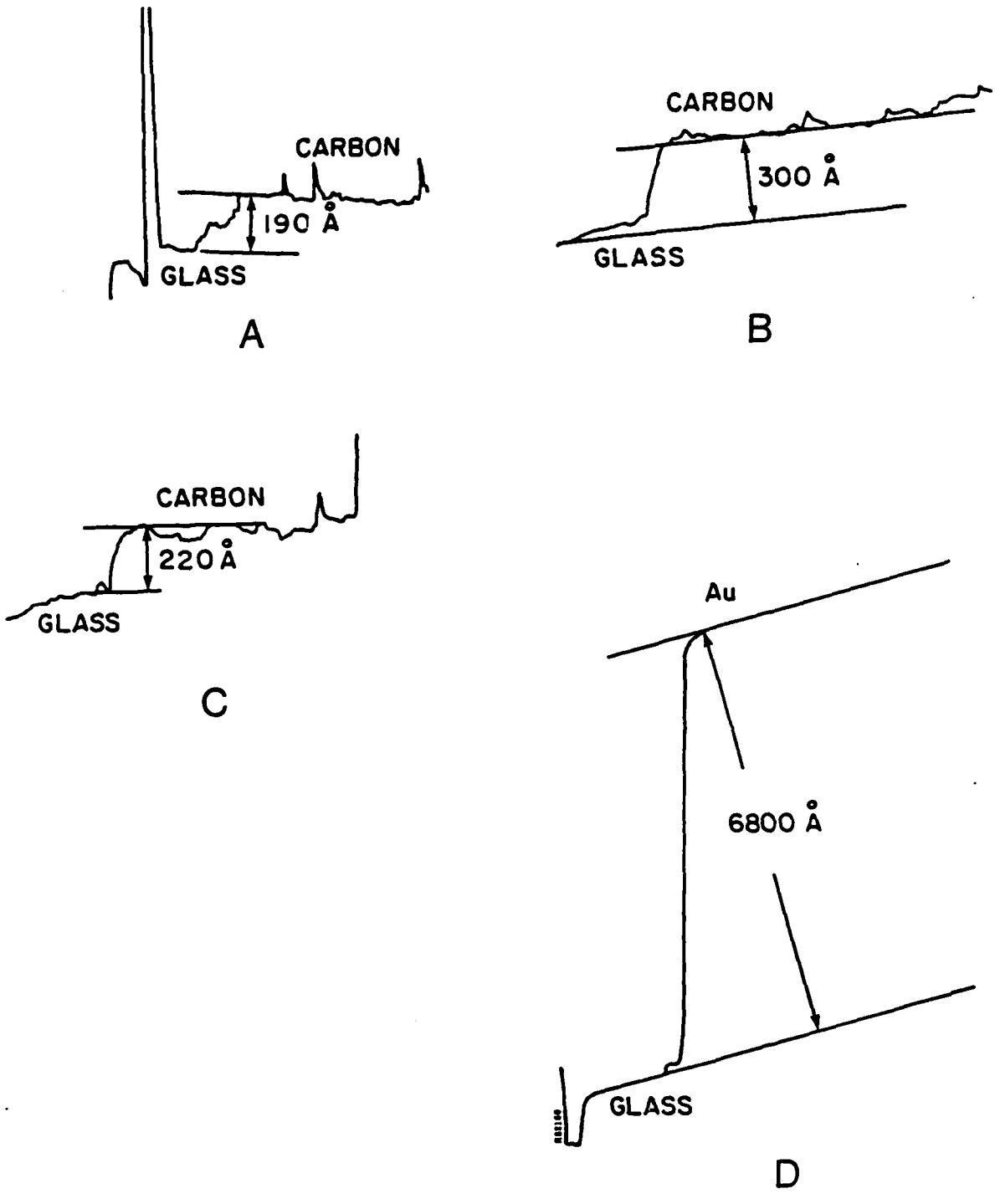

FIGURE 13. DEKTAK MEASUREMENTS ON GLASS OF CARBON AND Au LAYER THICKNESSES. (A, B and C are the three layers of carbon laid down on the Au absorber for the first Au/C mask used.)

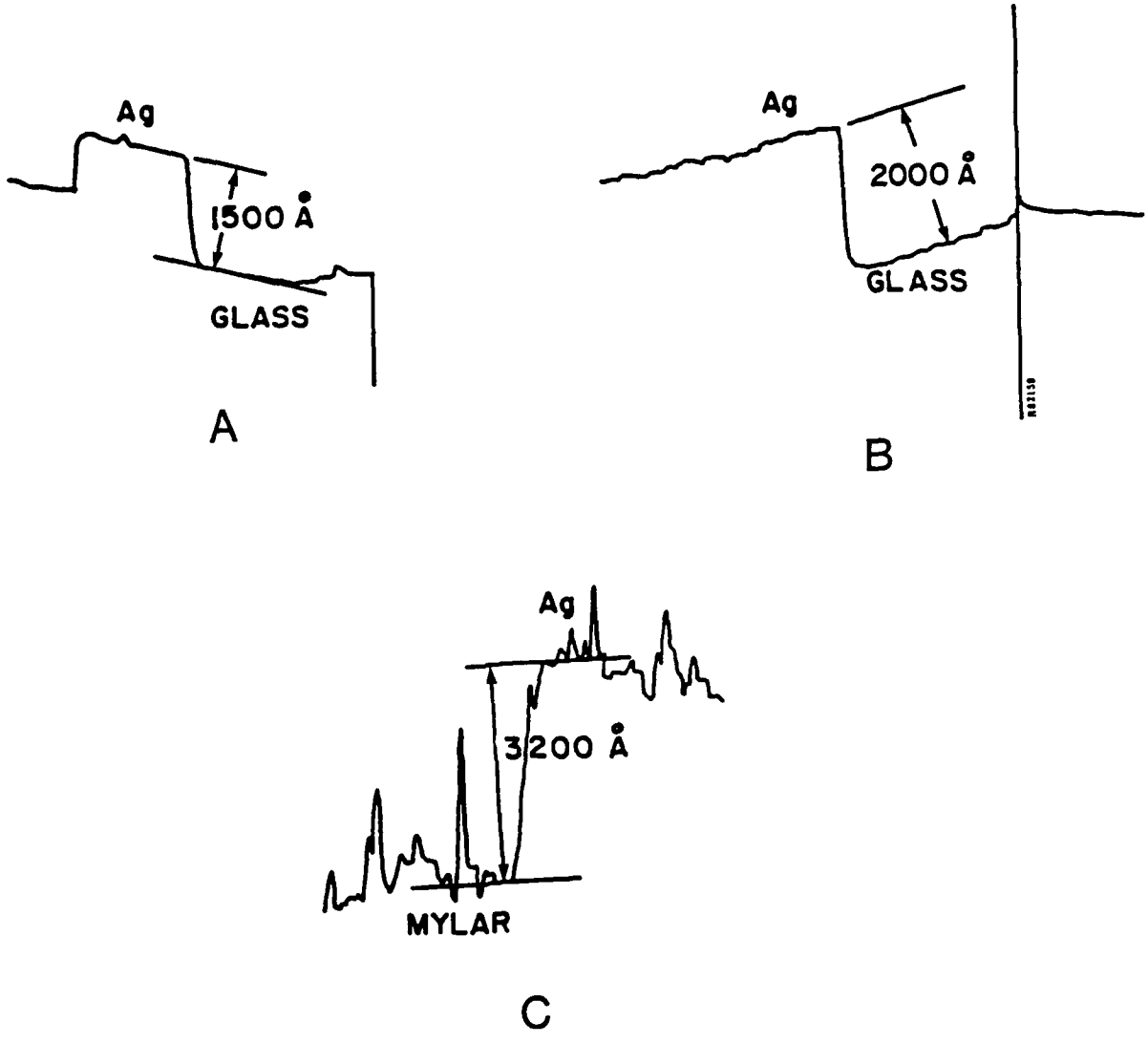

FIGURE 14. DEKTAK MEASUREMENTS OF THE Ag EVAPORATION ONTO MYLAR PELLICLE. (A and B are measurements of the evaporation monitor glass slides. C is a measurement of the total Ag thickness of the pellicle itself.)

showed a rough Ag surface. This roughness prevented a precise measurement of the carbon layers that were subsequently laid down on the silver surface.

5.2.2 Initial Carbon Deposition on X-ray Masks

Mr. Joe Comer of the Hanscom Air Force Base carried out the initial carbon deposition runs for this program. The apparatus consists of an evacuated bell jar, two pointed graphite rods in near proximity, the pellicle to be coated behind a mask, and two glass slides to monitor the deposited carbon thickness. Since no deposition rate monitor was available for the carbon coatings, an oil coated glass slide acted as a visual indicator for the thickness of carbon being deposited during a run. The 6800 Å gold coated pellicle was used for the first run. The vacuum in the evaporator unit was about 2×10^{-5} torr, pumped with a liquid nitrogen cold trapped diffusion pump. For each run, the carbon arc source which creates the deposited carbon lasted generally for three to five seconds.

5.2.3 Gold/Carbon Mask

Figure 13 shows the Dektak measurements made on the monitor glass slides for each carbon deposition run for the first Au/C mask. The three thicknesses were measured to be 190 Å, 300 Å and 220 Å. In an independent kind of measurement, Mr. Joe Comer determined the second carbon thickness using a stereomicrometer parallax measurement of electron micrographs. This is a rather delicate technique in which a carbon film is floated from a glass slide upon which it was originally deposited and coated on both sides with a very thin layer of gold. An electron micrograph is then taken using an electron microscope. The micrograph is then viewed with stereographic eyepieces. The result of this measurement is 313 $\pm$ 30 Å. This is in very good agreement with the Dektak measurement of Figure 13B.

In addition to the three carbon films laid down on the Au (Figure 13) there was also a small area of carbon (deposited next to the 220 Å thick area) which has a thickness of about 100 Å. The final parameters of this first experimental mask are listed in Table 3.

TABLE 3. X-RAY MASK PARAMETERS

Material	Thickness	Diameter
Mylar	2.5 microns	2.54 cm
Au	6800 Å	1.60 cm
C	100 Å	--
C	220 Å	1.35 cm
C	520 Å	1.1 cm
C	710 Å	0.65 cm

The complete mask is shown in the upper left of Figure 15. The "pac-man" configuration of carbon layers on the Au was meant to place bare Au next to each carbon layer thicknesses. All the C layers are not visible in this photograph. Figure 15A is a photomicrograph of this mask showing portions of the bare Au, the 100 Å and 510 Å carbon layers.

5.2.4 Silver/Carbon Mask

The carbon layer deposition on silver mask was performed using a different mask arrangement, one in which seven separate carbon depositions on the silver were carried out. The carbon layer configuration for the silver mask is also shown in Figure 4. Unfortunately, the glass slide monitor approach for this case was faulty. Basically, a single glass slide was used whereby only a small portion of the glass slide was exposed to the carbon deposition for each run so that a step wedge of carbon layering was established on the glass slide. However, Dektak measurements of this set of carbon layers gave inconsistent results so that the carbon thicknesses laid down on the silver mask cannot be adequately established. Attempts to measure the carbon layer thicknesses directly on the pellicle could not be done due to the severe roughness of the Ag and, presumably, the mylar as well. The photomicrograph in Figure 16B illustrates this roughness very well.

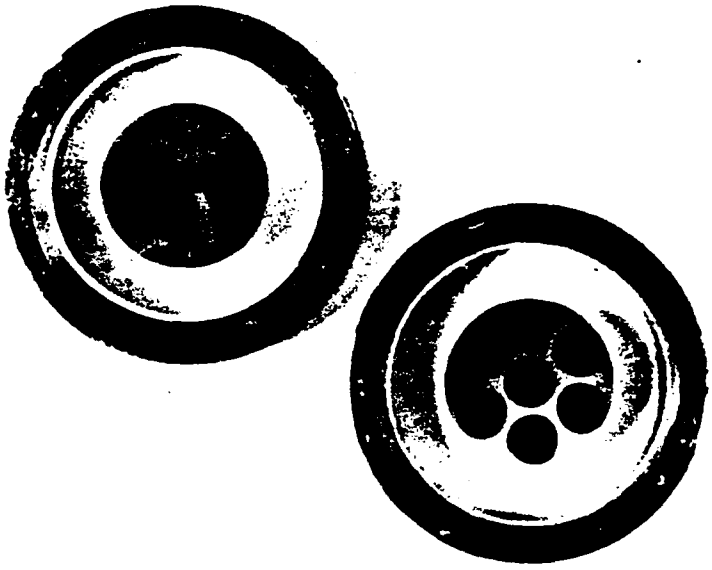

FIGURE 15. PHOTOGRAPH OF THE Au/C AND Ag/C X-RAY MASKS.

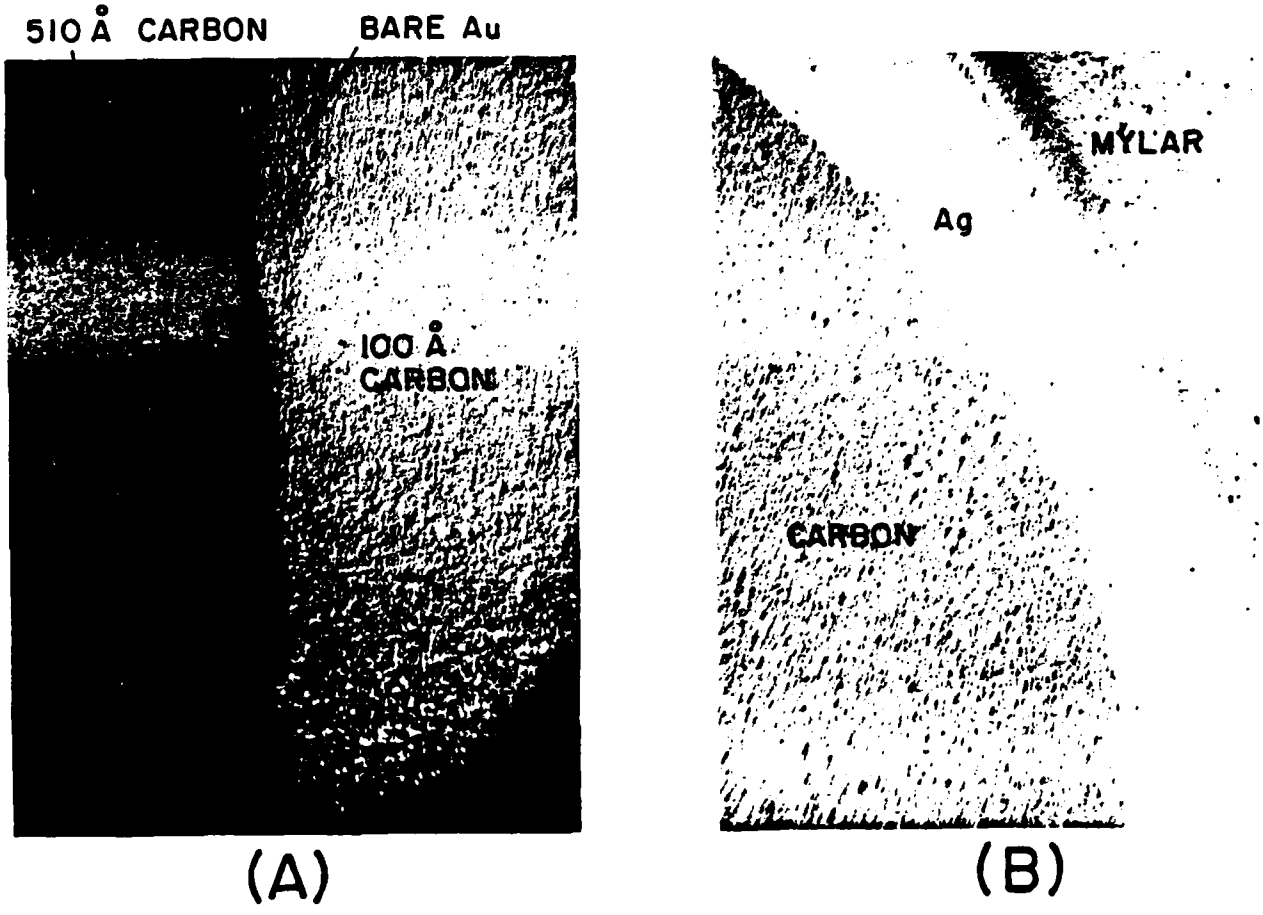

FIGURE 16. NOMARSKI (DIC) PHOTOMICROGRAPH OF SELECTED AREAS OF THE EXPERIMENTAL X-RAY MASKS: A - Au/C MASK AND B-Ag/C MASK.

5.2.5 Spinning of the PBS Resist on Silicon Wafers

The coating of PBS resist on cleaned silicon 2 inch diameter wafers generally resulted in coating thicknesses in the range of 2600-3500 Å. Low spin speeds of 1000 rpm are necessary to obtain this thickness of PBS coatings. A number of problems have been encountered in the PBS resist spinning. These include streaks and various other kinds of defects in the coating. It was thought that high humidity in the room in which the resist was being coated may be a factor in its poor coating performance. As a consequence, a number of wafers were coated in a humidity controlled environment. These coated wafers appeared to have significantly fewer defects than those coated at Spire Corporation and were subsequently used for experiments.

5.2.6 X-Ray Irradiations

The Sloan multi-target, electron beam evaporator unit was again used as the x-ray source for these experiments. The apparatus to hold the wafer and mask is basically the same as sketched in Figure 7. For these experiments, the mask pellicle is placed facing upward at a distance of 15 cm from the x-ray target. A coated wafer is laid down on top of the pellicle and makes surface contact with the carbon and gold (silver) of the mask.

Three different characteristic x-ray sources are used with characteristic energies of 1.49 keV, 2.98 keV, and 4.51 keV. However, for a complete evaluation of these experiments, the bremsstrahlung component for each x-ray source needs to be carefully considered.

For the three x-ray targets used, the maximum electron beam currents that did not result in any surface melting were 40 ma for Al, 80 ma for Ag and 10 ma for Ti. The low current for the Ti is due to its low specific heat and low thermal conductivity to the water cooled target support. The electron beam striking the target was not a circular spot but, rather, a broad line of approximately 1 cm x 1 mm. Since only one dimensional dose profiles are being measured in these experiments, the broad electron beam on the target was not considered a significant problem. The vacuum level during each radiation run was in the range of 2×10^{-6} torr. After each irradiation, the apparatus was allowed

to cool down before venting the chamber with nitrogen gas. Use of the Ag and Ti targets produced significant heating to the experimental apparatus above the target. For both, a mask pattern was easily observed on the coated wafer after irradiation and before development. This is probably due to the heat which was generated from the target and transmitted through the aluminized mylar heat shield and the mask to the resist on the wafer.

5.2.7 Resist Development

For each irradiated wafer, the same development procedure was employed. The wafer was placed in a 2 inch diameter wafer holder, placed in the developer solution for ten seconds, taken out and shaken off once, then placed in the rinse solution and softly agitated, for 60 seconds. After this, the wafer was gently blown dry with dry nitrogen gas. In all cases with the Au/C mask, a pattern was observed on each irradiated wafer.

6.0 INITIAL MEASUREMENTS AND RESULTS OF DOSE PROFILES

6.1. Ellipsometer Measurements

After the development of the exposed PBS-coated wafers, the dose data is contained within the thicknesses of each rather thin PBS layers. To measure such layers, an ellipsometer was used. The ellipsometer measurements were done using a Rudolph Research Auto EL III ellipsometer. The light source is an He:Ne laser with a wavelength of 6328 A. The basic equation of ellipsometry can be stated as

$$\rho = (\tan \Psi)\, e^{\,i\Delta}$$

where ρ is the ratio of the complex reflection coefficients of the incident and reflected light from the sample, $\tan \Psi$ is the ratio of the real to imaginary reflection coefficient magnitudes, and Δ is a difference in phase of the two beams.

Nulling ellipsometers, such as the Auto EL III, generally employ a polarizer, an analyzer, and a compensator, each of which is aligned along the axis in which it is located. The polarizer is located in the incident beam axis, the analyzer, in the reflected

beam axis and the compensator is located in the incident beam axis. A compensator is fixed at some azimuthal angle with respect to the plane of incidence while the other two components are rotatable automatically during the measurement period. The measurement consists of setting an angle of incidence, usually 70^{o}, with respect to the sample which is mounted with its surface at the intersection of two axis. The polarizer and analyzer are then rotated alternately until the intensity of the reflector beam is reduced to a minimum (as sensed by the photodetector). At that null condition, the angular azimuthal angle of the polarizer and the analyzer are determined. These two measured angles are directly convertible by simple linear equations into the polarization parameters Ψ and Δ. Once Ψ and Δ are determined, a simple computer program is used to determine the index of refraction and thickness of the transparent film on the silicon substrate. If the film is absorbing, however, it is not possible to determine uniquely the index of refraction and thickness from a single Ψ and Δ measurement with the presently available software from the manufacturer.

Figure 17 is a graphical representation of the Ψ and Δ that would be measured for transparent films of arbitrary thickness and refractive index on silicon substrate by the ellipsometer using a light source of wavelength 6328 Å and at an angle of incidence of 70 degrees. Each line in the family of closed curves is the locus of the Ψ and Δ produced by films of increasing thickness but constant refractive index. All curves of constant refractive index must go through a single point, the Ψ and Δ coordinates of the bare silicon substrate. Intuitively, this must be so, since Ψ and Δ for all film covered surfaces, must approach the Ψ and Δ of the substrate as the films get thinner and thinner. Similarly, as the films get thicker and approach the cycle thickness, the Ψ and Δ again must approach the Ψ and Δ coordinates of the bare substrates because, at the cycle thickness, the film/substrate system behaves as if no film is present. For the PBS resist, the index of refraction has been measured to be about 1.53, and this gives a cycle thickness of about 2620 Å. In measuring various resist thicknesses on silicon, therefore, one needs to know an approximate film thickness as the ellipsometer will only measure between 0 - 2620 Å, or 2620 Å - 5240 Å, and so on. As an experimental consideration, the

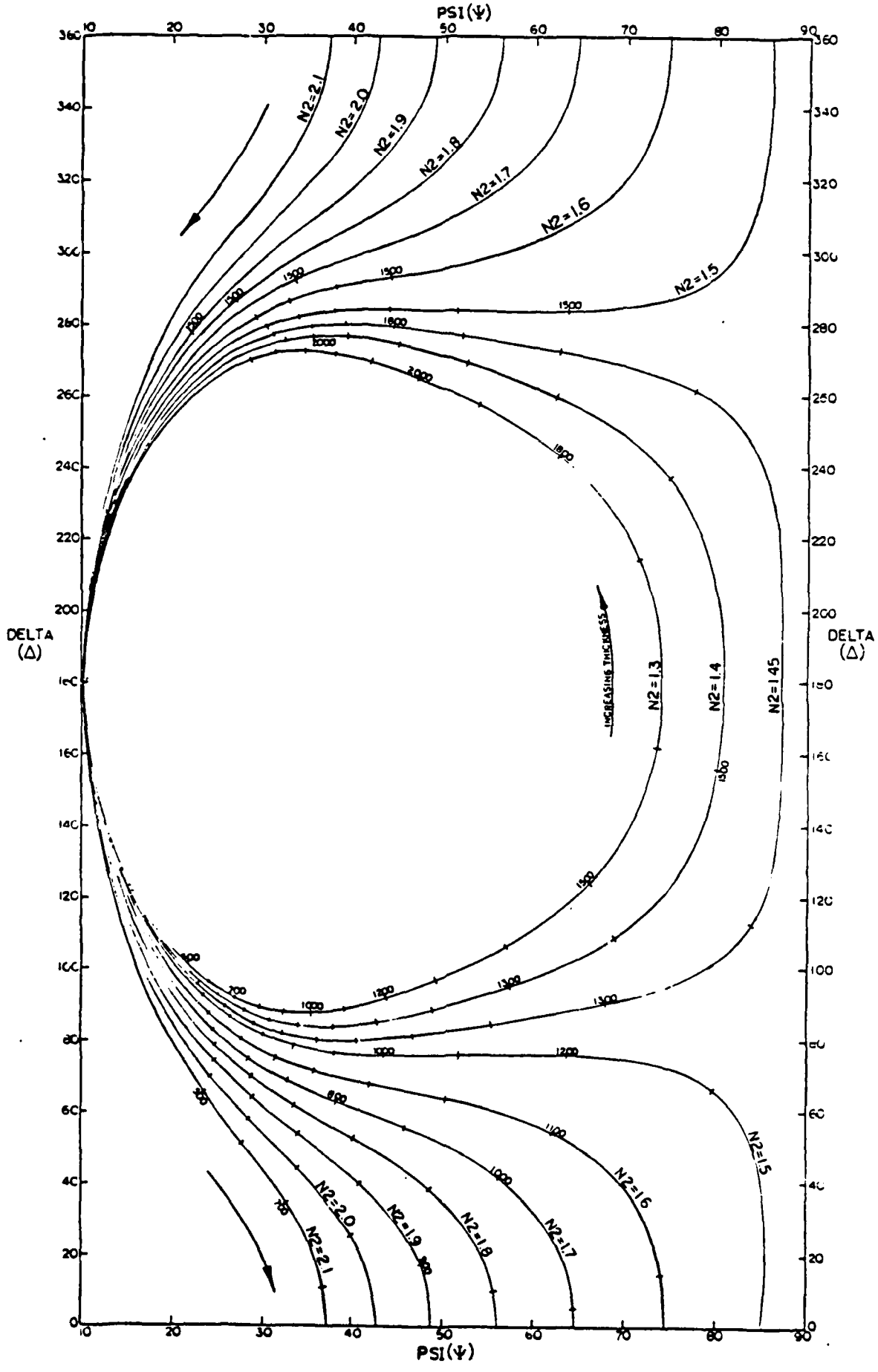

FIGURE 17. Ψ AND Δ VS. REFRACTIVE INDEX AND THICKNESS OF TRANSPARENT FILM ON SILICON SUBSTRATES. (Wavelength is 6328 Å.)

ideal resist thicknesses to be measured should vary between one-third and two-thirds the cycle thickness which, in the case of PBS resist, would be approximately 870 - 1740 Å. Very thin PBS resist films or those near the cycle thickness often lead to a null result in the measurement process.

6.2 Measurement Results

Typical ellipsometry data is illustrated in Table 4. The ellipsometer gives, for each reading, a value for Ψ, Δ, the index refraction, and the thickness of the film above the silicon substrate. The last column is the thickness difference between the unexposed resist region for each wafer and the various measured thicknesses. Plotting this column against the thickness of carbon in the first column will be a measure of the dose profile through the carbon material. Note that, for each measured wafer, the index of refraction stays fairly constant throughout the measurement of the different regions on that wafer.

The dose profile data is plotted in Figure 18. The Ti data is shifted upwards for convenience of display, and the Ag source profile curves are from data not listed in Table 4.

6.3 Comment on Dose Profile Data

The data shown for the Al K_α case would appear to be fairly easily explainable. The 1.49 keV X-rays from the aluminum source produce a dose enhancement next to the gold interface (0 carbon thickness) which is fairly readily absorbed in about 200 Å of carbon. As we move up in energy to the Ag L_α case, the dose profile definitely reaches no asymptote, but appears to continue downward as the carbon thickness reaches 710 Å. In fact, the silver data looks remarkably similar to the Ti K_α data and this is somewhat surprising. The titanium X-ray is 4.5 keV, about 50% greater than that for silver, yet the dose profile appeared to be similar in shape. What is missing, and not accounted for by our theorical analysis to date, is the potential presence of bremsstrahlung in the X-ray sources.

In Appendix I is a published paper which presents these data along with a theoretical analysis by Dr. John Garth of RADC.

TABLE 4. TYPICAL ELLIPSOMETER MEASUREMENT DATA

Ag L_α (II) (3/18/82)

Region	Δ	Ψ	INDEX	THICKNESS (A)	DIFF (A)
Unexp. Resist	261.7	20.88	1.531	2192	0
Au	355.3	82.16	1.535	1305	887
100A	294.2	68.64	1.533	1410	782
220A	288.3	54.60	1.532	1515	677
520A	286.6	43.76	1.530	1640	552
710A	285.1	37.72	1.528	1746	445

Al K_α (6/7/82)

Region	Δ	Ψ	INDEX	THICKNESS (A)	DIFF (A)
Unexp. Resist	276.9	28.24	1.525	1989	0
Au	284.4	36.36	1.526	1776	213
100A	283.9	35.20	1.527	1801	188
220A	282.2	32.88	1.525	1860	129
520A	282.7	33.40	1.526	1845	144
710A	281.8	32.32	1.527	1870	118

Ti K_α (6/7/82)

Region	Δ	Ψ	INDEX	THICKNESS (A)	DIFF (A)
Unexp. Resist	73.84	43.76	1.523	982	0
Au	84.44	27.40	1.518	620	362
100A	82.80	28.64	1.515	657	325
220A	81.68	29.56	1.513	684	298
520A	78.84	31.92	1.518	747	235
710A	77.56	33.56	1.518	790	192

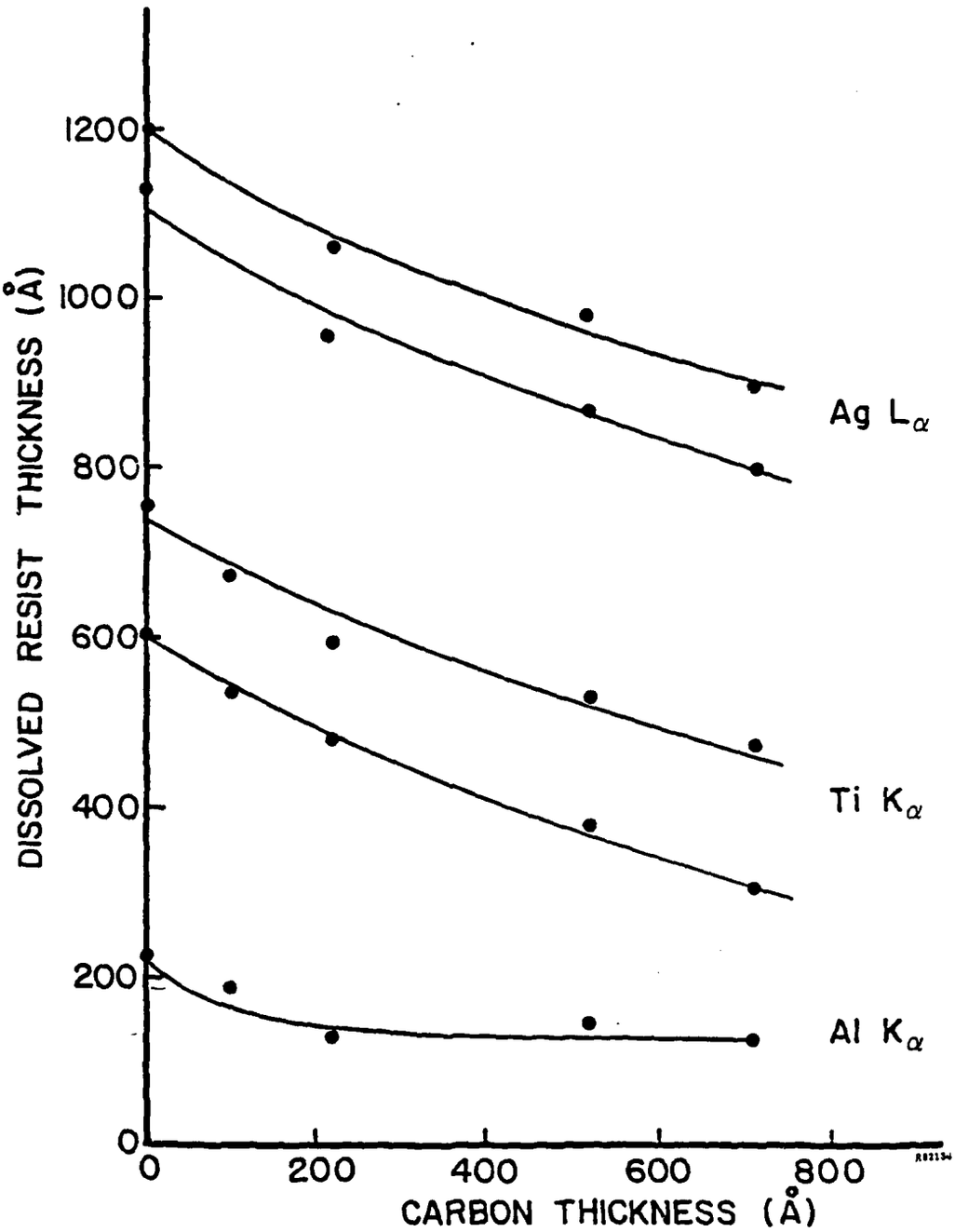

FIGURE 18. DOSE PROFILES IN PBS RESIST USING Au/C MASK. (Data plotted from ellipsometer measurements such as tabulated in Table 2.)

7.0 BREMSSTRAHLUNG CALCULATIONS

7.1 Estimates for Al and W Irradiated with 18 keV Electrons

To make a reasonable estimate for the bremsstrahlung radiation produced in Al and W by 18 keV electrons, data from the Atomic and Nuclear Data Tables was used.[6] Absorption of this radiation in the target material as a function of energy was estimated using an accurate x-ray cross section compilation.[7] The results are illustrated in Figure 19. A comparison of the estimated spectrum at 18 keV for Al is made with a measured spectrum (generated with 3 keV electrons)[8] shown in the inset of Figure 19. The two spectra for Al are at least consistent with one another taking into account the wide difference in electron accelerating voltages used. The ratios of the K_α line height to the peak in the bremsstrahlung distribution are two and a half orders of magnitude for the measured spectrum (at 3 keV), and a little over two orders of magnitude for the calculated spectrum (at 18 keV). Table 5 summarizes the pertinent data of these spectra.

TABLE 5. Al AND W CHARACTERISTIC/CONTINUUM COMPARISONS FOR 18 keV ELECTRONS

	Al	W
Characteristic line	K_α	M_α
Characteristic yield (photons/electron)	9.3×10^{-3}	$\sim 3.4 \times 10^{-3}$
Total bremsstrahlung yield (photons/electron)	0.66×10^{-3}	1.91×10^{-3}
Continuum mean energy (keV)	6.7	9.6
Characteristic/bremsstrahlung yield ratio	14.1	1.8

7.2 Bremsstrahlung Estimates for Al, Ti, Cr and Ag Irradiated with 10 keV Electrons

In this section, rough estimates for the bremsstrahlung components in Ti, Cr, and Ag target sources irradiated by 10 keV electrons will be made using this calculation and an equation from Evans.[9] The equation is:

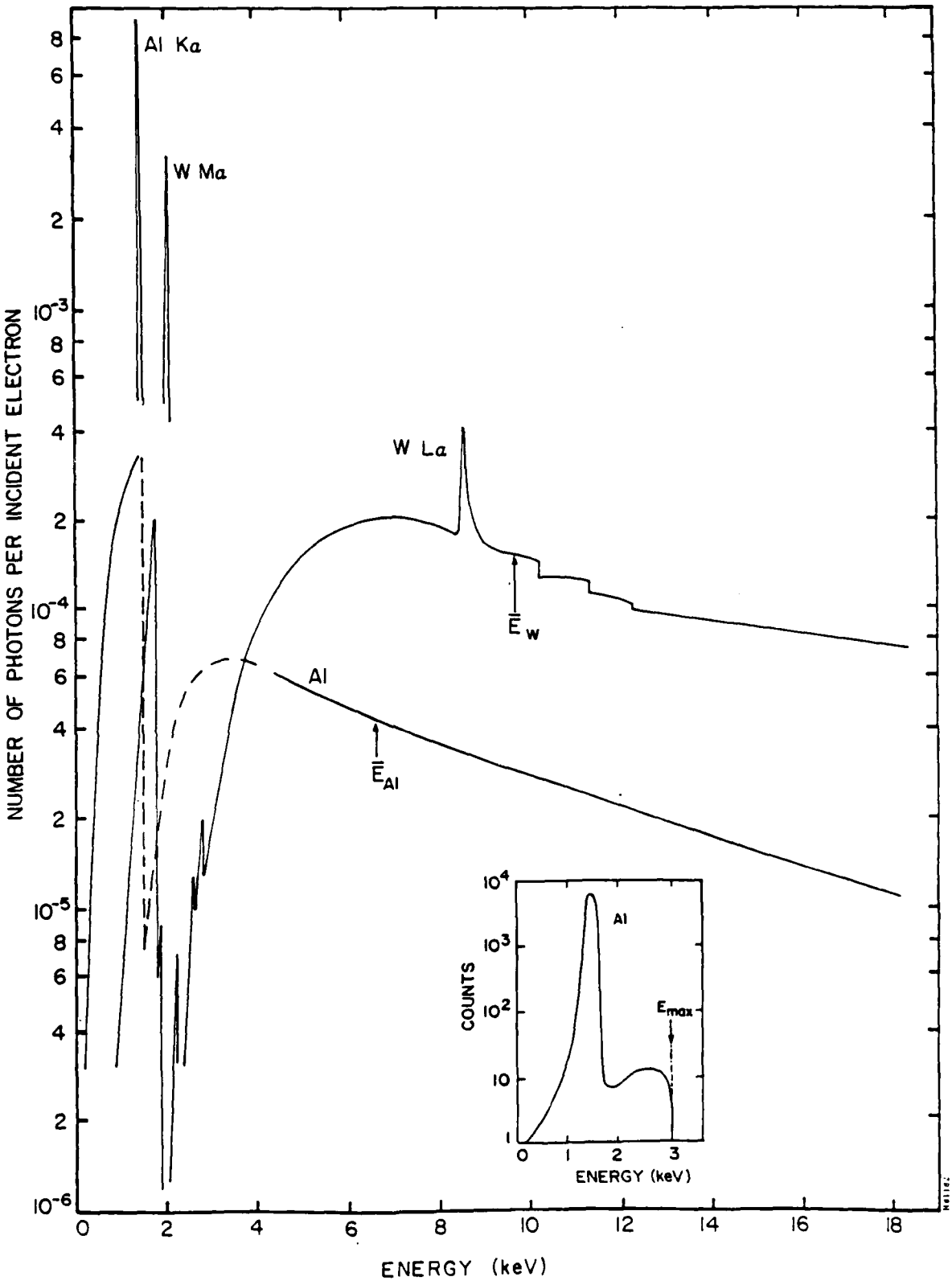

FIGURE 19. BREMSSTRAHLUNG DISTRIBUTIONS AND CHARACTERISTIC LINES FOR Al AND W TARGETS BOMBARDED WITH 18 keV ELECTRONS. (The inset is a measured Al spectrum produced by 3 keV electrons from Reference 8).

$$I = k \times Z \times E^2$$

where I is the total bremsstrahlung energy in MeV and E is the initial kinetic energy of the incident electrons.

We can use this equation in two different ways. First, we can use the experimental determination of k as 7×10^{-4}/Mev. This leads to the fraction of incident electron energy which is converted into bremsstrahlung in a thick target to be:

$$I/E = 7 \times 10^{-4} Z \times E$$

If we assume that we can use this formulation at the low energy of 10 keV, the amount of bremsstrahlung energy produced per 10 keV electron can be calculated. Similarly, taking the characteristic photon yield for each target and multiplying it by the photon energy for each gives the amount of characteristic photon energy produced per 10 keV electron. These two energies are listed in columns 4 and 6 of Table 6. Note that Cr is added as a potential x-ray source target. The ratio of the amount of bremsstrahlung energy produced to the amount of characteristic photon energy produced is listed in the last column in the table. As the Z of the target element increases from aluminum to silver, the energy ratio increases from 0.195 to 2.9.

TABLE 6. BREMSSTRAHLUNG TO CHARACTERISTIC PHOTON ENERGY RATIO FOR 10 keV ELECTRONS

Element	Z	I/E (10^{-4})	Energy Bremss. / 10 keV elec. (keV)	# Char. ph. / incident elec. (10^{-4})	Energy ph. / 10 keV ele. (keV)	Bremss. / char. ph. energy
Al	13	0.9	9×10^{-4}	31 x	4.6×10^{-3}	.195
Ti	22	1.54	1.54×10^{-3}	5.9 x	2.66×10^{-3}	.58
Cr	24	1.7	1.7×10^{-3}	3.4 x	1.84×10^{-3}	.92
Ag	47	3.3	3.3×10^{-3}	3.8 x	1.13×10^{-3}	2.9

That is to say, for all of the photons generated in an Al target, the energy carried away by bremsstrahlung photons is about 1/5 of the total photon energy produced while, for silver, the energy is about 3/4 of the total produced. This particular approach in estimating bremsstrahlung components leads to the conclusion that silver, while irradiated with 10 keV electrons, is primarily a bremsstrahlung source. For titanium, about 1/3 of the total photon energy produced is bremsstrahlung and for chromium, almost one half of the total is bremsstrahlung. These results would seem to indicate that the silver radiation produced for these experiments is significantly harder in energy than one might at first expect. The Ag source data shown in Figure 18, therefore, is not so surprising when bremsstrahlung is properly included in the analysis.

A different approach to estimating bremsstrahlung for the various target sources is to take the calculated data for aluminum and tungsten (Section 7.1) and interpolate that data as a function of Z for titanium, chromium, and silver. The total bremsstrahlung yield (photons per electron) for aluminum and tungsten for an electron energy of 18 keV was calculated to be 0.66×10^{-3} and 1.91×10^{-3}, respectively. Taking the difference between these two numbers and dividing by the number of Z units between Al and W, , i.e., 61, one ends up with an interpolation constant of 0.021×10^{-3} per Z unit. First, however, the bremsstrahlung yield for aluminum needs to be reduced from 18 kilovolts incident electron energy to 10 kilovolts. This results in a bremsstrahlung yield for aluminum to be 0.20×10^{-3} when using the equation above. The estimated bremsstrahlung yields and the comparisons with the characteristic photon yields for each of the target elements is tabulated in Table 7. Again notice that, for silver, the percent of bremsstrahlung photons to the total number produced in the source is greater than 50%. Either approach gives no easy way to estimate the mean energy of bremsstrahlung for each case. This needs to be calculated using accurate bremsstrahlung yield tables for each element. The estimates made here are presented to indicate the extent of the bremsstrahlung problem for these experiments.

TABLE 7. ESTIMATION OF BREMSSTRAHLUNG YIELDS FOR Al, Ti, Cr AND Ag IRRADIATED WITH 10 ke / ELECTRONS

Element	Bremss Yield	Char. ph. Yield	# Bremss ph. / # char. ph.	% # Bremss ph. of total ph.
Al	0.20×10^{-3}	31×10^{-4}	.065	6
Ti	0.26×10^{-3}	5.4×10^{-4}	0.48	32
Cr	0.27×10^{-3}	3.4×10^{-4}	0.79	44
Ag	0.42×10^{-3}	3.8×10^{-4}	1.11	52

7.3 Significance of Continuum Radiation on Pattern Quality

What do these calculational results signify? For the W target, about 35% of the photons produced are bremsstrahlung, while for the Al target, about 6% are bremsstrahlung. Figure 20 illustrates the potentially deleterious effects that bremsstrahlung can produce in the lithography process. X-rays traveling through the transparent regions of the mask irradiate the photoresist (region A), in a sharply defined area. The high energy component, however, passes through the resist and creates a new radiation source in the Si substrate. While the fluorescent yield for Si is only about 5%[10], photoelectrons are created and excited Si atoms de-excite via the creation of Auger electrons. These radiations deliver dose to the back side of the resist material isotropically and can affect the edge definition produced by the mask.

A potentially more severe problem exists as illustrated in region B of Figure 20. The energetic continuum photons may pass through the high-Z absorbing layers of the mask and continue on to irradiate the resist and substrate layers. At first sight this may be a tolerable situation, since the hydrocarbon-like resists are fairly insensitive to high energy x-rays. Furthermore, the radiations created in the Si substrate may be significantly deeper than before, since only the energetic portion of the continuum is transmitted through the high-Z layer. This may mean that the dose delivered to the underside of the resist layer is lower for region B than for region A. However, this is not the source of extraneous radiation that is the main concern.

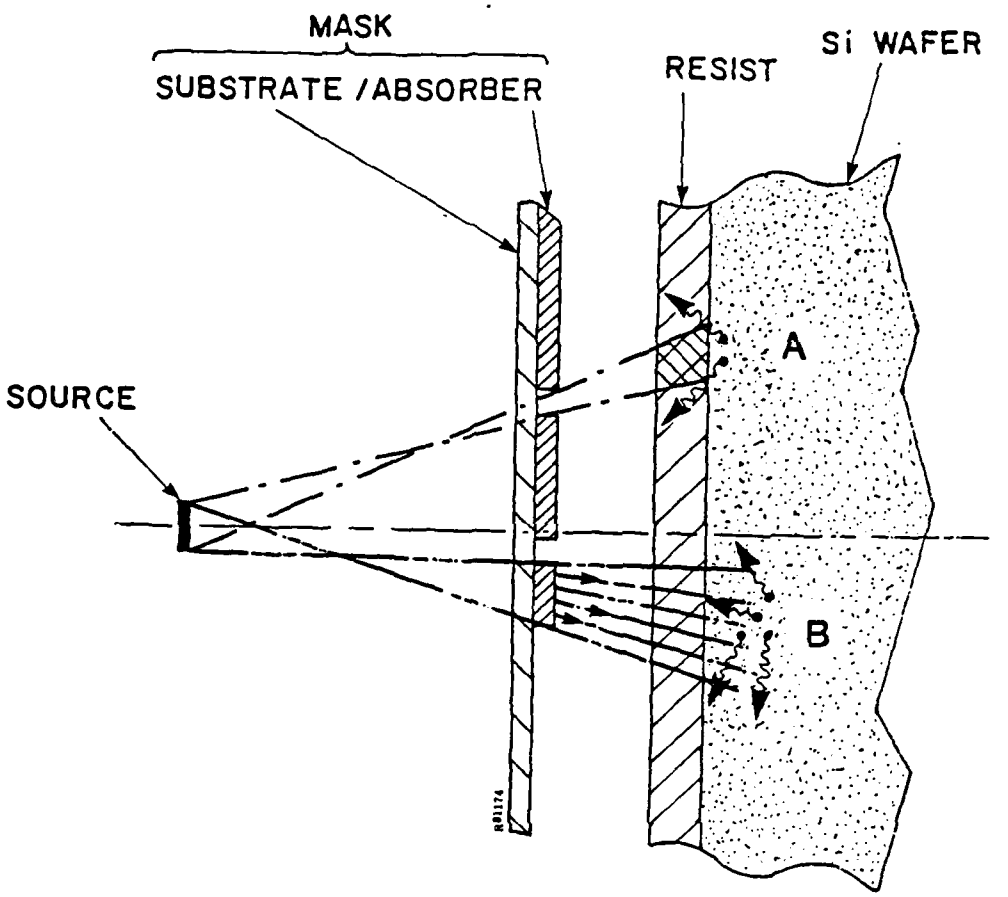

FIGURE 20. ILLUSTRATION OF EFFECTS ON THE X-RAY LITHOGRAPHY PROCESS CAUSED BY SOURCE BREMSSTRAHLUNG (A: Si fluorescence degrading edge definition; B: Absorber transmitted radiations reducing pattern contrast.)

For 10 keV x-rays impinging upon a 6000 Å thick layer of Au, the transmission is 87%.[7] The fact that the high-Z layer on the mask has ionizing radiation passing through it implies that the high-Z layer becomes a potential radiation source. This radiation source is comprised of Auger electrons and Au M_α (~2.4 keV) x-rays. These radiations can be quite efficient in exposing a typical hydrocarbon resist material. The result is overall reduced pattern contrast.

While a number of workers have demonstrated reduced contrast patterns,[11] absorption of Au radiations with a hydrocarbon layer,[12] or in some cases higher doses beneath absorber layers,[13] no one to date has compiled a quantitative data base with measured spectra to address this important problem. Buckley of Perkin Elmer Corporation admits that mask contrast is decreased when their W source is run at 20 kV.[14]

7.4 X-Ray Spectrum Alteration

The x-ray source used for these experiments is a Sloan electron beam evaporator unit. Since the electron beam source of the evaporator cannot have its accelerating voltage changed, the only way to alter any of the x-ray spectra used in these experiments is by filtration. That is to say, x-rays produced by a particular metal target are then filtered by a thin film of the same metal before they reach the x-ray mask and wafer.

7.4.1 Ag Filtration of Ag Source

Figure 21 illustrates how a spectrum may be altered for the case of Ag (Z = 47). Using a computer program called TUBE (from the NRL XRF, Program[15]), the continuum and principal lines of Ag are generated for the case of 10 keV electrons. The relative size of the continuum generated by TUBE is in some doubt at present, so that the main characteristic peak (L_α at 2.95 keV) ratio to the height of the continum must be estimated.

If the electron beam generated spectrum is passed through a Ag filter, x-ray absorption will occur as a function of x-ray energy according to the absorption curve of Figure 21. For example, at the L_α characteristic energy 2.95 keV), the mass absorption coefficient, μ/ρ, is 5.31×10^2 g/cm^2. Using ρ = 10.48 g/cm^3, and a thickness of two (2) microns (2×10^{-4}cm), this line would be reduced in intensity by a factor of

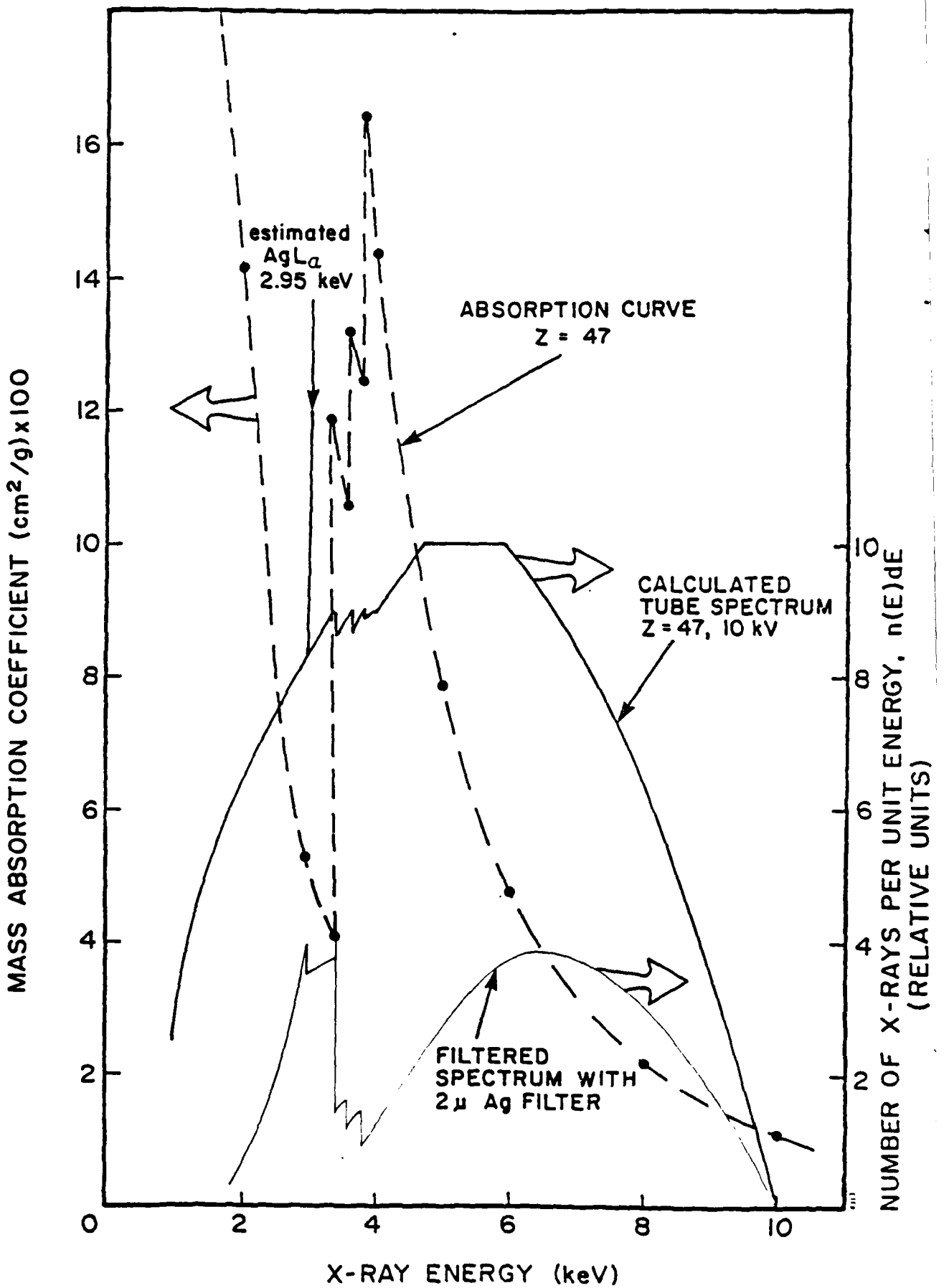

FIGURE 21. FILTERING OF SILVER X-RAY SPECTRUM BY SILVER FILTER.

exp ($-5.31 \times 10.48 \times 2 \times 10^{-2}$), or 0.329. The original height of 12 in Figure 21 for the L_α line, is reduced to 4. At each energy, the mass absorption coefficient is found, a new factor calculated, and a new n(E) dE found. When this is done for the whole spectrum, the filtered Ag spectrum is determined as illustrated. The filtered spectrum appears to be a binary distribution, with centers at 3 keV and 6.5 keV. Whether or not these two distributions have near equal peak heights depend, of course, on the relative contributions of the characteristic line and continuum.

7.4.2 Ag Filter

A Ag filter of two microns (2×10^{-4} cm) was made by evaporating Ag to that thickness onto a 2.5 micron mylar pellicle. Glass slides, coated along with the pellicle, were measured by profilometry. This Ag filter will be placed in front of any x-ray mask in order to filter the x-ray spectrum.

8.0 DOSE PROFILE MEASUREMENTS USING A SILVER/CARBON MASK

8.1 Ag/Carbon Mask

A new x-ray mask has been made. Using, as for previous masks, a 2.5 micron thick mylar pellicle (1-inch diameter) as the mask substrate, 7000 Å of Ag was first laid down by evaporation. Two glass slides were also coated to determine the actual Ag thickness deposited on the pellicle.

8.1.1 Sputtering of Carbon Absorption Layers

Ion beam sputtering was used to deposit thirteen (13) different known carbon thicknesses on the Ag layer. The ion beam sputtering apparatus produces a 30 kV Ar^+ beam which strikes a water cooled target. The incident beam sputters the target material so that a substrate surface in close proximity will become coated with sputtered material from the target. Pure carbon in the form of a thin graphite sheet was used as the target material. The substrate was a one inch diameter mylar pellide, coated with 7000 Å of Ag, placed behind a 13 hole aluminum mask.

8.1.2 Rate Deposition Monitor

An Inficon (model XTM) rate deposition monitor was used to measure the thickness of each sputtered carbon layer as it was being laid down. To calibrate the rate deposition monitor for this application, carbon was first sputtered onto a polished surface of a 2-inch

diameter Si wafer through the 13 hole aluminum mask. The monitor head was positioned next to the Si wafer, a position which would not be changed for the sputter coating of the x-ray mask. The heights of the thirteen carbon layers sputtered onto the Si wafer were measured with an in-house profilometer (Sloan Dektak Profilometry System). By comparing each measured height and the rate deposition monitor reading, a calibration of the monitor was made for each of the thirteen areas. Since the flux of sputtered atoms (for ion beam sputtering) is fairly well directed, small variations over a diameter of one inch on a stationary substrate should occur. In this case the variations were less than 20%. The method of calibration used here yields a separate calibrating factor for each carbon area, so that the accuracy of the final height of each carbon layer of the mask is limited, primarily, to the accuracy of the profilometry data. This accuracy is on the order of $\pm$5%.

8.1.3 Carbon Deposition by Sputtering

Carbon was deposited by ion beam sputtering onto the Ag mask in ten separate sputtering runs. For the first run, every hole but one of the 13 holes in the mask was covered with a piece of copper tape. About 300 Å of carbon was sputtered (as measured by the calibrated rate deposition monitor). For the next run, a second hole on the aluminum mask was uncovered along with the first hole. After another 300 Å (or so) of carbon deposition, the Ag mask had two layers of carbon on it differing in height by the deposition depth of the second run. This procedure was used for ten runs, with the amount deposited per run selected to yield a useful set of carbon layer thicknesses. Each carbon layer had a diameter of six millimeters.

8.1.4 Ag/Carbon Mask Parameters

The carbon thicknesses laid down on the 7000 Å Ag mask (supported by a 2.5 micron thick mylar substrate) are listed on the following page.

These thicknesses are all derived from the calibrated rate deposition monitor readings taken during each sputter run. Independent measurements of these thicknesses, such as by profilometry or by ellipsometry could not be done. The basic surface roughness of the evaporated Ag in the mylar prevented a meaningful profilometer measurement to be made for any of the carbon heights. Ellipsometry cannot measure carbon thicknesses as carbon is an absorbing medium and there are no available programs from the ellipsometer manufacturer (Rudolph Research, Inc.) for measuring absorbing media.

Area Number	Carbon Thickenss (A)
1	1688
2	1349
3	1117
4	931
5	666
6	496
7	226
8	128
9	118
10	73
11	76
12	36
13	35

8.2 Fabrication of a Second Au/C Mask

A standard 1-inch pellicle with 2.5 micron thick mylar was used. Au was evaporated over most of the pellicle surface to a thickness of 6500A. This thickness was measured on a witness plate (a glass slide) which had been placed near the pellicle during the evaporation of Au. Profilometry, using a Sloan Dektak, was performed across regions of the slide where the Au had been scratched away to reveal bare glass.

8.2.1 Carbon Sputtering

An ion beam sputtering apparatus was used again to sputter coat various thicknesses of carbon onto the Au. A thirteen hole Al mask was used such that various holes were covered or uncovered to produce 13 different thicknesses of carbon on the Au. A calibrated rate deposition monitor, with its sensor close to the Al mask-covered pellicle, was used to determine the carbon thickness laid down during each run. The monitor was calibrated by sputter coating some carbon onto a glass slide with the sensor in place. By measuring the thickness of carbon laid down (by profilometry) and comparing that thickness to the monitor reading, a ratio (tooling factor) was found and programmed into the monitor read-out.

8.2.2 Carbon Thickness Determination

After depositing the thirteen carbon layers of varying thicknesses on the Au-covered pellicle, a second calibration run was performed by placing a section of glass slide behind the Al mask and coating it in a single sputter coating run. By measuring the heights of the thirteen layers of carbon, small variations in the sputtering distribution could be measured and corrected for. The final carbon thicknesses for the Au/C mask are illustrated in Figure 22.

8.2.3 Design of Au/C Mask

The thinnest layers of carbon are near the center of the pellicle, while the thickest are on the outer perimeter. The rationale for this is due to the uneven coating (or developing) of the PBS resist material. Since the thin layers are now located in close proximity to one another, small variations in the PBS layer should not critically affect the final developed resist heights corresponding to these thinnest carbon layers. As a result, any detrimental effect on the measurement of dose due to resist thickness variations should be minimized.

8.3 Experimental Exposure Curves for PBS

Three exposure curves were determined for the PBS resist using three different x-ray sources: Ag, Al and Ag with Ag filtration. For each source used, a section of a single coated wafer was exposed for a preselected time. Exposure time, depending on the expected source strength at the wafer, varied from one (1) minute to twenty (20) minutes. Figure 23 shows the results of these experiments, viz., the exposure curves for PBS plotted on linear graph paper. Note the remarkable linearity of the dissolution rate vs. irradiation time (varies linearly with dose). The slopes for each curve give the relative exposure dose strength for each source. The ratio in slopes for the Ag source and Ag filtered by Ag source is 4.35.

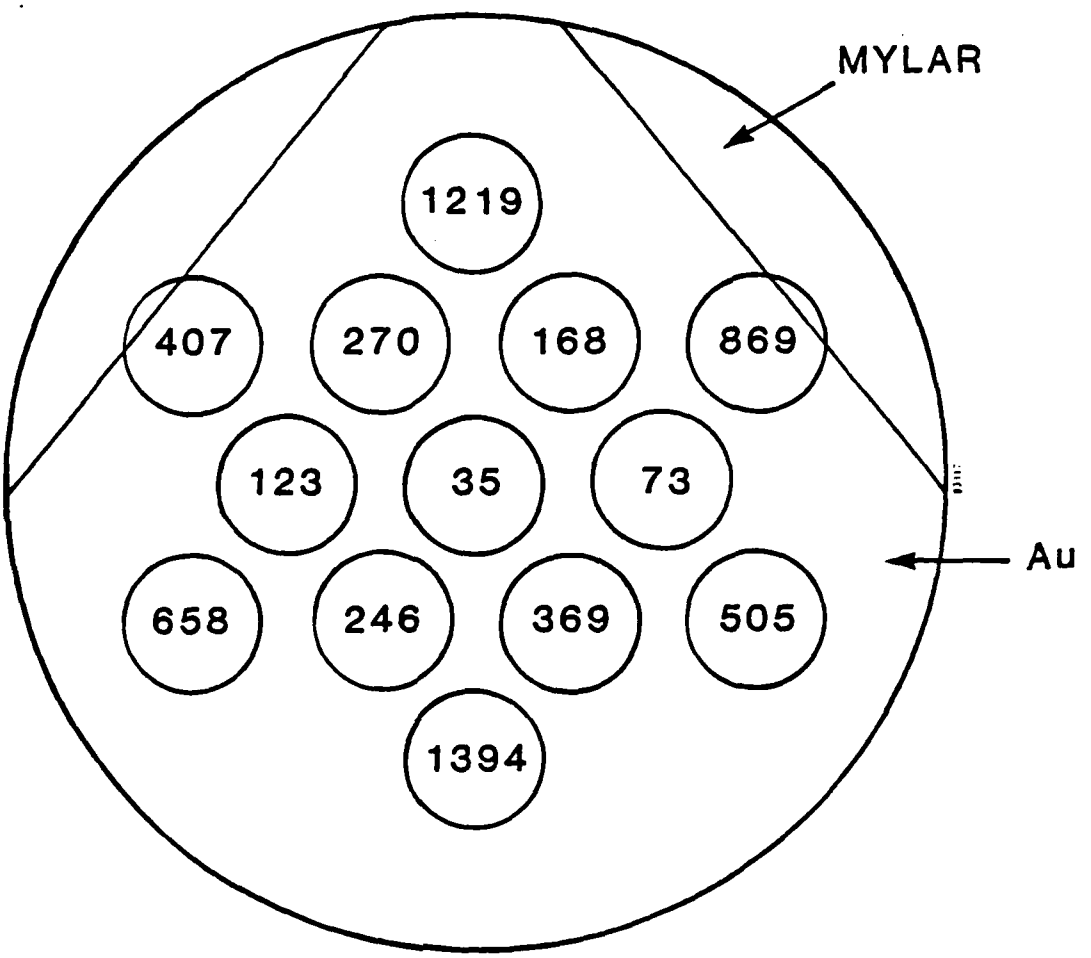

FIGURE 22. CARBON THICKNESS VALUES IN ANGSTROMS FOR SECOND Au/C MASK. (The circular diameter is 1-inch.)

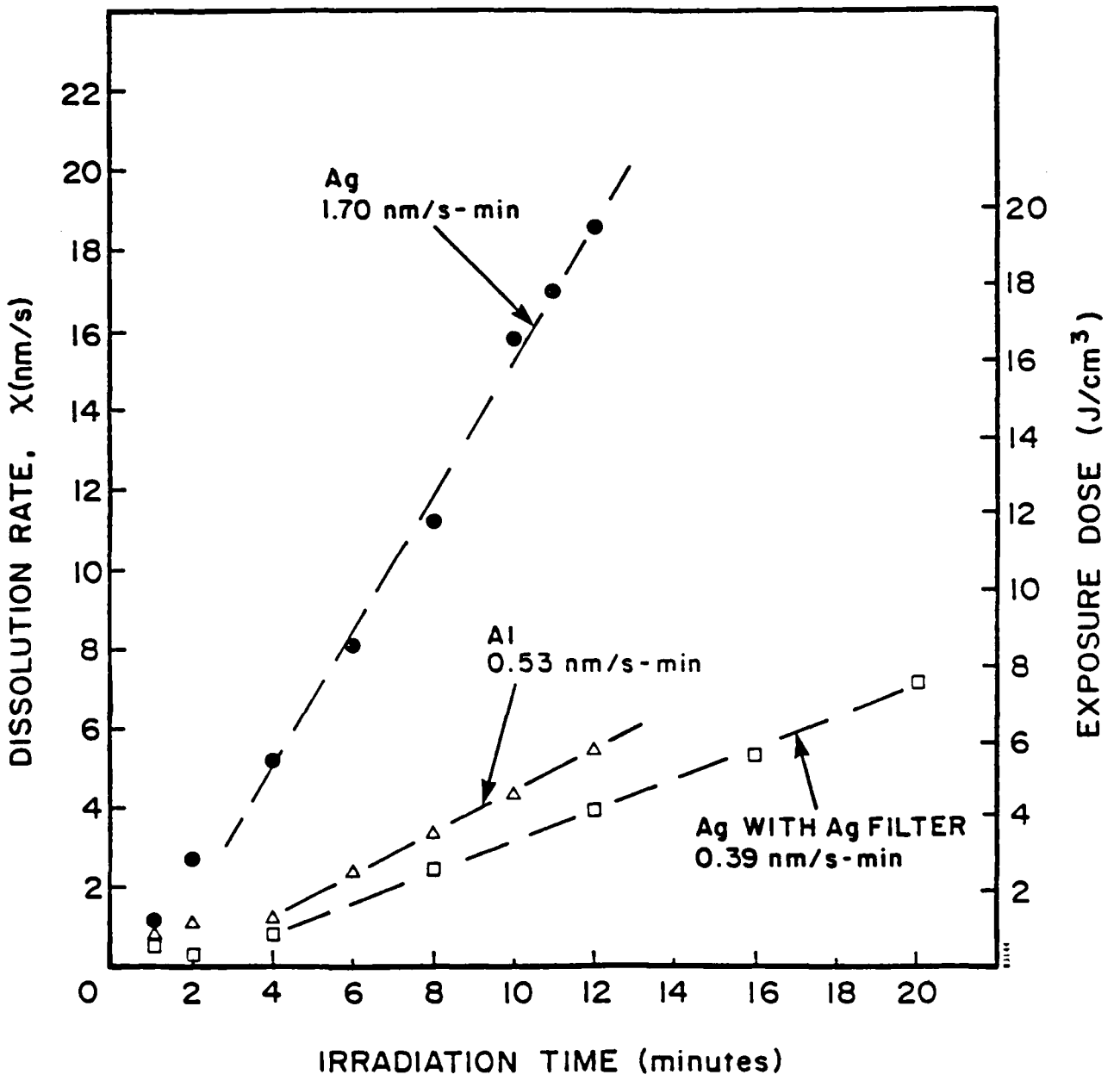

FIGURE 23. PBS EXPOSURE CURVES FOR Al, Ag AND FILTERED Ag SOURCES.

Figure 24 shows the curves plotted on log-log paper. The expected curve shape for all positive resists is:

$$\chi \alpha (\text{dose})^{\beta}$$

and these curves fit that shape quite well. The power exponent does vary from 1.11 to 1.18 (i.e., $\pm$ 3%), which indicates very little dependency on the source spectrum. The exposure times for the two Ag source irradiations vary by a factor of 4.13 for a given dissolution rate. Using the attenuation calculated for the Ag filter in Section 7.4.1, the difference in transmitted flux of the L_α line is 3.04. The difference in the two factors is to be expected since the x-ray energies around the L_α line are attenuated much more strongly than the L_α line.

8.3.1 Dose Measured by Dissolution Rate

What has not been determined so far is the actual absorbed x-ray dose in the PBS. This required an independently calibrated detector, such as x-ray film, exposed in an identical fashion as the coated wafers to the X-ray sources. An interim calibration may be estimated from the data of Phil Blais[5]. Blais determined the dose in units of J/cm^3 for his exposure curve measurements and plotted dose vs. dissolution rate. He found a slope of 0.0571 microns/min/J/cm^3 which translates as 0.95 nm/s/J/cm^3. The inverse slope, 1.05 J/cm^3/nm/s, may be used, as a first approximation, as a factor connecting the dissolution rates determined in these experiments with exposure dose. There may be considerable uncertainty in this procedure as the development solution he used (77% 5 methyl 2-hexanone and 22% 2-pentanone) is significantly different from the development solution used in these experiments (MIAK/MPK, 75%/25%). The inverse slope is used for the exposure dose scale seen on the right vertical axis of Figure 23.

8.4 Dose Profile Curves

8.4.1 Al Source Irradiations

Three Al source irradations were performed at three different irradiation times: 10, 15 and 20 minutes. The standard procedure was used in all irradation studies: Spin coat

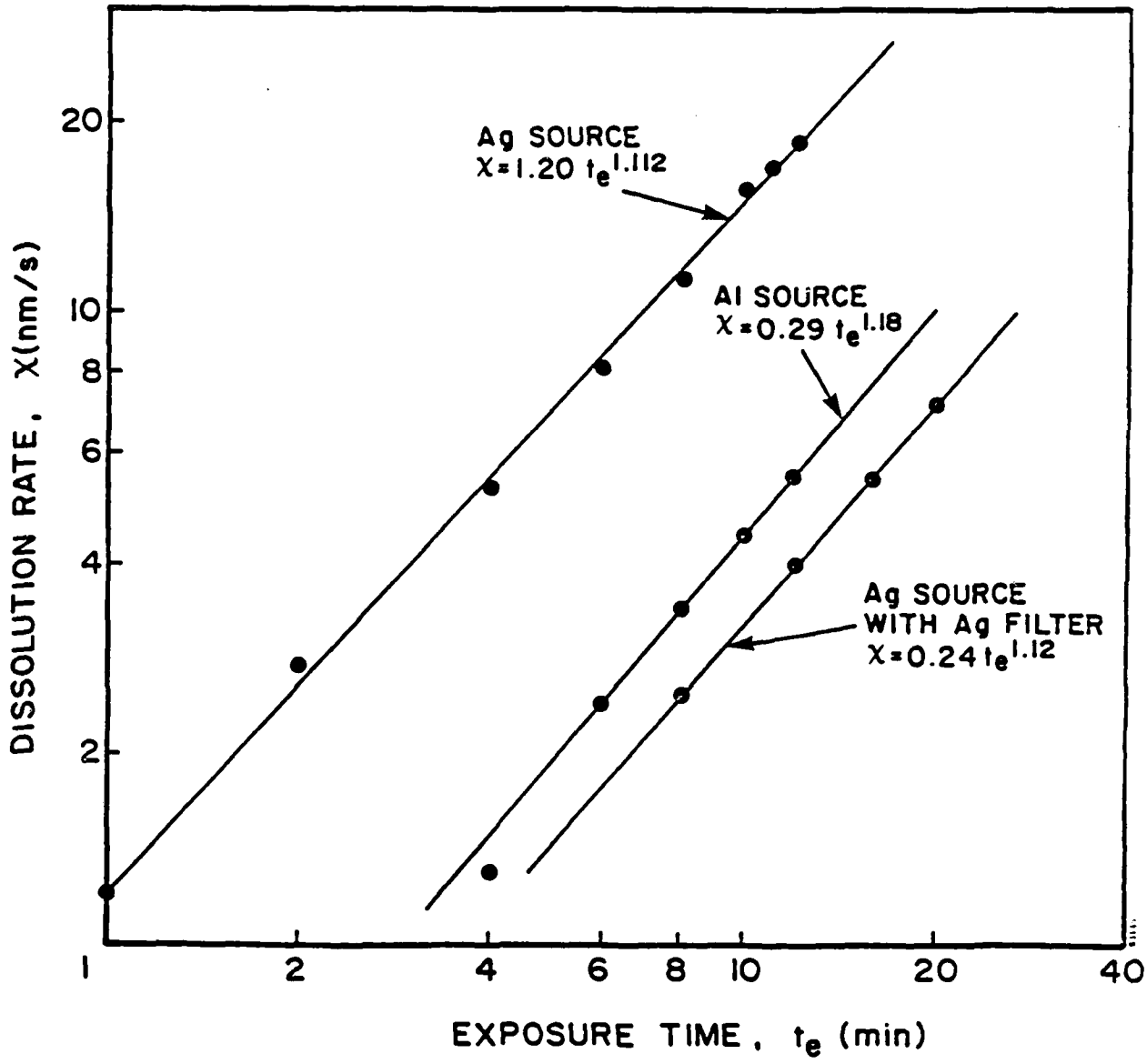

FIGURE 24. PBS EXPOSURE CURVES PLOTTED TO DERIVE EXPOSURE EXPONENTS

to ~3000A thickness, prebake at 120° C for 30 minutes, store in dry N_2, irradiate for pre-selected time, develop for 10 seconds, rinse for 60 seconds, dry with N_2, and measure with ellipsometer. The Al source data is shown in Figure 25. The data sets are quite consistent with one another with the greatest scatter in the 20 minute irradation set. Basically, these data are consistent with the previously obtained data of Al source and Au/carbon mask and which can be found in Appendix I.

8.4.2 Ag Source Irradiations

Two Ag source irradiations were performed, one with and one without the 2 micron thick Ag filter. The data is shown in Figure 26. The dotted lines are drawn to guide the eye; they are not least squares fitted. There does appear to be a slight difference in the two curves. Both curves reach an asymptote, the filtered profile at a carbon thickness of 350 A and the unfiltered Ag source's profile at 380 A.

8.4.3 Ti and Cr Source Irradiations

Figure 27 shows the dose profile curves for the Ti and Cr source irradiations. These curves, produced by K_α lines of 4.51 KeV (Ti) and 5.41 KeV (Cr) respectively, are significantly different than the Ag source curve (Figure 26) in that they appear to contain two exponential curves before the final asymptotes are reached. If the first exponential is extended to the final asymptote level, the intercept carbon thicknesses are 500 A (Ti) and 580 A (Cr). The multiple points in each curve are the results of separate ellipsometer measurements.

8.4.4 Ag Mask Profile Summary

The carbon thicknesses to which the first exponential of each profile can be extrapolated to the asymptote are plotted vs. x-ray energy in Figure 28.

This procedure of characterizing profile curve is not based on any theoretical model. Figure 28 is simply a convenient way to summarize the data obtained using the Ag mask.

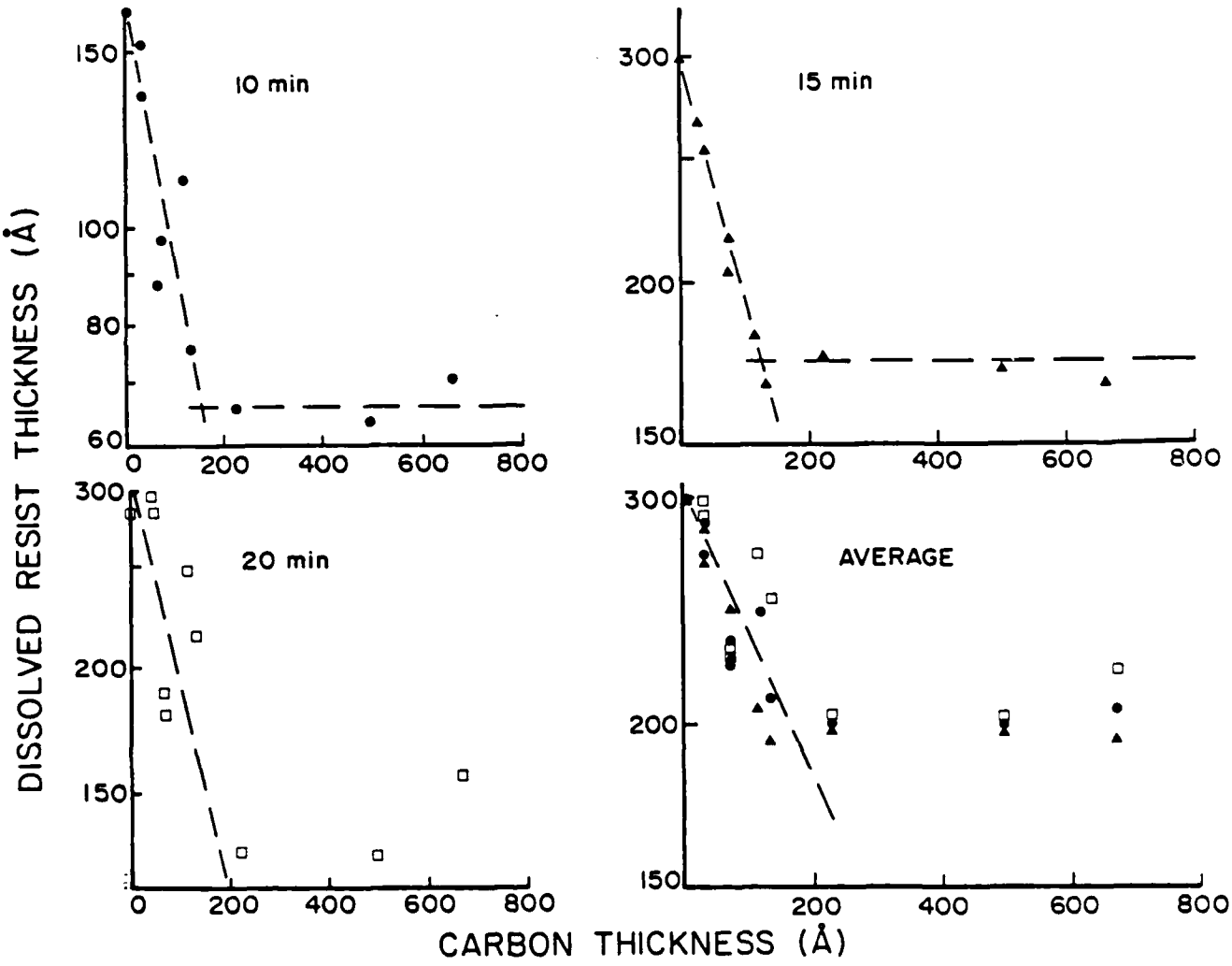

FIGURE 25. DOSE PROFILE CURVES FOR Al IRRADIATIONS USING THE Ag/C MASK.

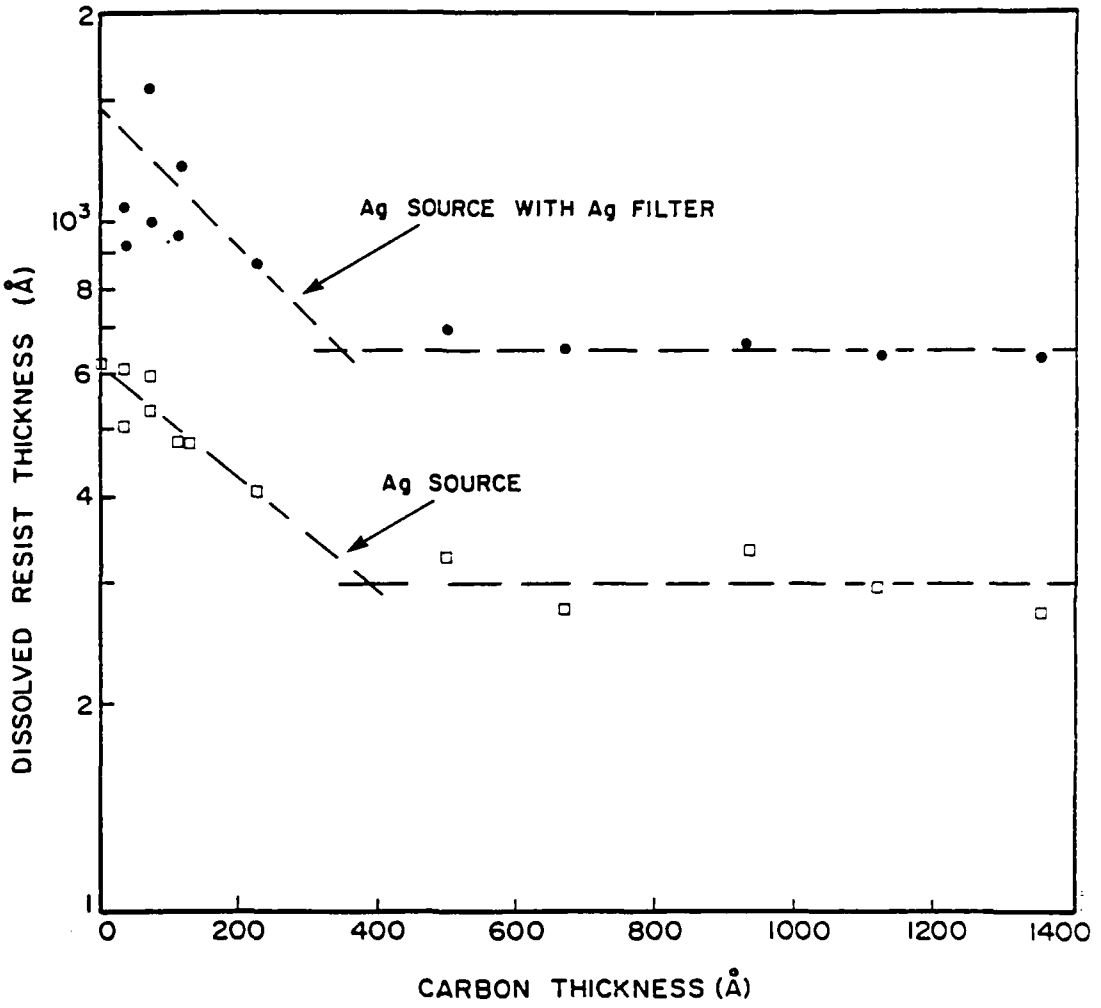

FIGURE 26. DOSE PROFILE CURVES FOR Ag AND FILTERED Ag IRRADIATIONS.

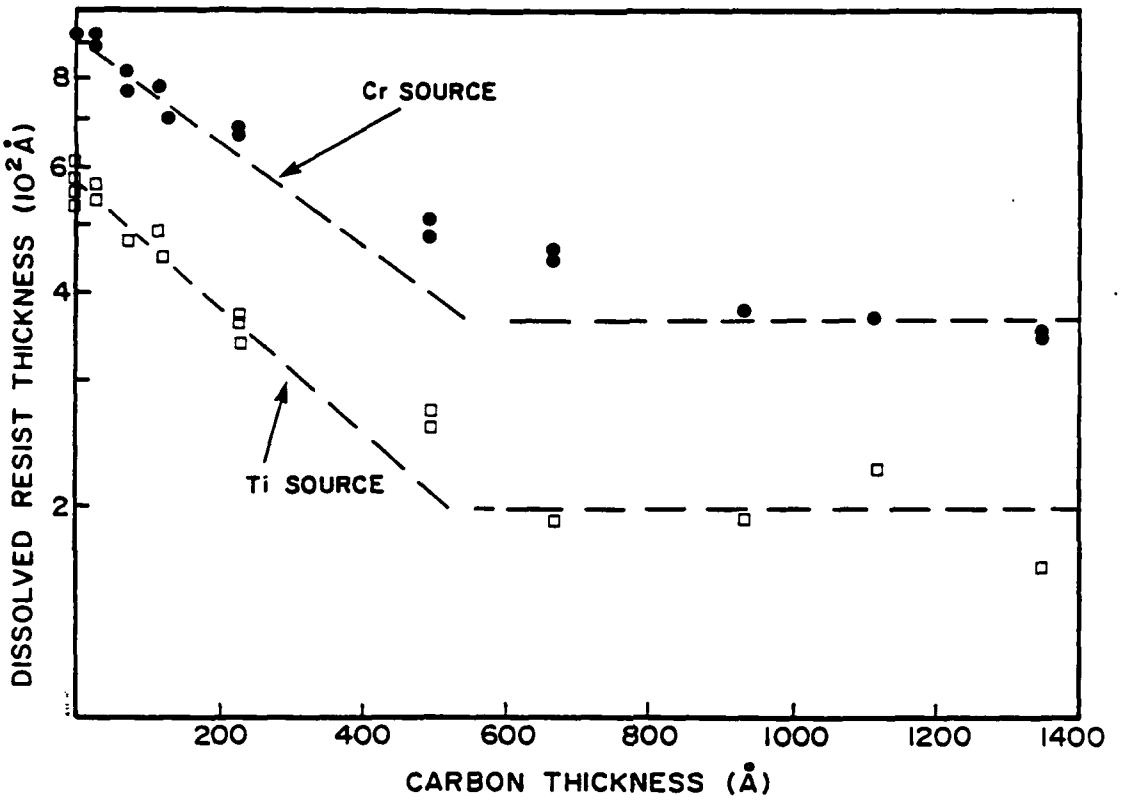

FIGURE 27. DOSE PROFILE CURVES FOR Ti AND Cr IRRADIATIONS.

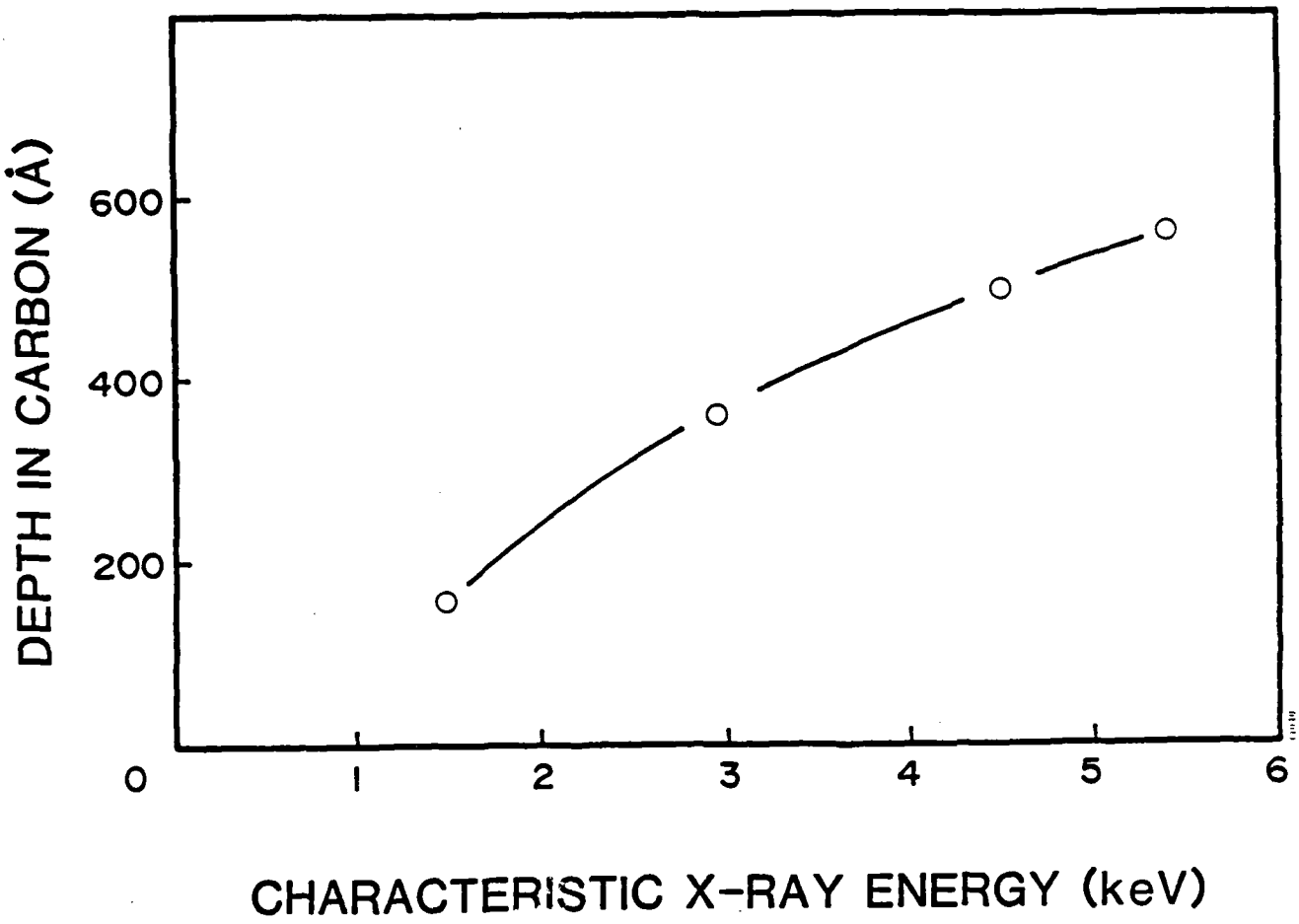

FIGURE 28. DEPTH IN CARBON ASYMPTOTE IS FIRST REACHED FOR Ag MASK PROFILES VS. CHARACTERISTIC X-RAY ENERGY.

9.0 SUMMARY AND CONCLUSIONS

The first attempt to measure dose profiles near interfaces of two materials with a large difference in atomic number, Z, and irradiated with soft x-rays, has been completed. The purpose was to ascertain the character and the depth of such dose profiles in one or both materials and attempt to correlate, whenever possible, the results with existing theoretical models. The experimental challenge was primarily one of measurement technique. The material depths envisioned (and realized) for these profiles were indeed quite small (i.e., 50-1000 A).

Originally, the plan was to carry out absorption experiments with very thin films, using a variable electron energy source, exchangeable x-ray targets and a state-of-the-art Si(Li) detector. However, this approach proved to be fund-limited in the middle of the contract period. As a result, a second less costly (and far less flexible) experimental approach was taken. By means of an electron beam evaporator with fixed electron energy (10 keV), and a number of exchangeable targets, a soft x-ray source was realized.

The second choice for a detector was a photoresist. PBS (poly (butene-1-sulfone)) resist was chosen for this purpose since its sulphur content raised its sensitivity to higher energy x-ray sources and its etch rate-dose response appeared to be linear. By fabricating Au (6800 A) and Ag (7000 A) masks on 2.5 micron thick "mylar" films and then depositing carbon films with a range of thicknesses on those masks, a number of "absorption" experiments could be carried out with a single x-ray irradiation. The experimental interfaces were actually three material interfaces (i.e., metal, carbon, resist). In terms of absorbed dose, however, the carbon and resist could be viewed as a single low Z material next to a high Z material. X-ray irradiations were done for a range of exposure times. By maintaining strict process controls on the exposed resist, etch rates (highest in those areas adjacent to the bare metal mask) decreased with increasing carbon film thickness. The validity of using the measured etched depth in the resist as a measurement of exposure dose was confirmed by generating a number of exposure curves for PBS. The PBS etch rate responded linearly to the length of exposure time over the times used in these experiments.

Measurements of the processed, exposed resist film thicknesses were done by optical ellipsometry in an outside laboratory. Not having easy access to an ellipsometer proved to be a significant shortcoming in this experimental work. While every other step in the measurement process was in-house and readily available, the thin resist film thickness measurement step was not. As a result iterative, repetitive measurements to optimize the overall technique were never carried out.

In spite of the difficulty in obtaining time on an ellipsometer, two sets of dose profiles (one for each mask) were obtained. The Au/C mask dose profiles (except for the Al source profile) did not compare well to the first theoretical model calculations (see Appendix 1.) A second, more realistic model that included bremsstrahlung in the source, and that calculated a spectrum of Auger electrons generated in the metal mask, was designed and compared to the Au/C profiles (see Appendix 2). This comparison is plotted in Figure 29 for the Ag source and Al source profiles. Taking into consideration that only four carbon thicknesses were deposited on the first gold mask, the experimental data and theory agree quite well. A similar comparison to the Ag/C mask dose profiles has not been done.

Conclusions one may draw from these experiments are as follows. First, one can measure (however crudely) dose profiles of soft x-ray-irradiated high Z/low Z material interfaces using a resist film as a dosimeter. Two, the experimental dose profiles can be predicted fairly well with a realistic calculational model that includes source bremsstrahlung. Such a model can have important uses in modeling a full-scale x-ray lithographic system. Three, for x-ray lithography, mask generated radiations can be eliminated by depositing a thin (1500 A) organic film to the exposed metal portions of the mask. Four, the loss of spatial resolution in x-ray-produced lithographic patterns due to high Z/low Z interfaces should be in the range of 0.1 microns.

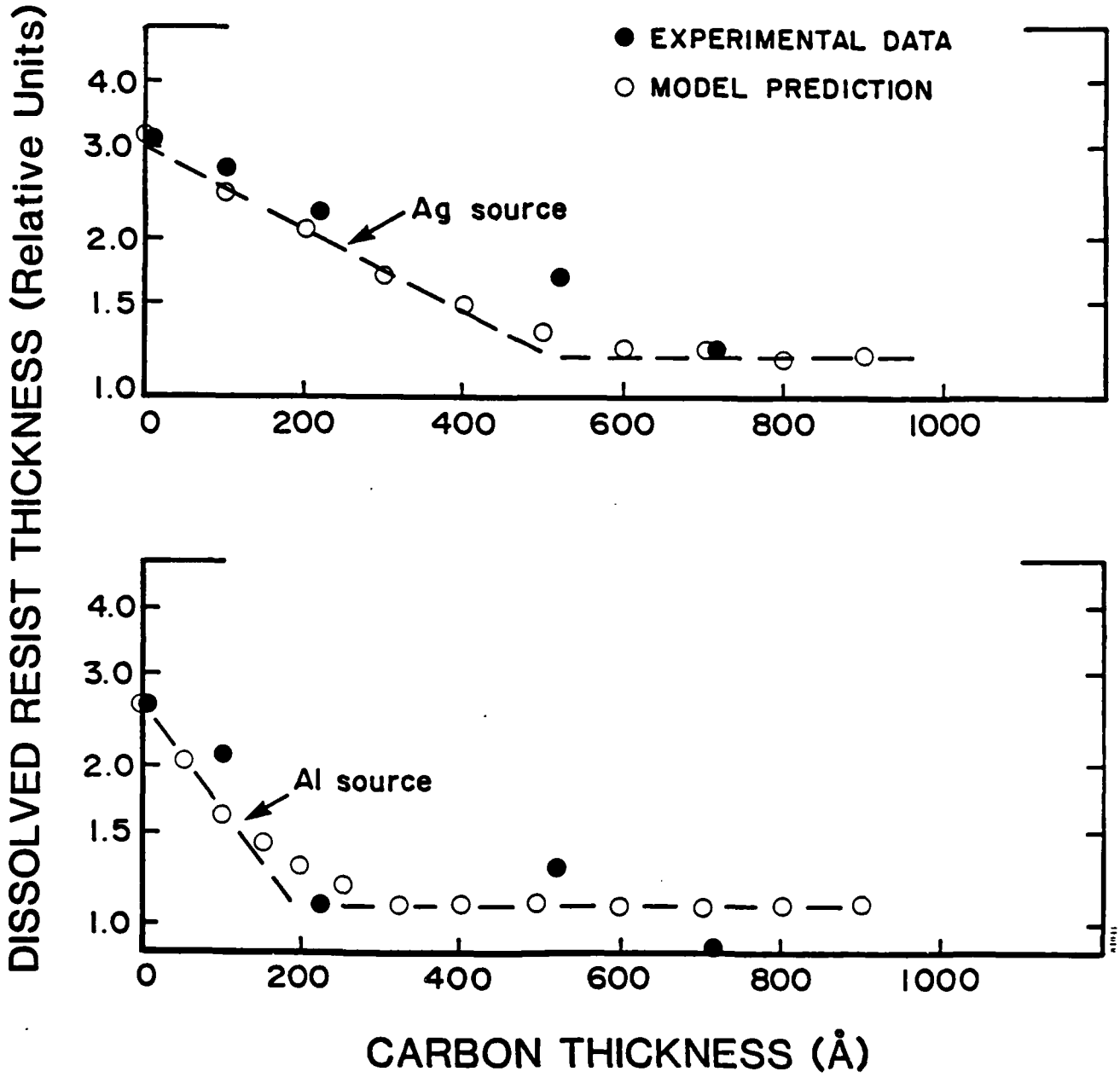

FIGURE 29. COMPARISON OF Au/C MASK DOSE PROFILE DATA FOR Ag AND Al SOURCES WITH THEORETICAL MODEL (Appendix 2).

REFERENCES

1. Green, M. and Cosslett, V. E., "Measurement of K, L and M Shell X-ray Production Efficiencies," Brit. J. Appl. Phys. 2, 91), 425 (1968).

2. Sullivan, Paul A., "X-ray Lithography System Complete with interdigital Transducer System," Report No. AFCRL-TR-75-0573, Hughes Research Laboratories, 1975.

3. L. F. Thompson and M. J. Bowden, J. Elect. Chem. Soc. 120, 1722 (1973).

4. P. D. Blais, "X-ray Resist Technology" Kodak Microelectronics Seminar Proc., Interface p80, Kodak Report No. G-130 p. 79.

5. P.D. Blais, Westinghouse Research Center, Pittsburg, PA, private communication.

6. R.H. Pratt et al, Atomic Data and Nuclear Data Tables 20, 175-209 (1977).

7. W.J. Veigele et al, X-ray Cross Sections Compilation, Kaman Nuclear Report No. KN-798069-2 (1969).

8. C.M. Dozier, D.B. Brown et al, J. Appl. Phys, 47, 3732, (1976).

9. R.H. Evans, The Atomic Nucleus, (McGraw-Hill, NY), p. 615, (1955).

10. C.M. Lederer et al, Table of Isotopes, 6th Edition (John Wiley & Sons, New York)(1967).

11. P.A. Sullivan & J.H. McCoy, IEEE Trans. ED-23, 412 (1976).

12. J.R. Maldonado et al, J. Vac. Sci. Technol 12, 1329 (1975).

13. R. Feder et al, J. Vac. Sci. Technol 12, 1332 (1975).

14. W.D. Buckley and G.P. Hughes, J. Electrochem. Soc., 128, 1106 (1981).

15. J. W. Criss, Naval Research Laboratory (Fortran Program, NRLXRF (Documented by Cosmic Software Management of Information Center, Athens, GA, DOD No. 00065).

APPENDIX I

IEEE Transactions on Nuclear Science, Vol. NS-29, No. 6, December 1982

SOFT X-RAY INDUCED ENERGY DEPOSITION IN A THREE-LAYERED SYSTEM: Au/C/PBS

J. C. Garth
Rome Air Development Center
Solid State Sciences Division
Hanscom AFB, MA 01731

and

B. W. Murray and R. P. Dolan
SPIRE Corporation
Bedford, MA 01730

Abstract

An experimental and theoretical study of soft x-ray generated dose profiles in the Au/C/PBS three-layered system has been performed using x-rays from Al, Ag and Ti targets. Experimental measurements of etched photoresist thickness as a function of carbon layer thicknesses of several hundred Angstroms were performed. Theoretical dose profile calculations were made for the Al K_α, Ag L_α, and Ti K_α x-ray line energies using a 3-layer extension of the semi-empirical electron transport model of Burke and Garth (1977) and Garth (1981). From the etch rate-exposure characteristic of PBS, predictions of the etched thickness vs carbon thickness were obtained and compared with the data. Qualitative agreement was obtained, but a quantitative discrepancy was found, attributable to the neglect of high energy bremsstrahlung-produced electrons in the theoretical model.

Introduction

Few measurements have been made of energy deposition profiles in solids for x-rays in the 1 - 20 keV energy range. It is well known that the effective range for secondary electrons at a few keV is several hundred Angstroms[1]. Thus dose measurements at distances of this order of magnitude are necessary for characterizing the dose profile near interfaces between different materials[2]. In a study of spurious effects in x-ray lithography, Maldonado et al[3], using Pd L_α (2.84 keV) x-rays, studied the x-ray exposure of a negative resist material as a function of organic layer thickness next to gold. It was found that there was a substantial dose increase in the photoresist due to photoelectrons emitted from the gold into the photoresist which could be eliminated by an intervening organic layer several thousand Angstroms thick.

It was suggested by Burke[4] that a photoresist etching experiment similar to that of Maldonado et al could be used as radiation dosimeter for measurements of soft x-ray dose-depth profiles over distances of several hundred Angstroms. Such data could then be used as an experimental check of an electron transport model, such as the semi-empirical model of Burke, Garth and Chadsey[5-8] extended for multi-layers, for use in predicting the dose profiles in microelectronic devices in x-ray test environments. Data and prediction models of this type would be likewise useful for optimizing x-ray lithography systems[9] and predicting radiation doses received by underlying oxide layers in devices under fabrication.[10]

In this paper we present photoresist etching measurements obtained with x-ray spectra from aluminum, silver and titanium targets for a well specified three-layer system consisting of gold, carbon and and PBS [Poly(butene-1 sulfone)][11]. The semi-empirical model of Burke, Garth, and Chadsey is extended to layered media using the "two-flux" transport equation of Garth[8] and, with the aid of the etched rate vs dose response curve for PBS[12], calculations of etched photoresist vs carbon thickness are made and compared with the experimental data.

Experimental

In Figure 1 we show schematically the experimental mask used to measure the dose profile in a photoresist near to a gold interface. A 2.54 cm diameter pellicle+ with a 2.5 micron thick mylar film was used as a substrate and mask support. A 6800 Å thick gold film of diameter 1.6 cm was evaporated on the mylar substrate. Within the diameter of the gold film, three thin carbon films of decreasing diameters were deposited with thicknesses of 220 Å (next to the gold), 310 Å and 190 Å. A small area of carbon 100 Å thick was also deposited next to the 220 Å thick area. The parameters of the mask are listed in Table 1:

Table 1. Film Parameters

Material	Thickness	Diameter
mylar	2.5 μm	2.54 cm
Au	6800 Å	1.60 cm
C	100 Å	--
C	220 Å	1.35 cm
C	520 Å	1.10 cm
C	710 Å	.65 cm
C	710 Å	.65 cm

The carbon film thicknesses were measured with a Sloan Dektak and by stereomicrometer parallax measurements of electron micrographs. Measurements by both techniques were in substantial agreement to ±10%.

The radiation detector for these experiments was the positive electron beam resist, PBS (Poly(butene-1 sulfone)).[11] This resist was chosen because of its sulfur content which enhances its sensitivity to Ag L_α radiation. Figure 2 shows the absorption coefficient for PBS; the sharp edge is due to the K edge of sulfur.

While PBS, like other organic resists, behaves as[12]

$$\chi \propto K D^{\beta}$$

where χ is the dissolution rate (μm/min), K and β are constants, and D is the dose (J/cm³), its etch rate response (measured using Ag L_α radiation) is nearly linear over the dose range of 10-50 J/cm³, as

+ National Photocolor Corp., Mamaroneck, New York

0018-9499/82/1200-1985$00.75 ©1982 IEEE

shown in Figure 3.[13] (Note: Assuming a density of 1.2 gm/cm^3 for PBS, 1 J/cm^3 = .833 x 10^5 rad.) This implies that spatial variations in surface dose will result in initial dissolution rates which vary, above a threshold D_c about 10 J/cm^3, nearly linearly with $D - D_c$.

The PBS resist developer and rinse solutions were purchased from KTI Chemicals, Inc. Resist was spun on 5 cm diameter polished Si wafers to thicknesses of 2500-3200 A at spin speeds in the range of 1000-1500 rpm. Coated wafers were pre-baked at 120°C for 30 minutes. After irradiation, development of exposed resist for 15 seconds at 21°C in MIAK/MPK (75%/25%) followed by a 60 second rinse in IPA/MIAK (60%/40%).

Developed resist thickness measurements were performed on a Rudolf Research ellipsometer (model Auto El III). Resist thicknesses in the range of 200-3000 A were generally encountered. Reproducibility of measurement was generally ± 5A. The dissolved resist thickness for a given region of exposed resist was determined by subtracting the measured resist height for that region from the measured height of the unexposed resist region.

The x-ray source used for these experiments was a Sloan multi-target E-beam evaporator unit with a 270° electron gun producing 10 keV electrons. Beam current was set for each target so that melting did not occur. The Au/C pellicle mask and the resist coated Si wafer were placed in a specially designed support 15 cm above the x-ray target. To protect the mask from excessive target heat, a 2.5 μm thick aluminized mylar shield was placed 5 cm beneath the mask. Pertinent data for x-ray production are listed in Table 2.

Experimental Results

The experimental data for dissolved PBS thickness (A) as a function of total carbon film thickness (A) is given in Figure 4 for five data runs made for three x-ray targets (Al,Ag and Ti). The irradiation times for these runs are as given in Table 2 and are roughly in inverse proportion to the x-ray absorption at the characteristic line wavelengths (Figure 2). Smooth curves (dashed curves in Figure 4) are drawn through the data points for each run. Each curve shows a steady decrease with increasing carbon thickness. As we find when we compare model predictions (solid curves in Figure 4) with the data, this persistent decrease rather than a more rapidly levelling off behaviour is attributable to the presence of higher energy electrons with a longer effective range in the PBS.

Theoretical

In this paper we consider energy deposition produced only by the characteristic x-rays from aluminum, silver and titanium at 1.49, 2.98 and 4.51 keV respectively. In calculating the dose profile, we employ the semi-empirical model of Burke, Garth and Chadsey extended from a two-medium to a two-medium, three-layer configuration. When we compare our predictions with the experimental data, we infer that the bremsstrahlung spectrum, particularly from the silver and titanium targets, is much more important than we first thought and probably dominates the characteristic x-ray line contribution. We intend to report the calculations taking into account the bremsstrahlung spectrum in a later publication.

Semi-Empirical Model Extension

The gold-carbon-PBS system is a three-medium transport problem; as far as the electron transport is concerned, the material geometry may be regarded as two semi-infinite slabs of gold and photoresist facing each other with an intervening layer of carbon of variable thickness. When the carbon thickness is zero, we have the two-medium problem described extensively in Burke and Garth[5] and Garth[8].

It turns out that within the approximations we employ, the formulas involving the transport properties of three different media are unnecessarily unwieldy and complicated. We therefore assume that we can treat the carbon and PBS as having the same transport (scattering) properties, but different source electron energies and intensities in regions separated by a plane representing the carbon/PBS interface. Hence we utilize formulas obtained by solving the "two-flux" transport equations[8] in two semi-infinite media with a plane partition in the second half space. Detailed derivations of these formulas will be published elsewhere[15].

In order to increase the speed of the computations (performed on a mini-computer), we approximated the full photoelectron and Auger electron spectrum arising from gold, carbon and PBS (some 30 different lines total!) using a single average electron energy and intensity for source electrons from each material (i.e., a total of three electron energies, one from each region). While this is not a particularly accurate approximation, it turns out that because of the neglect of the bremsstrahlung produced photoelectrons, a more accurate calculation for these lower energy electrons is unnecessary for the purposes of this paper.

Table 2. X-ray Exposure Data

Target Element /Char. Line	X-ray Energy (kev)	Electron Beam Power(W)	X-ray Power at 15 cm† (μW/cm^2)	PBS sensitivity* (mJ/cm^2)	Irrad. Time (min)	Unatten. resist dose** (J/cm^3)	Au atten. dose (J/cm^3)
Al Kα	1.49	400	42	17	20	55	2.33
Ag Lα	2.98	800	20	29	45	37	2.29
Ti Kα	4.51	100	6	117	240	15	4.2

† Based on a source/sample distance of 15 cm, and x-ray generation data from reference 14.

* Data obtained from reference 12, for a dose of 20 J/cm^3.

** Unattenuated dose delivered to surface of resist, not corrected for aluminized mylar electron shield nor 6800 A Au.

Application to Au/C/PBS

We first consider the case of Al K_α radiation (1.49 keV) impinging on the gold-carbon-photoresist system. In Figure 5, we show the predicted dose profile in Au/PBS when the carbon thickness is 0 A. The lower curves show the separate profile contributions induced in the system by the gold and PBS photo- and Auger electrons respectively. The upper curve gives the total dose profile obtained when the separate contributions are added together.

The important result for zero carbon thickness is that the relative dose in the PBS is a factor two higher at the interface than the equilibrium dose value (all doses are normalized relative to the equilibrium dose in PBS). In other words, there is a net dose enhancement in the PBS due to the photoelectrons introduced from the gold.

Figures 6 and 7 give the corresponding dose profiles for the case of 200 A and 400 A thicknesses of gold. Similar to Figure 5, the lower parts of each figure give the separate profiles due to electrons arising from gold, carbon and PBS and the upper curve shows the total dose profile. Figure 6 shows that the separate photoelectron contributions from the three regions have resulted in an essentially constant profile in the PBS while Figure 7 shows a slight net dose depression in the PBS next to the C/PBS interface.

Figure 8 shows the dose profile in Au/C/PBS for the case of Ti K_α radiation (4.51 keV) for 5 thicknesses of carbon ranging from 0 A to 800 A . As in the Al K_α case, the dose profile in PBS goes from a large net dose enhancement when the carbon thickness is zero to a net dose depression at the C/PBS interface as the carbon film thickness is made large.

Theoretical Response Curve

We are now in a position to make a theoretical estimate of the etched photoresist thickness vs carbon thickness for comparison with the experimental data. To make this estimate, we must use the mathematical form of the dose response curve (Figure 3) and an approximate exponential form for the dose profile shape in PBS.

We first note that, according to Figure 3, the etch rate in PBS as a function of the surface dose D is given by the equation

$$dx/dt = k\,[D(x) - D_c] \qquad (1)$$

where dx/dt is the etch rate (in A/min), D_c is the "critical dose" (where the dose response curve goes to zero), D(x) and D_c are given in J/cm3, and k is a proportionality constant approximately equal to 460 (A/min)/(J/cm3). D(x) is a known function of x, and equation (1) describes the fact that, as material is etched off, the surface position sweeps through the dose profile and the rate of etch varies with the position according to the exposure received at location x.

As the resist is etched in a predetermined length of time T, the photoresist is etched off to a distance L. To obtain L, we separate the variables x and t in equation (1) and integrate:

$$T = \int_0^T dt = \frac{1}{k}\int_0^L \frac{dx}{[D(x) - D_c]} \qquad (2)$$

If the dose profile in the PBS has the approximate form

$$D(x) = A(d)\exp(-Bx) + C \qquad (3)$$

where A may be positive, zero, or negative and C is the equilibrium dose, we can integrate equation (2) analytically. Then, with some manipulation, we obtain the analytic expression

$$L = (1/B)\log([1+A/(C-D_c)]\exp(-B\,L_0) - A/(C-D_c)) \qquad (4)$$

where L_0 is defined as

$$L_0 = k\,T\,(C - D_c). \qquad (5)$$

We next need to obtain a prediction for the etched thickness L as a function of the carbon thickness d. We assume (in equation (3)) that the dose profile D(x) depends on d only through the amplitude A(d), which goes from a large positive value (enhancement) to a small negative value (depression). Actually D(x) in the PBS consists of three contributions from photoelectrons from each material each of which has slightly different exponential behaviour depending on the electron energy. According to the semi-empirical model extension[15], the sum of the three dose contributions has the form

$$D(x) = A_1(d)\exp(-B_1x) + A_2(d)\exp(-B_2x) - A_3(d)\exp(-B_3x) + C \qquad (6)$$

where the indices 1, 2 and 3 refer to photoelectron contributions from the three media gold, carbon and PBS respectively.

We make the simplifying approximations that

$$A(d) = A_1(d) + A_2(d) - A_3(d) \qquad (7)$$

and

$$B = (1/3)(B_1 + B_2 + B_3) \qquad (8)$$

which we insert into equation (3). If A(d) has the simple form A(0) exp (-B d), the shape of L as a function of d is shown schematically in Figure 9 in which L starts with a maximum at d = 0 and rapidly reaches a flat plateau as d increases. The more complete expression (7) turns out to have about the same shape as Figure 9.

Etched Thickness vs Carbon Thickness Comparison

Figure 4 shows the comparison of our theoretically predicted etched resist thickness curves with the experimental data we discussed earlier. Each theoretical curve has a shape similar to Figure 9 and flattens out much sooner than the corresponding experimental data. The height of each theoretical curve has been adjusted to lie near the experimental points by adjusting the value of the equilibrium dose C.

The discrepancy between theory and experiment which can be qualitatively explained by the presence of higher energy electrons probably due to bremsstranlung radiation from the targets. This discrepancy might be reduced experimentally by filtration to increase the characteristic line-to-bremsstranlung intensity ratio. To account for it theoretically would require estimating the intensity of the bremsstrahlung spectrum and performing a sum of electron dose profile contributions resulting from these

x-rays. This is a much lengthier computation and has not been done to date.

Discussion

Does this experimental technique have promise as a practical dosimeter for measuring dose profiles over distances of several hundred Angstroms? For example, it would be of interest in dosimetry of microelectronics in x-ray and gamma-ray environments to be able to measure changes in dose over very small distances near device material interfaces and boundaries.

It is not easy to answer this question at this time since there are still a number of experiments and calculations that need to be done for known x-ray spectra in the 1 - 10 keV range. Our etched thickness vs carbon thickness measurement seems to give a rather crude integral measurement of the dose profile and is inherently a low resolution measurement without much energy or shape discrimination. Hence, it appears that this technique is not very useful without a fair degree of knowledge of the x-ray spectrum present. Furthermore, as x-ray energies increase above 10 keV, the thicknesses of etched photoresist may become excessively large (thousands of Angstroms).

On the other hand, when the x-ray spectrum can be reasonably well estimated or determined, the semi-empirical electron transport model will furnish a convenient method for predicting dose profiles in multi-layered structures. The experimental technique could then be used as a verification procedure to check the model prediction for the test x-ray environment.

A number of follow-up experiments are underway and planned. Data has already been obtained for the same three target spectra for the silver/carbon/PBS system. If thin enough films of PBS can be constructed, a gold/PBS/.../PBS mask could be made, thus allowing measurements characteristic of the gold/PBS system without a third medium present to be made. Finally spectra can be filtered to change the relative amount of characteristic line and bremsstrahlung content in the x-ray spectrum.

Several refinements in the theoretical modelling could be made:

1. As already stated, the contribution of the bremsstrahlung portion of the x-ray spectrum should be taken into account, the resulting photo and Auger electrons generation determined, and the dose profiles calculated.

2. Instead of using a single average electron energy and intensity in each medium for each x-ray energy, the more complete specification of the photoelectron - Auger spectrum for each photon energy could be taken account in the photoelectron source functions used to generate the electron dose profiles.

3. A full solution of the three-medium, "two-flux" transport equation would result in a more complicated but exact treatment of the electron dose profile.

4. The exponential shape of the dose profiles inherent in the semi-empirical transport model overestimates the extent to which electrons arising in one medium penetrate another. Because the average electron energy in the electron flux drops rapidly with increasing depth of penetration, the dose profiles will drop more rapidly to zero than the exponential shape indicates. However, we believe this effect is relatively unimportant compared to 1, 2 and 3 above.

5. Rather than use the analytic model formula of equation (3), a numerical integration over the exact profile according to equation (2) should be performed. The disadvantage of this is that the etched thickness L is then no longer directly obtainable in closed form, but, as the undetermined upper limit of an integral, must be found by an indirect numerical procedure.

On the other hand, except for consideration 1 above, in view of the inherent coarseness and low "resolution" of the experimental data and the uncertainties in the x-ray intensity and equilibrium dose level in the photoresist, it is doubtful that some of the above refinements will be necessary.

Summary

The principal results of this study are:

1. We have applied the photoresist etching technique developed by Maldonado et al in the context of x-ray lithograpny to the problem of measuring energy deposition profiles in a different system with better defined material properties (i.e., no unspecified organic layers or resists). Some capabilities and limitations of the technique have been demonstrated for obtaining an indirect measurement of the dose profiles in a three-layer system over the dimensions of several hundred Angstroms.

2. We have successfully applied a three-layer extension of the semi-empirical electron transport model of Burke, Garth and Chadsey to obtain useful predictions of the dose profile.

3. Using the exposure characteristics of the resist, we derived a theoretical estimate of the etched resist thickness vs carbon thickness of the Au/C/PBS system. A quantitative discrepancy was found when compared with the experimental data. This discrepancy is due to the apparent contribution of high energy electrons observed experimentally. This could probably be accounted for theoretically if the bremsstrahlung components as well as the characteristic line components of the x-ray spectra are taken into account.

The authors would like to acknowledge the valuable contributions of Mr. Joseph J. Comer of the Solid State Division at RADC for preparing the carbon films for the experimental mask used in our experiments.

References

1. See, for example, R. Feder, E. Spiller and J. Topolian, J. Vac. Sci. Tech. 12, 1332 (1975).

2. E. A. Burke and J. C. Garth, IEEE Trans. Nucl. Sci. NS-26, 4868 (1979).

3. J. R. Maldonado, G. A. Coquin, D. Maydan, and S. Somekh, J. Vac. Sci. Tech. 12, 1329 (1975).

4. E. A. Burke (private communication).

5. E. A. Burke and J. C. Garth, IEEE Trans. Nucl. Sci. NS-23, 1838 (1976).

6. E. A. Burke, IEEE Trans. Nucl. Sci. NS-24, 2505 (1977).

7. W. L. Chadsey, IEEE Trans. Nucl. Sci. NS-25, 1591 (1978).

8. J. C. Garth, IEEE Trans. Nucl. Sci. NS-28, 4145 (1981).

9. P. A. Sullivan and J. H. McCoy, IEEE Trans. Electron Devices, ED-23, 412 (1976).

10. K. F. Galloway, S. Mayo, and P. Roitman, J. Electrochem. Soc. 126, 2245 (1979).

11. L. F. Thompson and M. J. Bowden, J. Electrochem. Soc. 120, 1722 (1973).

12. P. D. Blais, "X-ray Resist Technology", Kodak Microelectronics Seminar Proc. Interface '80, Kodak Report No. G-130, p. 79.

13. P. D. Blais, Westinghouse R&D Center, Pittsburgh, PA, private communication.

14. M. Green and V. E. Cosslett, Brit. J. Appl. Phys. 2, 425 (1968).

15. J. C. Garth (to be published).

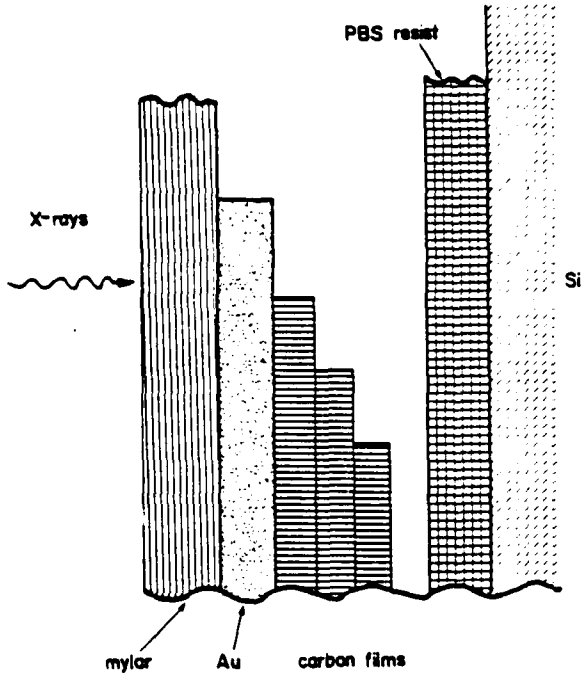

Figure 1. Experimental Au/C mask and PBS film configuration.

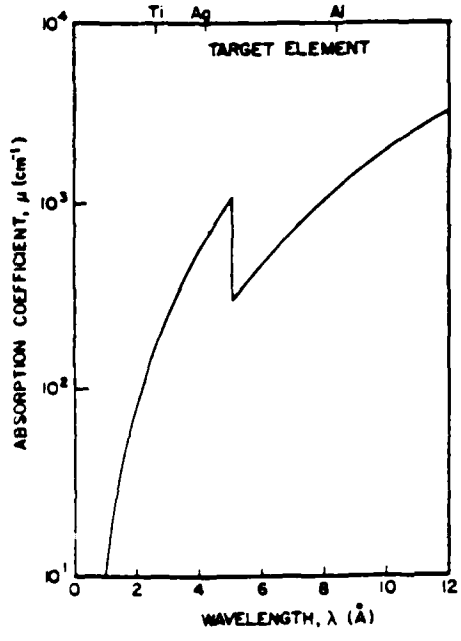

Figure 2. X-ray absorption coefficient vs wavelength (Å) for PBS.

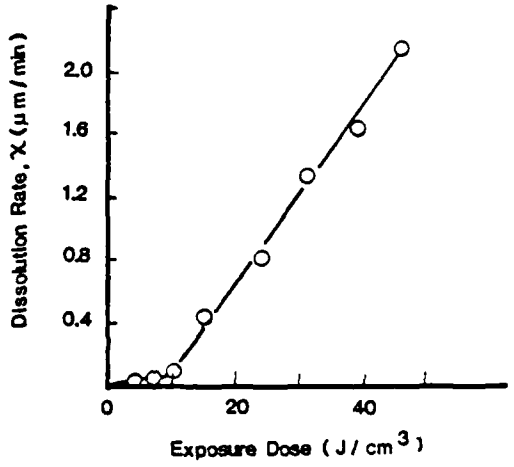

Figure 3. PBS characteristic exposure curve.

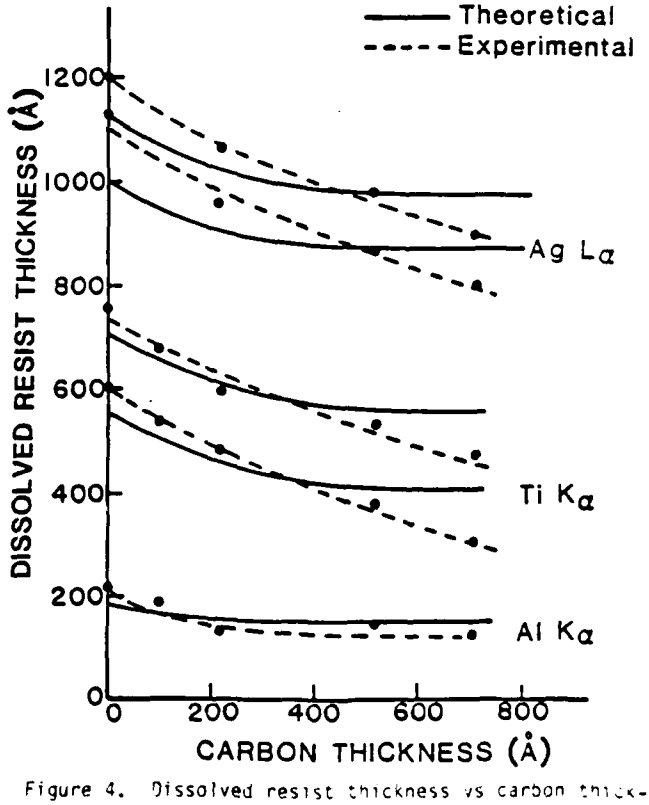

Figure 4. Dissolved resist thickness vs carbon thickness. The filled circles are the data points, the dashed curves are smooth curves drawn through the data, and the solid curves are the theoretical predictions (where the equilibrium dose parameter has been adjusted to bring each curve close to the experimental data).

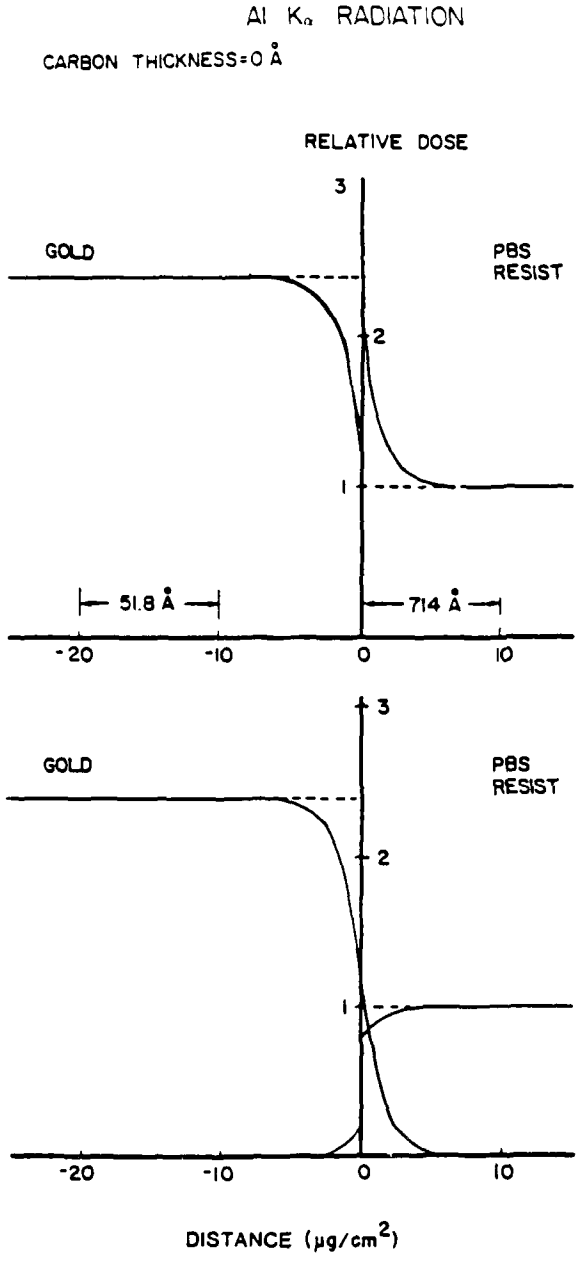

Figure 5. Semi-empirical model dose profiles for Al K_α x-rays in Au/PBS (carbon layer thickness = 0 A). Upper curve: total dose profile. Lower curves: individual profiles due to gold and PBS photoelectrons.

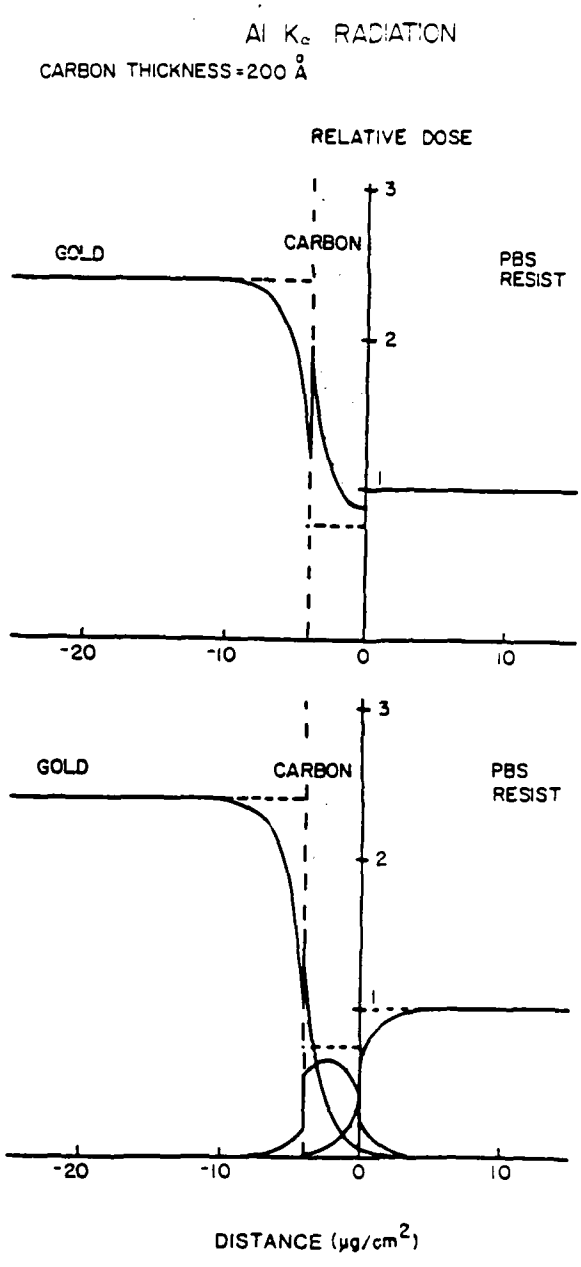

Figure 6. Semi-empirical model dose profiles for a 200 A thick carbon layer in Au/C/PBS. Upper curve: total dose profile. Lower curves: individual profiles due to gold, carbon and PBS photoelectrons.

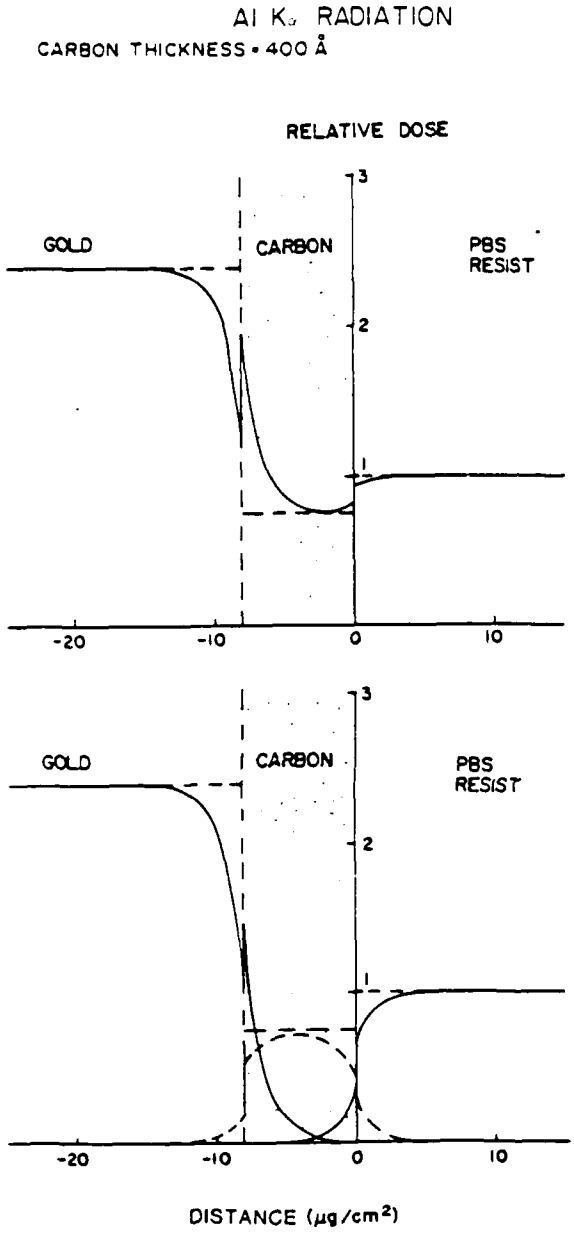

Figure 7. Same as Figure 6 but for a 400 Å thick carbon layer.

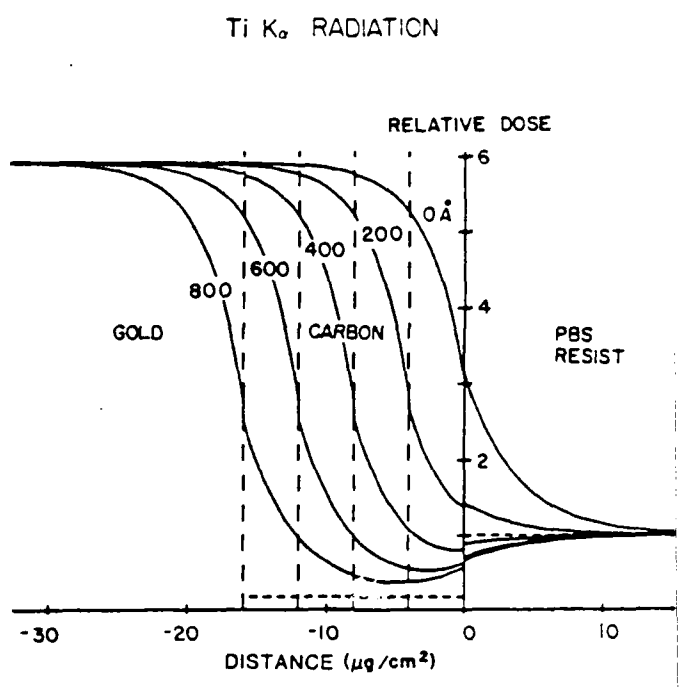

Figure 8. Semi-empirical model dose profiles for Ti K_α x-rays in Au/C/PBS for five thicknesses of carbon (0, 200, 400, 600, and 800 Å).

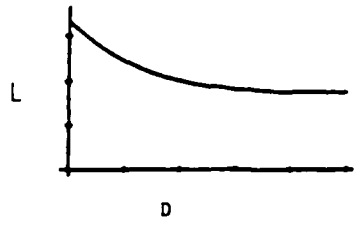

Figure 9. Schematic curve of etched thickness L vs carbon thickness d (see text).

APPENDIX 2

J. C. Garth; Proc. of SPIE, Vol. 393, Electron-Beam,
X-ray and Ion-Beam Technologies for Submicrolithographies II
Mar. 14-15, 1983, pp. 78-86.

Theoretical model for photoelectron transport in x-ray lithography systems

J. C. Garth
Solid State Sciences Division, Rome Air Development Center
Hanscom Air Force Base, Massachusetts 01731

Abstract

We have developed a theoretical model for calculating the dose received by a resist behind an x-ray absorbing mask in an x-ray lithography system. The model enables the dose-depth profile due to photoelectrons entering the resist from the mask to be predicted as a function of x-ray target material, excitation voltage, mask material and thickness, and chemical composition of the resist.

As an application, we have calculated the dose profile in the resist PBS next to a Au mask irradiated by x-rays from Ag and Al targets operated at 10 kilovolt beam voltage. The characteristic line and continuum spectrum from the targets are computed, the absorption by the Au mask obtained, and an approximate photoelectron and Auger electron spectrum in the gold and PBS is evaluated. The dose-depth curve next to the gold-resist interface is found using the analytic electron transport model developed by Burke and Garth (1979). The calculations show that the dose profiles obtained using bremsstrahlung-produced electrons extend deeper than profiles that are computed from characteristic photon radiation alone. At 10 kV, this effect is found to be much greater for Ag than for Al.

Introduction

Various combinations of x-ray sources, mask materials, and resists have been considered for x-ray lithography systems. A key factor of interest in x-ray lithography is image contrast, the ratio of the x-ray resist dose without mask absorption to the dose with the absorber present. The dose from photoelectrons injected into the resist from the absorber lowers this ratio and hence is undesirable.

Photoelectron generation in x-ray lithography configurations has been examined experimentally[1,2,3], but only one detailed theoretical study has been published.[4] Maldonado et al.[1] made the first study of photoelectron effects and developed the method of measuring the dose using the technique of measuring the resist etch rate as a function of thickness of an intervening layer between the mask and the resist. Hundt and Tischer[2] pointed out the effect of dose enhancement by the substrate as well as the mask, while Saitoh at al[3], using a Mo x-ray source, a Au mask and several resists (FPM, SEL-N, and CMS), found that image contrast could be improved considerably by introducing a 6 micron thick mylar film between the mask and the wafer. They also pointed out that the continuum radiation generated at the same time as the Mo L_α radiation is filtered less by the gold mask and is responsible both for more photons and more energetic electrons than the characteristic line radiation.

Recently Garth, Murray and Dolan[5] studied the system of the resist PBS (Poly(butene-1 sulfone)) next to a gold mask with various layers of evaporated carbon separating the gold and the resist (Figure 1). Three different x-ray target spectra were used: Al, Ag, and Ti bombarded by 10 keV electrons (a Sloan E-beam evaporator unit was used as the source). Measurements of the etched PBS thickness were made as a function of the thickness of the carbon layers (Figure 2). Two data sets each were taken for Ag and Ti x-rays and one for Al. Theoretical predictions were made assuming that the x-rays were monochromatic with the characteristic lines from the targets (Al K_α (1.49 keV), Ag L_α (2.98 keV), and Ti K_α (4.51 keV)). Qualitative agreement was found, but the experimental curves do not reach a plateau with increasing carbon thickness as soon as the theoretical model. We believe that this indicates the presence of electrons of higher energy than those included in the model.

The purpose of this paper is to describe a method for calculating the dose profile in the x-ray resist taking into account the full characteristic line plus continuum spectrum from the x-ray target. We have applied it to the case of PBS next to a 6800Å thick gold mask irradiated by x-rays from Ag and Al excited at 10 kV. In the case of Ag, it is apparent from the calculated photon spectrum after filtration by the Au that the contribution to the dose in the x-ray resist due to the continuum spectrum considerably exceeds the characteristic line contribution.

Theoretical Model

The model consists of three main parts. These parts consist of prediction of (1): the photon intensity spectrum from a target anode, including the effects of target absorption and filtration by the Au mask, (2) the energy spectrum of the dose due to photoelectrons and Auger electrons generated in the mask and the resist, and (3) the electron dose profile in the resist obtained using a simple analytic transport model.

Photon spectrum

It was surprisingly difficult to locate a complete algorithm for finding both the characteristic line intensity and the continuum spectrum from an x-ray target. A highly recommended, but fairly complicated, algorithm is the TUBE algorithm contained in the large x-ray fluorescence code "NRLXRF" developed by J. W. Criss.[6] Brown and Nagel[7] have recently described an improved, but not yet available version of TUBE and show comparisons of predicted spectra with experimental results.

After examining TUBE from NRLXRF, we decided to develop a simplified algorithm involving fairly low memory storage which we could programm in BASIC for our Tektronix 4051 minicomputer. For the principal characteristic x-ray line for the target, we used fit formulas for the K and L line efficiency obtained by Blais[8] from data by Green and Cosslett.[9] The number of photons per incident electron N is given by

$$N = \varepsilon \ (E_0 - E_x)^{1.63} \qquad (1)$$

where E_0 is the incident electron energy (keV), E_x is the shell ionization energy, and the efficiency ε is

$$\varepsilon = 3.2\text{x}10^{-4}\ e^{-z/10.92} \tag{2}$$

and

$$\varepsilon = 8.5\text{x}10^{-5}\ e^{-z/32.0} \tag{3}$$

for Kα and Lα radiation respectively (Z is the atomic number of the target).

As in the TUBE algorithm, we used the well-accepted[10] formula of Kramer for the continuum spectrum

$$N_c(E) = k\ Z\ (E_0 - E\ )/E \quad \text{(photons/electron/keV)} \tag{4}$$

where E_0 and E are the electron beam and photon energies respectively (keV) and we used the value $k = 2.2 \times 10^{-6}$. Also as in TUBE, we corrected this spectrum for target absorption using the Philibert correction formula.[10]

To save computer memory, we used the x-ray parameter fits originally in the FRAME code[11] (listed by Shen and Russ[12]) to give a simple method for obtaining x-ray absorption coefficients, absorption edge energies, and energies of characteristic lines of all elements and compounds used for target, mask and resist.

As an example of this part of our algorithm, we have calculated the x-ray photon intensity spectrum from Ag (Figure 3) and Al (Figure 4) for 10 kV beam voltage. In each case, there are three curves: (a) the spectrum uncorrected for x-ray absorption within the target, (b) the spectrum after correction, and (c) the spectrum after filtration by a Au mask. The height of the characteristic line peak has the units of number of photons per incident electron while the continuous curve is in units of photons/keV per incident electron. (To make a valid comparison of the relative strength of these contributions, the height of the characteristic peak should be compared to the area of the continuum curve over a 1 keV interval.)

Comparing Figures 3 and 4, we see that the magnitude of the continuum in Al is about a third that of silver, while the Al K_α line height is greater than that of Ag L_α. Though the continuum in Al is not negligible, we shall find later on that it makes very little difference to the photoelectron dose profile. The spectrum in Figure 3 clearly shows, however, that after filtration by the Au mask, bremsstrahlung intensity dominates the characteristic line intensity; We find later that the shape of the calculated dose profile reflects this, but perhaps not as much as one might expect.

At this point, we have sufficient information to calculate the photon absorption dose to the resist (and to the Au mask, if desired). Denoting the filtered spectrum (as shown in Figures 3c and 4c) by $g(h\nu)$ and neglecting electron transport effects, the total dose in the mask and resist are given by

$$D_{io} = \int_{h\nu(min)}^{h\nu(max)} g(h\nu)h\nu\ \mu_i(h\nu)d(h\nu)\ , \qquad i = 1,\ 2 \tag{5}$$

where $h\nu$ is the photon energy, and $\mu_i(h\nu)$ is the x-ray absorption

coefficient for the ith material (i = 1 for gold and 2 for PBS). For the range of integration, we have used $h\nu(max)$=10 keV and $h\nu(min)$=1 keV.

Photoelectron Spectrum

The energies and intensities of photoelectrons and Auger electrons in the mask and the resist are needed for calculating the photoelectron contribution to the dose at the gold-resist interface. Since each element has its own peculiar energy level structure, we illustrate our calculational approach with Au and PBS as our main examples.

Photoelectron energies. Let us first consider the photoelectron energies: Photons in the energy range from 1 to 10 keV are absorbed by exciting electrons in the inner shells of atoms in the mask and resist (Au, PBS). The photoelectron energy is just

$$E = h\nu - E_b \qquad (6)$$

where E_b is the shell binding energy. For example, there are five M-levels in Au in the 1 - 10 keV energy range. For photons below the M_5 edge (2.22 keV), we assume that photoelectrons are excited only from the highest N shell (.76 keV). At the other extreme, above the M_1 edge (3.45 keV) photoelectrons from all five M levels and the N level are excited, giving rise to photoelectrons with six different energies.

Auger electron energies. In principle, there are a large number of Auger transitions of a given type (KLL, LMM, LMN, etc.) that can contribute to Auger electron generation[13]. Looking at published Auger electron data[14], there is a principal MNN Auger peak for Au at 2.02 keV and a KLL peak for S (in PBS) at 2.105 keV. We make the possibly too crude assumption that only one Auger electron energy is produced when a given shell is excited (K, L, M, etc.). We will assume that when any of the M levels of Au are excited, 2.02 keV Auger electrons are produced in gold and if the K level of sulfur in PBS is excited, a 2.105 kev Auger electron is produced.

Electron Intensities. The intensities of photoelectrons and Auger electrons are determined as follows:

(1) For each photon absorbed, we assume there is one photoelectron and one Auger electron being generated. If an electron is excited with energy below 1 keV we neglect it, since the electron range is too short for it to transport appreciably.

(2) If more than one level is excited, the relative probability of excitation of a given shell is proportional to the photoionization cross-section of the shell. Theoretical photoionization cross-sections as a function of photon energy for each element have been calculated and tabulated by Scofield[15].

Since it is awkward to use the Scofield cross sections, we use the simpler approach for obtaining the excitation probability described by Burke.[16] To illustrate the method, for simplicity, we consider the excitation of K and L shells near the K edge photon energy. The well-known "jump ratio" of the absorption coefficients just above and below a K edge energy is set equal to $(P_L + P_K)/P_L$ where P_L and P_K are the probabilities of excitation of the K and

L shell respectively. If we assume that the excitation of other levels is negligible, the total excitation probability, $P_L + P_K$, of all levels = 1. It follows that P_L equals the reciprocal of the K jump ratio. If we now neglect the variation of P_K and P_L with energy, we can calculate the intensity of K and L photoelectrons for any energy in this case. Neglecting fluorescence, if a K Auger electron is produced each time when a K shell is excited, the probability of excitation of a K Auger electron equals P_K.

Application to Au and PBS. In Figures 5 - 8, we have plotted the energy-intensity spectrum of photoelectrons and Auger electrons calculated for Au and PBS respectively, resulting from excitation by the x-ray spectrum q(hυ) after filtration by the gold. Rather than calculate a continuum of photoelectron energies, we adopted the approach of representing the continuum spectrum by a series of "lines" centered around the 9 energies, 1.5, 2.5,...,9.5 keV, with heights obtained by integrating the area under q(hυ) over 1 keV photon energy widths. This is in turn produced photoelectron "lines" spaced 1 keV apart in Figures 5 - 8. Each line represents an electron group that contributes to the calculated dose-depth profile in the resist.

What is calculated and plotted is the energy spectrum of the dose contribution of each photoelectron and Auger electron energy group. This dose contribution is defined by

$$\text{"electron dose"} = p_i E_i \; G(h\upsilon) \; \mu(h\upsilon) \quad (\text{keVcm2/g}) \tag{7}$$

where G(hυ) is the integral of q(hυ) over a 1 keV photon energy interval, μ is the absorption coefficient (Au or PBS), and E_i and P_i are the energy and excitation probability for each electron. The quantity above appears directly as a coefficient of the dose profile contribution we calculate later on.

The plots in Figures 5 - 8 give a great deal of insight as to what happens when Au and PBS are excited by Ag and Al spectra. First, in both cases, there is a far greater dose contribution by Au electrons than by those from PBS, since there is much greater x-ray absorption in Au. Secondly, there is a large Auger peak in both Au and PBS, because the same level giving rise to a series of photoelectron energies produces only an Auger electron of only one energy (by our assumption). Thirdly, the characteristic line contribution to the dose is clearly distinguishable in the Al spectrum (Figs. 7 and 8), but not in the Ag spectrum (Figs. 5 and 6). Finally, the bremsstrahlung has produced most of the electron dose intensity in Figures 5 and 6, but only a small amount in Figures 7 and 8.

Electron Dose Profile

Transport Model. The gold mask next to a resist irradiated by soft x-rays is an example of a two-medium electron transport problem in which electrons originating in either material move, scatter and lose energy depositing energy and charge on both sides of the interface. The gold and PBS may be regarded as semi-infinite media, because the electron range of electrons with 10 keV energy or below is less than the thickness of either material. The usual approach employed for modelling electron transport is the well-known Monte Carlo method.[17] In the absence of simpler analytical methods, this method is reliable, but it is also tedious and quite expensive in computer time.

The semi-empirical model for electron transport[4,16,18-20] was developed for calculating energy deposition near the plane interface between two semi-infinite media by x-ray produced electrons over the range from 1 keV to over 1 MeV. It had its beginning as a fit to Monte Carlo calculations for gold-silicon and gold-polyethylene interfaces[21]. By employing the concept of electron reflection back and forth between media with reflection coefficient equal to the electron backscatter coefficients of each material, a predictive model was developed which fit the Monte Carlo data well. This model involves a sum of simple exponential functions, each describing the contribution to the transport by a single energy group. Found to be an excellent first-order fit to the Monte Carlo data over the photon energy range from 10 keV to 2 MeV, it was extended down to 1 keV, adapted to predict x-ray photoemission from a material surface and was found to check well with published experimental x-ray photoemission data.[16]

Dose-Depth Relations. Let us first consider a beam of monoenergetic photons of energy $h\nu$ incident on the mask-resist interface. Consider the mask (Au) as medium 1 and the resist (PBS) as medium 2, characterized by the absorption coefficients μ_1 and μ_2 respectively. Let the photoelectrons or Auger electrons be excited with energies E_j and E_k and excitation probabilities p_j and p_k respectively. Then the dose in medium 2 as a function of distance x (expressed in gm/cm2), due to the electrons of energy E_j excited in medium 1, is given by[4]

$$D_{21}(x;E_j;h\nu) = \mu_1 p_j E_j \frac{R_1(E_j)}{R_2(E_j)} \frac{(1-\beta_1)(1+\beta_2)}{2(1-\beta_1\beta_2)} \exp(-B_2(E_j)x) \qquad (8)$$

where the coefficient $B_2(E)$ is given by the equation

$$B_2(E) = \frac{1-\beta_2}{1+\beta_2} \frac{2}{R_2(E)} \frac{n_2+1}{n_2} \qquad (9)$$

and the β_j and $R_j(E)$ are the backscatter coefficients and CSDA electron ranges for the two media, and n_2 is the power of energy in the range-energy relation for calculating $R_2(E)$. For complete definitions and methods for evaluating all transport parameters, we refer the reader to reference 4.

The total dose at a given photon energy due to x-ray absorption in medium 2 is simply

$$D_{20}(h\nu) = \mu_2(h\nu)\, h\nu \qquad (10)$$

To this should be added negative dose terms corresponding to the transport of electrons of energies E_k away from medium 2 into medium 1, i.e.,

$$D_{22}(x;E_k;h\nu) = -\mu_2 p_k E_k \frac{(1-\beta_2)(1+\beta_1)}{2(1-\beta_1\beta_2)} \exp(-B_2(E_k)x) \qquad (11)$$

The D_{21} and D_{22} terms should now be summed over each photoelectron and Auger electron energy produced by hν. In addition, for the spectrum of photons $q(h\nu)$, an integration of D_{21} and D_{22} with respect to hν must also be performed. (We have done this by summing over the dose contributions from the characteristic line plus 9 bremsstrahlung "lines" previously described.) The total dose in medium 2 is therefore given by

$$D_2(x) = \int_{h\nu(min)}^{h\nu(max)} q(h\nu)d(h\nu)\{ D_{20}(h\nu) + \sum_j D_{21}(x;E_j;h\nu) + \sum_k D_{22}(x;E_k;h\nu) \} \qquad (12)$$

The relative dose may then be defined by $D_2(x)$ divided by D_{20} as given by equation (5).

Application to PBS next to Au. The calculated relative dose profile in PBS for Ag and Al x-rays is shown in Figures 9 and 10. The curves obtained show the results for the case when the continuum spectrum is included and when it is left out. There is a clear difference between the curves in Figure 9, but the difference is not spectacular. With the continuum present, there appears to be a residual dose that penetrates deep into the resist due to the electrons of highest energy (3 - 7 keV, according to Figure 5). There is a small difference between the curves in Figure 10, yet the effect of the continuum contribution can be clearly seen.

A comparison of Figure 9 and 10 shows that the "mean" depth of the photoelectron-produced profile for the Ag spectrum is at least twice that of Al (about 400Å compared with 200Å). This is confirmed, at least qualitatively, by the experimental results in Figure 2.

Model Limitations

We wish to make some caveats regarding some uncertainties in the theoretical model given above. In developing the algorithm for the x-ray spectrum, it was difficult to arrive at a consensus for the magnitude of the constant k for the Kramer's bremsstrahlung spectrum (equation (4)). We used the value $k = 2.2 \times 10^{-6}$, but the value $k = 1.4 \times 10^{-6}$ would be obtained using the equations given by Evans.[22] The values of the continuum calculated by the recent version of TUBE[7] were some 25% higher than we have obtained.[23] We believe that the magnitude of the bremsstrahlung we predict is within a factor of 2 of what others would calculate; this does not qualitatively affect our conclusions as to the relative importance of bremsstrahlung.

Other uncertainties in the model include: (1) we have not yet located a theory that predicts the energies and intensities of x-ray produced Auger electrons. The tables by Coghlan and Clausing[13] have been the best guide we have found. (2) As pointed out in reference 5, exponentially-shaped dose profiles are not valid far from the interface. Unfortunately there are no better simple predictions available without going to a Monte Carlo calculation. (3) There have been few experiments to measure electron transport in the 1 - 10 keV energy range. The x-ray photoemission version of the semi-empirical model[16] gives good agreement with experiment, but the validity of the use of a CSDA electron range at these energies is open to question. Electron

transport in the 1 - 10 keV energy range is not yet well understood.

Summary

We have developed a flexible theoretical model for the soft x-ray photoelectron-produced dose profile in a resist next to absorbing mask. We have illustrated all stages of the model by calculating the relative dose profile in the resist PBS next to Au exposed to 10 kV x-rays from Ag and Al. The depth of the profiles predicted using the characteristic line photons from Ag and Al was enhanced by bremsstrahlung-induced electrons in Ag, but the small amount of bremsstrahlung from Al gave little change in the profile.

In the near future, we will extend this model to predict etched resist thickness vs carbon thickness response for comparison with new experimental data obtained recently by Murray and Dolan.[24] At the same time, we will be checking our model against data for x-ray spectra from other target elements and other mask materials beside Au.

Acknowledgements

The application of the semi-empirical electron transport model to x-ray lithography was begun by E. A. Burke of our laboratory. I also would like to thank him for his encouragement, Brian Murray and Russ Dolan of Spire Corporation for their enthusiasm and experimental support and P. A. Blais of Westinghouse Research and Development for valuable technical advice.

References

1. J. R. Maldonado, G. A. Coquin, D. Maydon, and S. Somekh, J. Vac. Sci. Technol. 12, 1329 (1975).
2. E. Hundt and P. Tischer, J. Vac. Sci. Technol. 15, 1009 (1978).
3. Y. Saitoh, H. Yoshihara and I. Watanabe, Jpn. J. Appl. Phys. 21, L52 (1982).
4. E. A. Burke and J. C. Garth, IEEE Trans. Nucl. Sci. NS-26, 4868 (1979).
5. J. C. Garth, B. W. Murray and R. P. Dolan, IEEE Trans. Nucl. Sci. NS-29, 1985 (1982).
6. J. W. Criss, "NRLXRF", COSMIC Program and Documentation DOD-65, Computer Software Management and Information Center, University of Georgia, Athens, GA 30602 (1977 and updates).
7. D. B. Brown and D. J. Nagel, Low Energy X-ray Diagnostics - 1981, edited by D. T. Attwood and B. L. Henke, AIP Conference Proceedings No. 75, American Institute of Physics, New York (1981).
8. P. A. Blais (private communication).
9. M. Green and V. E. Cosslett, J. Phys. D. 1, 425 (1968).
10. K. F. J. Heinrich, Electron Beam X-Ray Microanalysis, Van Nostrand Reinhold Co., New York (1981).
11. H. Yakowitz, R. L. Myklebust, and K. F. J. Heinrich, NBS Technical Note 796 (1973).
12. R. B. Shen and J. C. Russ, X-ray Spectrometry 6, 56 (1977).
13. W. A. Coghlan and R. E. Clausing, Atomic Data 5, 317 (1973).
14. W. Palmberg, E. Riach, E. Weber and N. C. MacDonald, Handbook of Auger Electron Spectroscopy (Physical Electronic Industries, 7317 South Washington Avenue, Edina, Minnesota 55435, 1972)

15. J. H. Scofield, Theoretical Photoionization Cross Sections from 1 to 1500 keV, Lawrence Livermore Laboratory Report UCRL-51326 (January 1973).
16. E. A. Burke, IEEE Trans. Nucl. Sci., NS-24, 2505 (1977).
17. Of many possible references, a good collection of papers pertinent to kilovolt electron Monte Carlo is Use of Monte Carlo Calculations in Electron Probe Microanalysis and Scanning Electron Microscopy, edited by K. F. J. Heinrich, D. E. Newbury and H. Yakowitz, NBS Special Publication 460 (Dec. 1976).
18. E. A. Burke and J. C. Garth, IEEE Trans. Nucl. Sci. NS-23, 1838 (1976).
19. J. C. Garth, IEEE Trans. Nucl. Sci. NS-25, 1598 (1978).
20. J. C. Garth, IEEE Trans. Nucl. Sci. NS-28, 4145 (1981).
21. J. C. Garth, W. L. Chadsey and R. L. Sheppard, IEEE Trans. Nucl. Sci. NS-22, 2562 (1975).
22. R. D. Evans, "The Atomic Nucleus", McGraw-Hill, New York, 1955.
23. D. B. Brown (private communication).
24. B. W. Murray and R. P. Dolan (private communication).

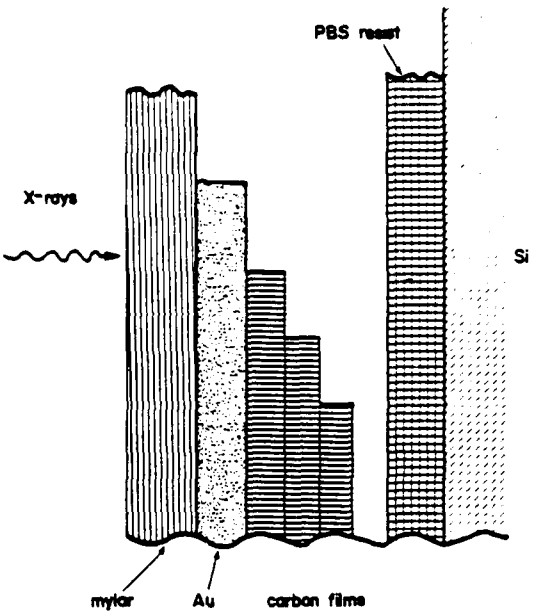

Figure 1. Experimental Au/C mask and PBS film configuration used by Garth, Murray and Dolan (ref. 5).

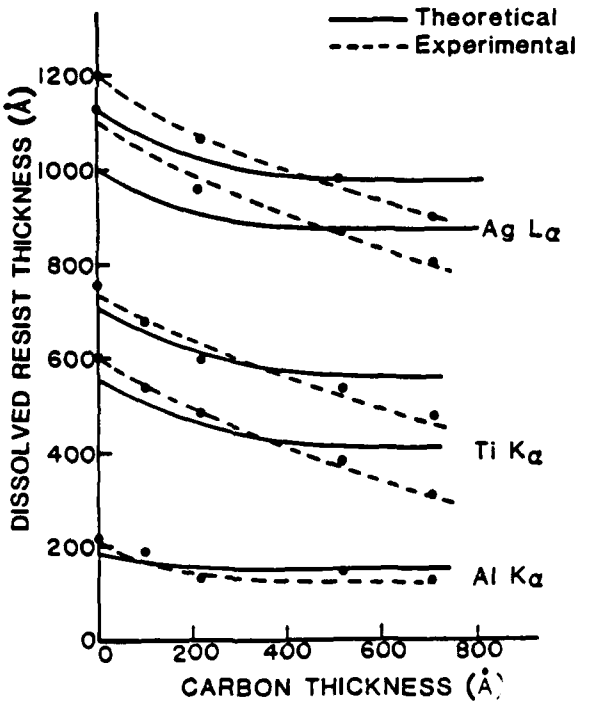

Figure 2. Etched PBS thickness vs carbon film thickness exposed to 10 kV x-rays from Ag, Ti and Al. Electrons produced by bremsstrahlung were not included in the theoretical curves (solid lines).

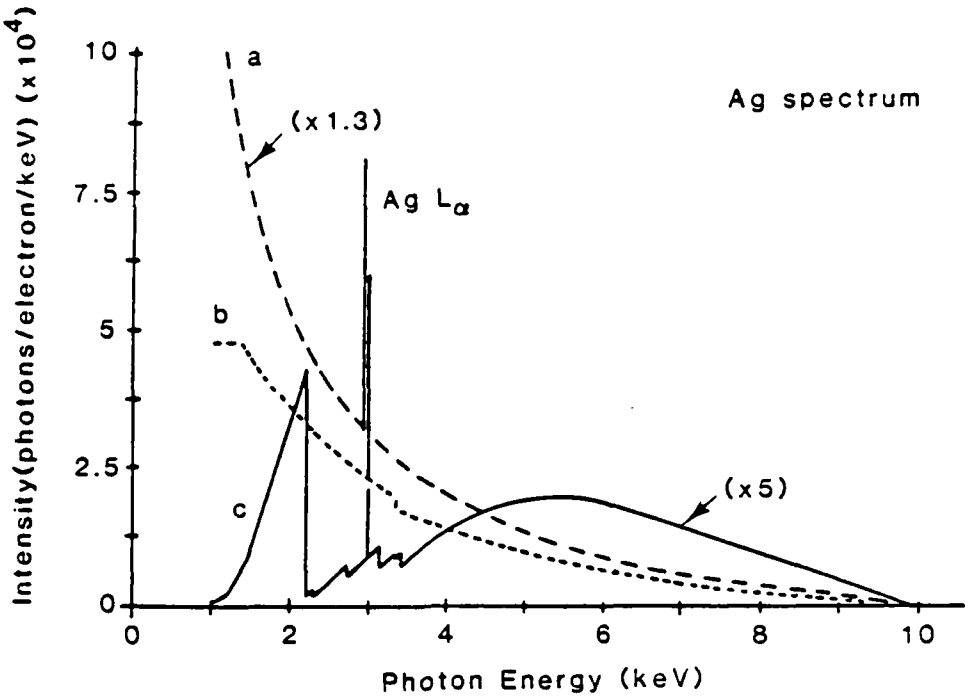

Figure 3. Calculated photon spectrum from Ag at 10 kV. a. Uncorrected for Ag target absorption. b. Corrected for absorption. c. Filtered by 6800Å Au.

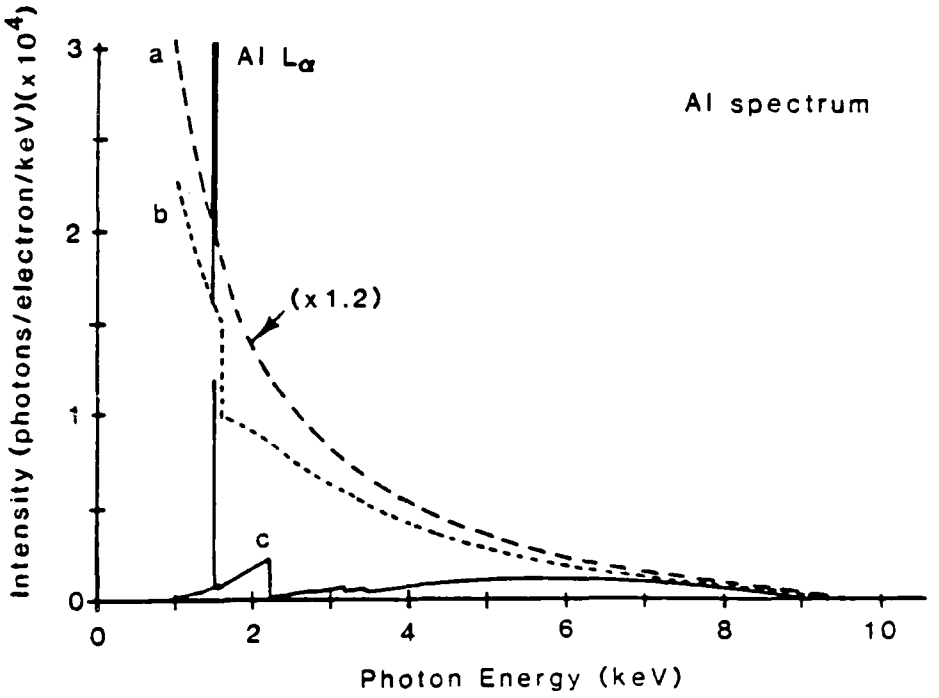

Figure 4. Calculated photon spectrum from Al at 10 kV. a. Uncorrected for Al target absorption. b. Corrected for absorption. c. Filtered by 6800Å Au.

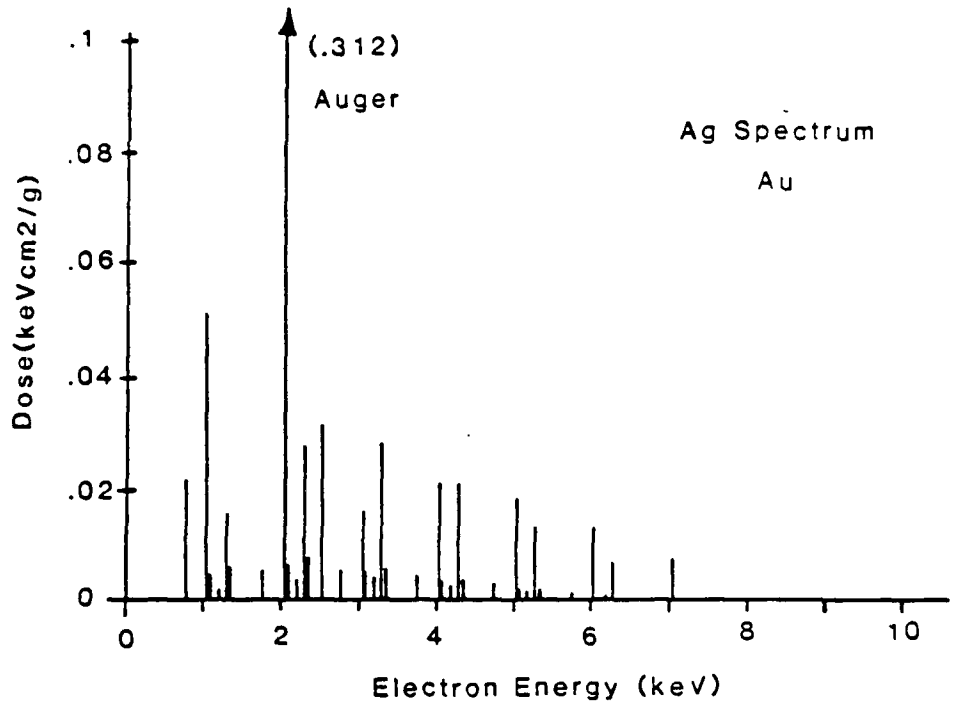

Figure 5. Calculated electron dose spectrum in Au produced by the Ag spectrum of Figure 3c.

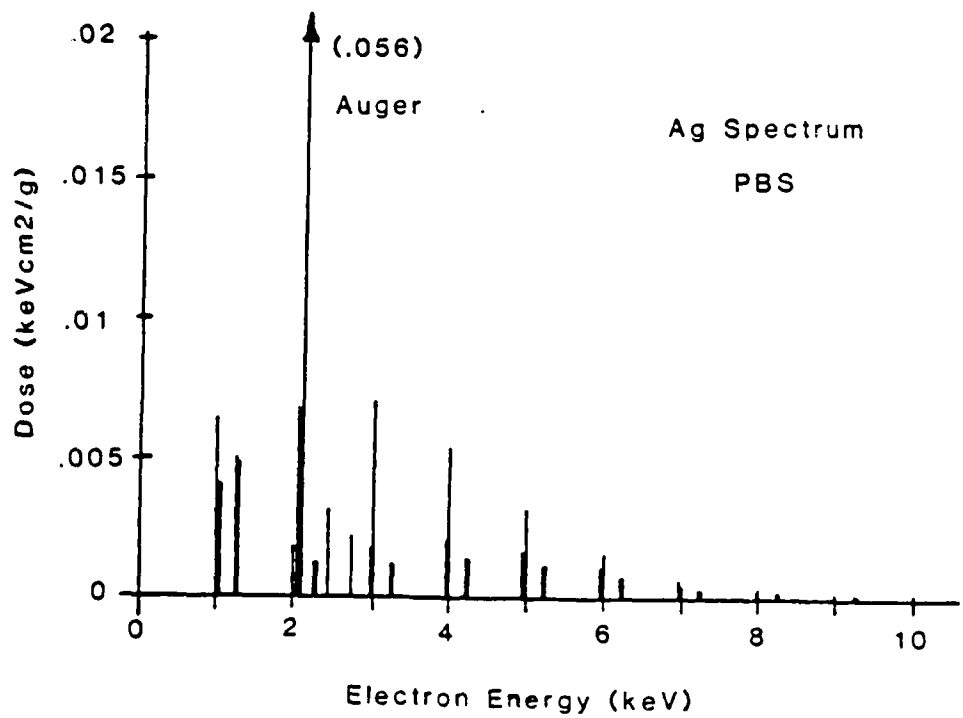

Figure 6. Calculated electron dose spectrum in PBS produced by the Ag spectrum of Figure 3c.

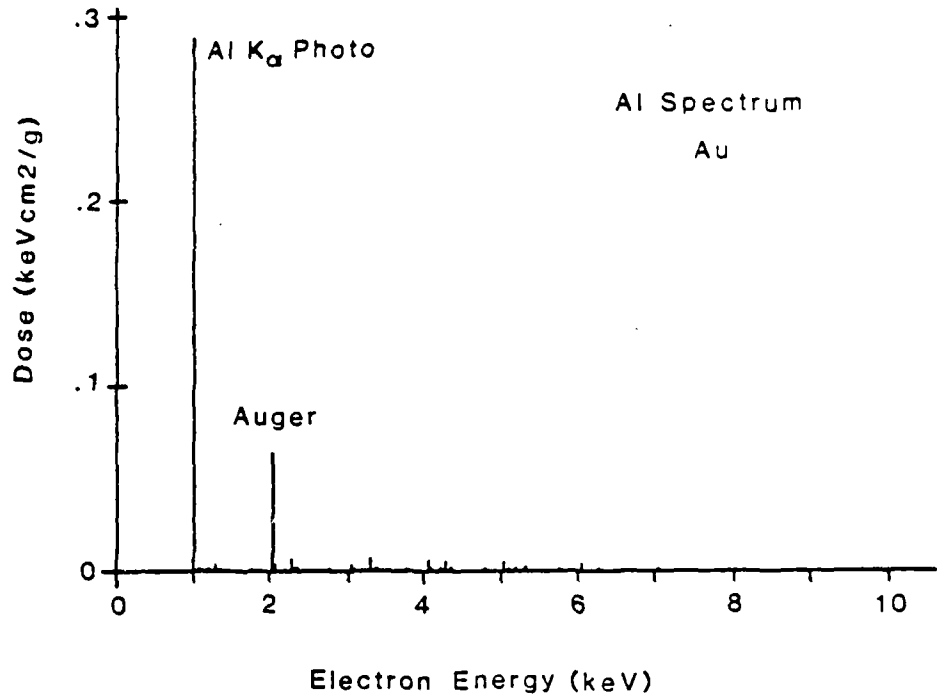

Figure 7. Calculated electron dose spectrum in Au produced by the Al spectrum of Figure 3c.

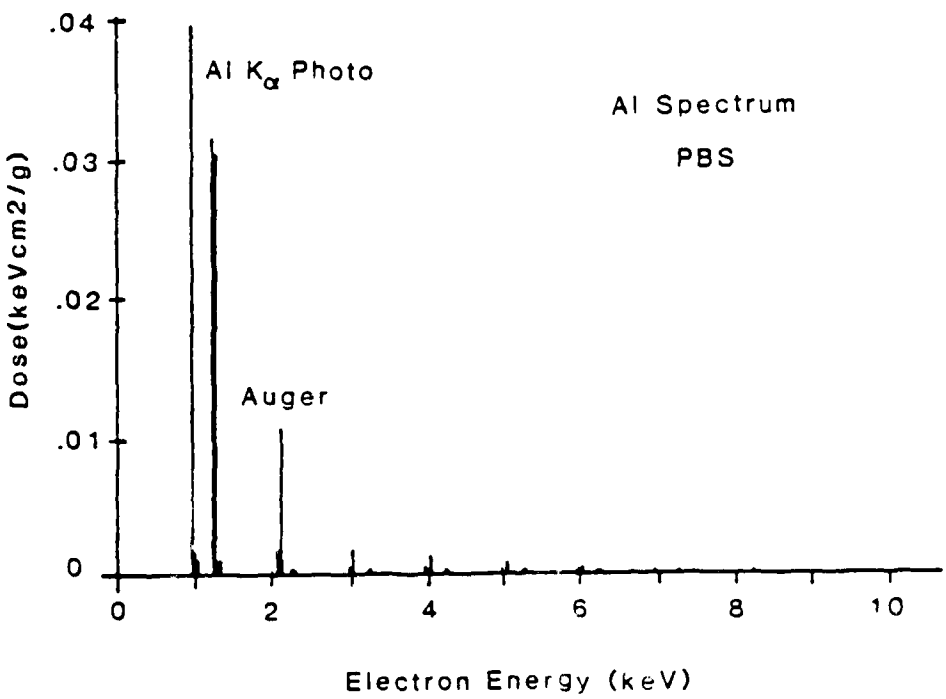

Figure 8. Calculated electron dose spectrum in PBS produced by the Al spectrum of Figure 4c.

AD-A149 552 LITHOGRAPHY RADIATION EFFECTS STUDY(U) SPIRE CORP 2/2
BEDFORD MA B W MURRAY NOV 84 RADC-TR-84-233
F19628-80-C-0196

UNCLASSIFIED F/G 14/5 NL

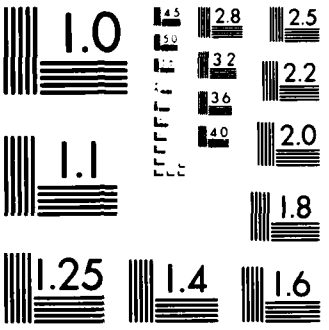

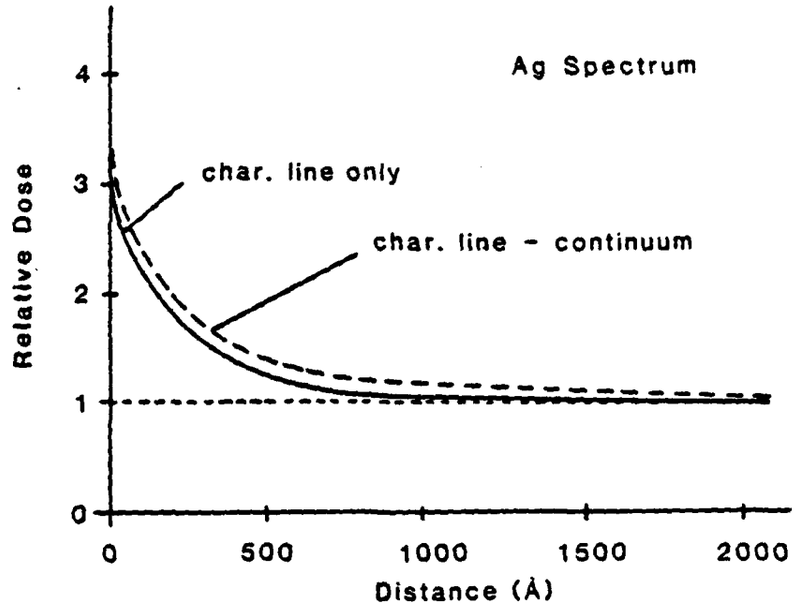

Figure 9. Relative dose profiles in PBS due to 10 kV Ag photon spectrum filtered by Au.

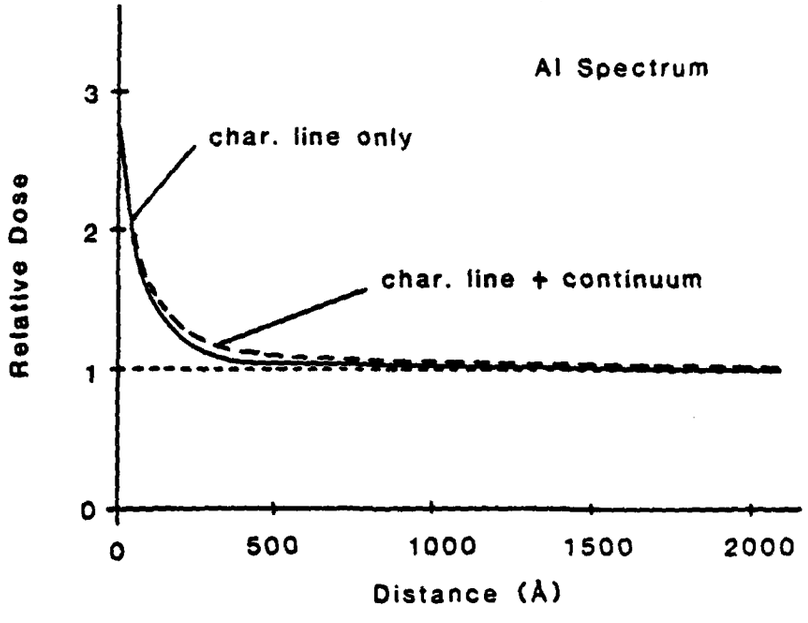

Figure 10. Relative dose profiles in PBS due to 10 kV Al photon spectrum filtered by Au.

MISSION
of
Rome Air Development Center

RADC plans and executes research, development, test and selected acquisition programs in support of Command, Control Communications and Intelligence (C^3I) activities. Technical and engineering support within areas of technical competence is provided to ESD Program Offices (POs) and other ESD elements. The principal technical mission areas are communications, electromagnetic guidance and control, surveillance of ground and aerospace objects, intelligence data collection and handling, information system technology, solid state sciences, electromagnetics and electronic reliability, maintainability and compatibility.

END

FILMED

2-85

DTIC